

The Origin of Galactic Cosmic Rays: Supernova Remnants

Siming Liu

Purple Mountain Observatory

liusm@pmo.ac.cn

**Yuliang Xin, Houdun Zeng, Xiao Zhang,
Qiang Yuan, Xiaoyuan Huang, Chuyuan
Yang, Yang Chen**

Outline

1: General Properties of Cosmic Rays

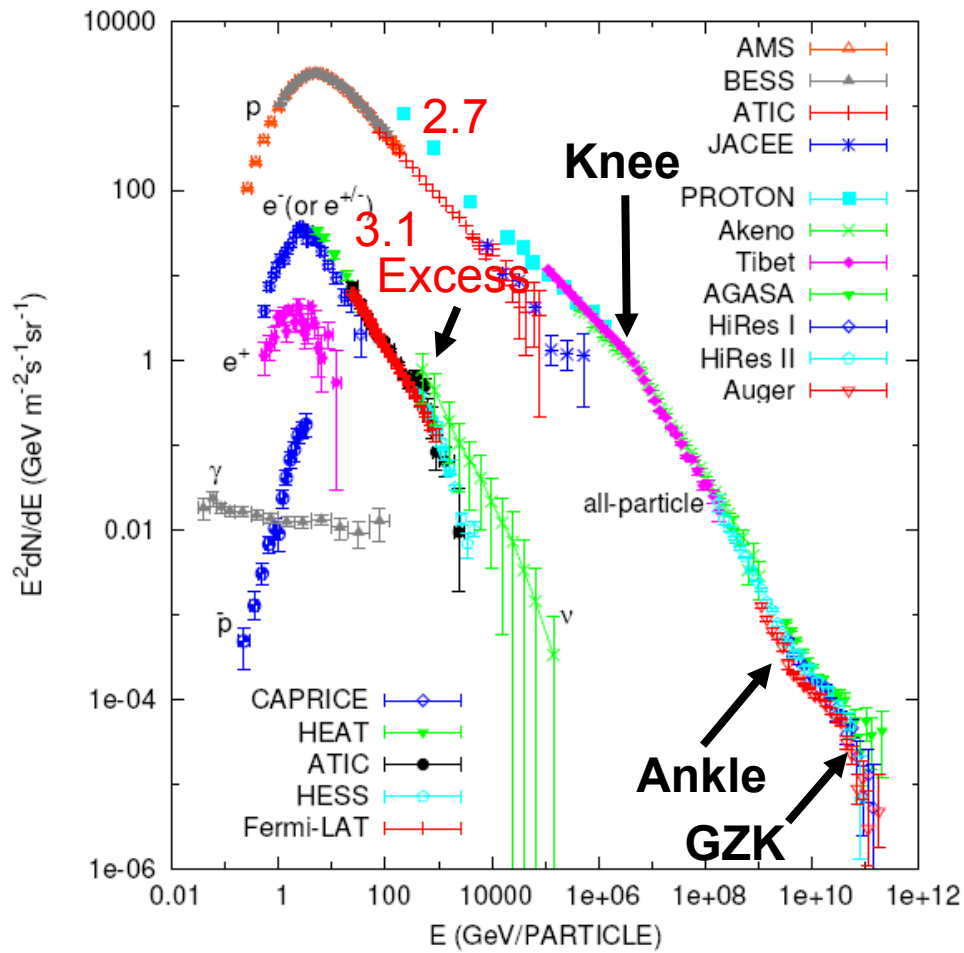
2: The Origin of Galactic Cosmic Rays:

Gamma-ray Observations of Supernova Remnants

3: Modeling of Individual SNRs with Multi-Wavelength Observations

4: Conclusions

1: Cosmic Rays



Dominated by Nuclei, there are also electrons, positrons and antiprotons

Age : $\sim 10^7$ Year

Energy density: $\sim 1\text{eV/cm}^3$

Power: $\sim 10^{41}\text{ erg/s}$
 $\sim 3\text{e}48\text{ erg/year}$

e/p $\sim 1\%$ at 1GeV

Leptonic Excess at $\sim 500\text{GeV}$

Spectral Knee at $\sim 1\text{e}15\text{eV}$
and Ankle at $\sim 1\text{e}18\text{eV}$

Maximum Energy: $3 \times 10^{20}\text{eV}$
 $\sim 50\text{ Joule}$

GZK Cutoff at $\sim 1\text{e}20\text{ eV}$

1: Modeling of Cosmic Ray Spectra

GALPROP

$$\frac{\partial \psi(\vec{r}, p, t)}{\partial t} = q(\vec{r}, p, t) + \vec{\nabla} \cdot (D_{xx} \vec{\nabla} \psi - \vec{V} \psi)$$

$$+ \frac{\partial}{\partial p} p^2 D_{pp} \frac{\partial}{\partial p} \frac{1}{p^2} \psi - \frac{\partial}{\partial p} \left[\dot{p} \psi - \frac{p}{3} (\vec{\nabla} \cdot \vec{V}) \psi \right] - \frac{1}{\tau_f} \psi - \frac{1}{\tau_r} \psi$$

Injection Power :

Proton $\sim 3 \times 10^{48}$ erg/year

Electron $\sim 4 \times 10^{46}$ erg/year

$$\alpha = 1.25, \beta = 3.56, R_\odot = 8.5 \text{ kpc}, z_s \approx 0.2 \text{ kpc}$$

3 SNRs/100 yrs with

1×10^{50} erg protons and

1×10^{48} erg electrons

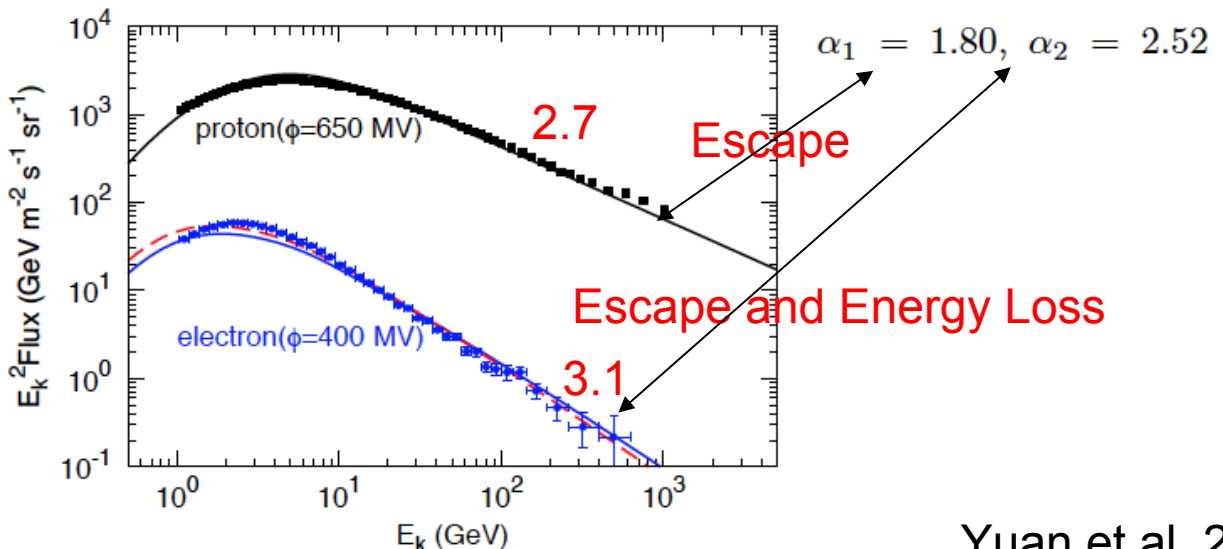
For each SNR.

10% efficiency for type Ia SNRs with a kinetic energy of 1×10^{51} ergs

$$q_f(R, z) \propto \left(\frac{R}{R_\odot} \right)^\alpha \exp \left[-\frac{\beta(R - R_\odot)}{R_\odot} \right] \exp \left(-\frac{|z|}{z_s} \right),$$

$$q(p) \propto \begin{cases} p^{-\alpha_1}, & p < p_{br}, \\ p^{-\alpha_2}, & p \geq p_{br}, \end{cases}$$

$$p_{br} c = 6 \text{ GeV}$$



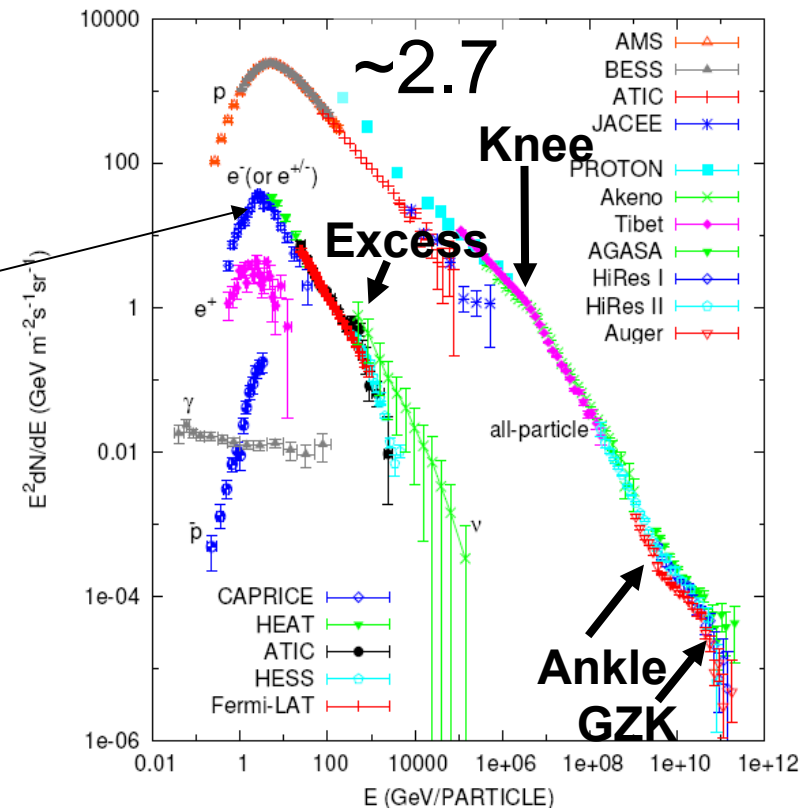
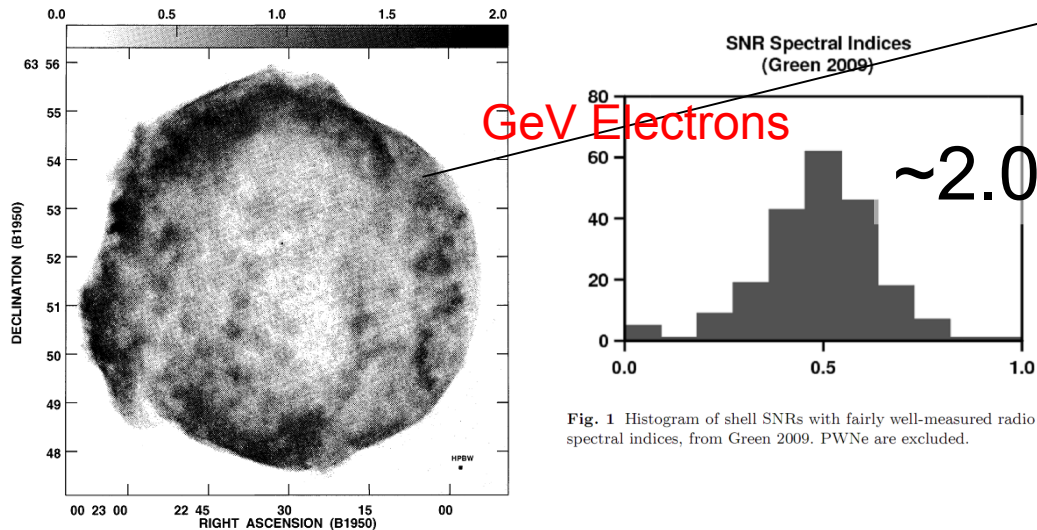
2: Radio Supernova Remnants and Galactic Cosmic rays

COSMIC RAYS FROM SUPER-NOVAE

By W. BAADE AND F. ZWICKY

MOUNT WILSON OBSERVATORY, CARNEGIE INSTITUTION OF WASHINGTON AND CALIFORNIA INSTITUTE OF TECHNOLOGY, PASADENA

Communicated March 19, 1934

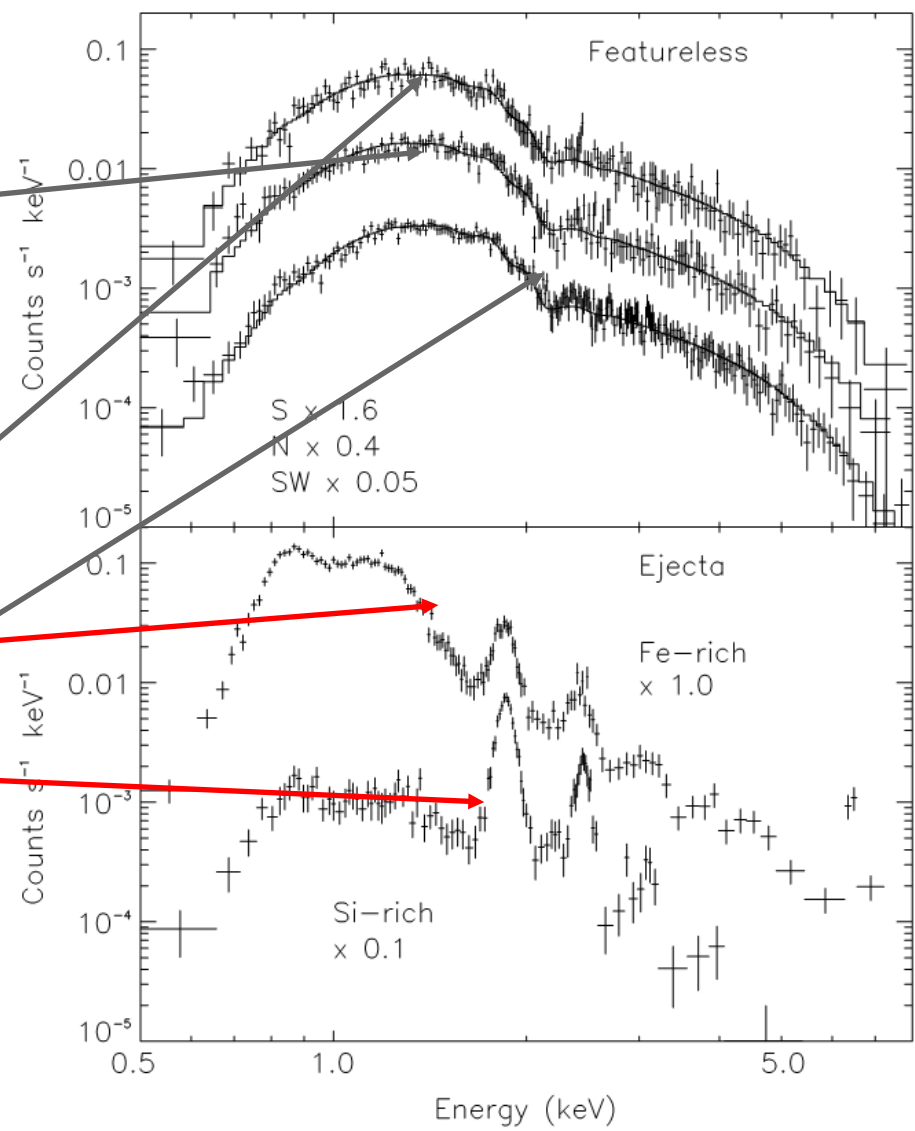
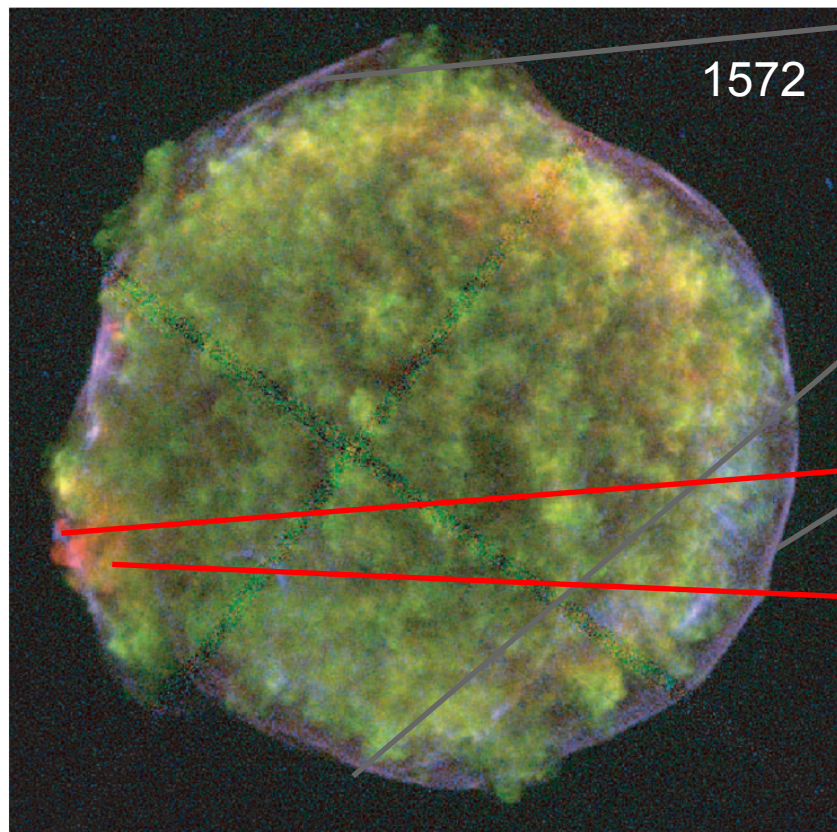


Magnetic fields in supernova remnants and pulsar-wind nebulae

2: Synchrotron X-rays

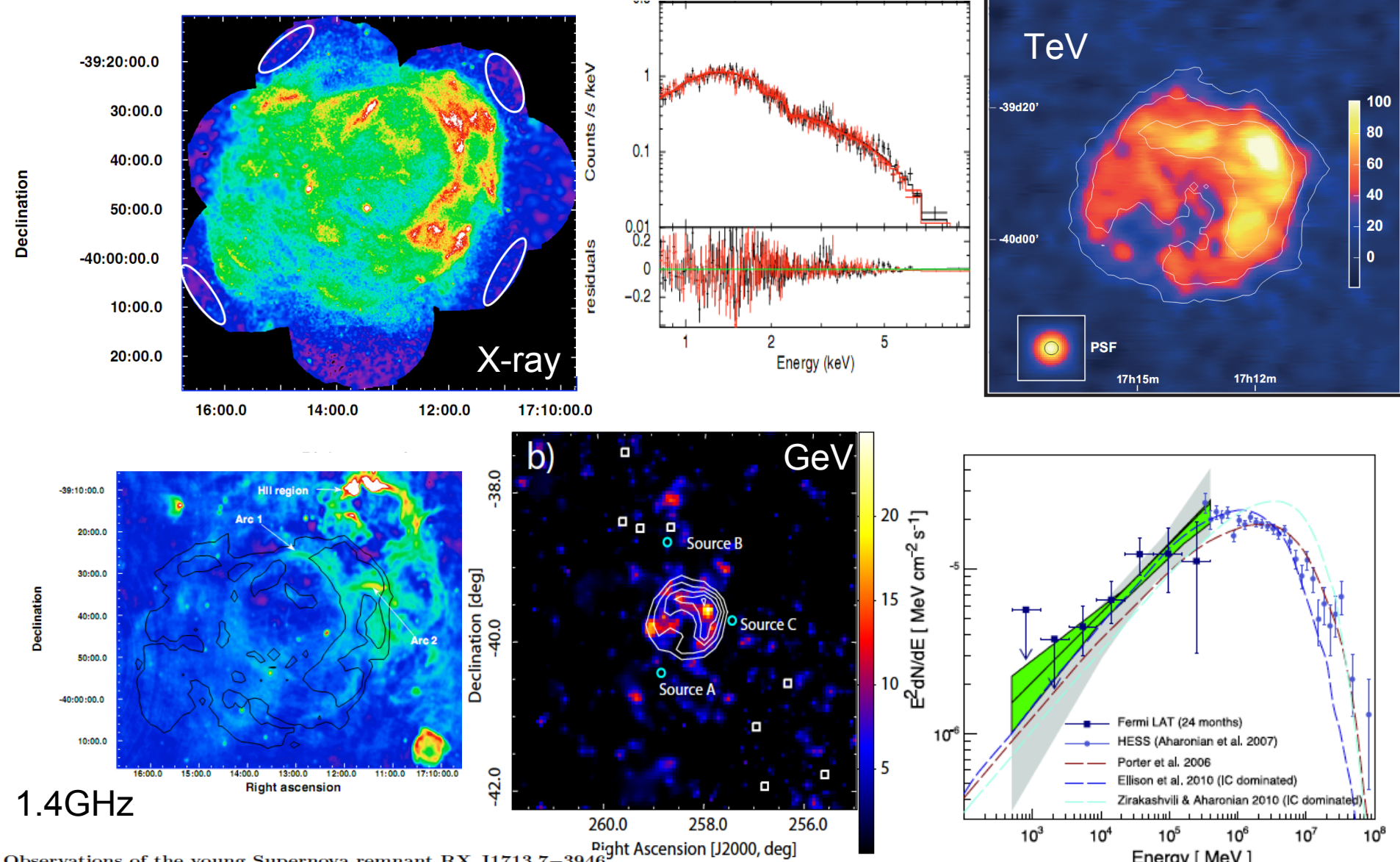
TYCHO'S SUPERNOVA REMNANT

TeV Electrons



2: Shell Type TeV SNRs

F. Acero¹, J. Ballet¹, A. Decourchelle¹, M. Lemoine-Goumard^{2,3}, M. Ortega⁴, E. Giacani⁴, G. Dubner⁴, and G. Cassam-Chenaï⁵



The X-ray emission of the supernova remnant W49B observed with *XMM-Newton*

M. Miceli^{1,2,3}, A. Decourchelle¹, J. Ballet¹, F. Bocchino³, J. P. Hughes⁴, U. Hwang^{5,6}, and R. Petre⁶

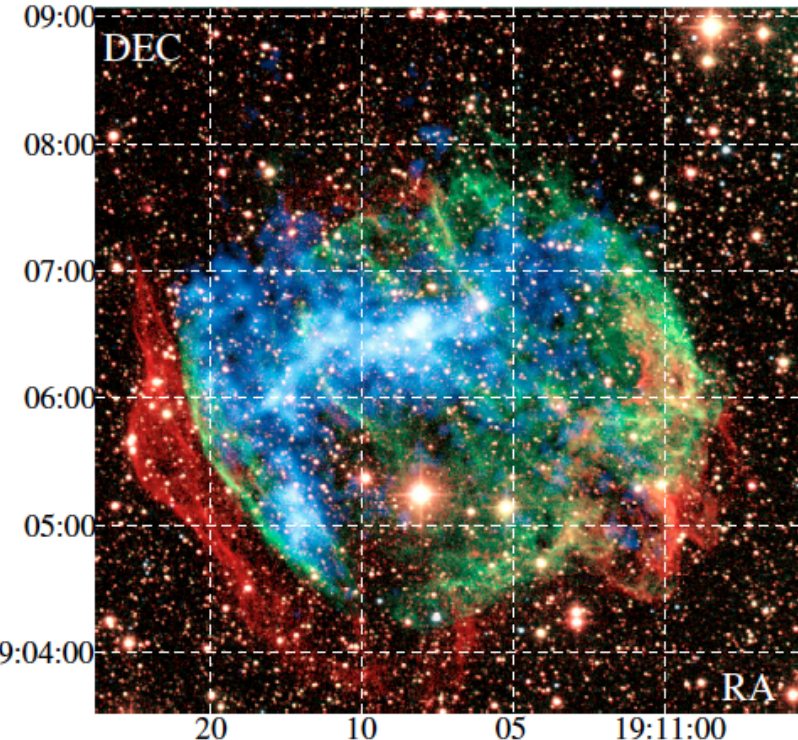
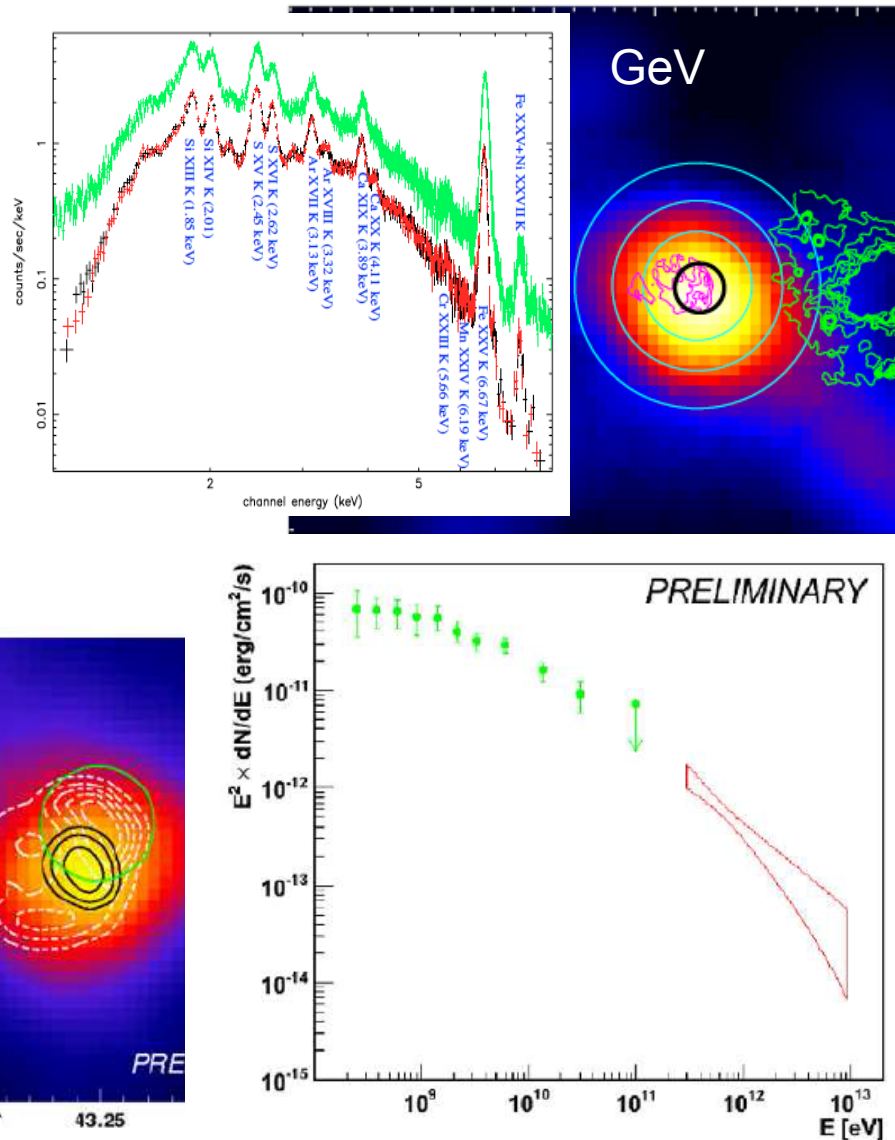


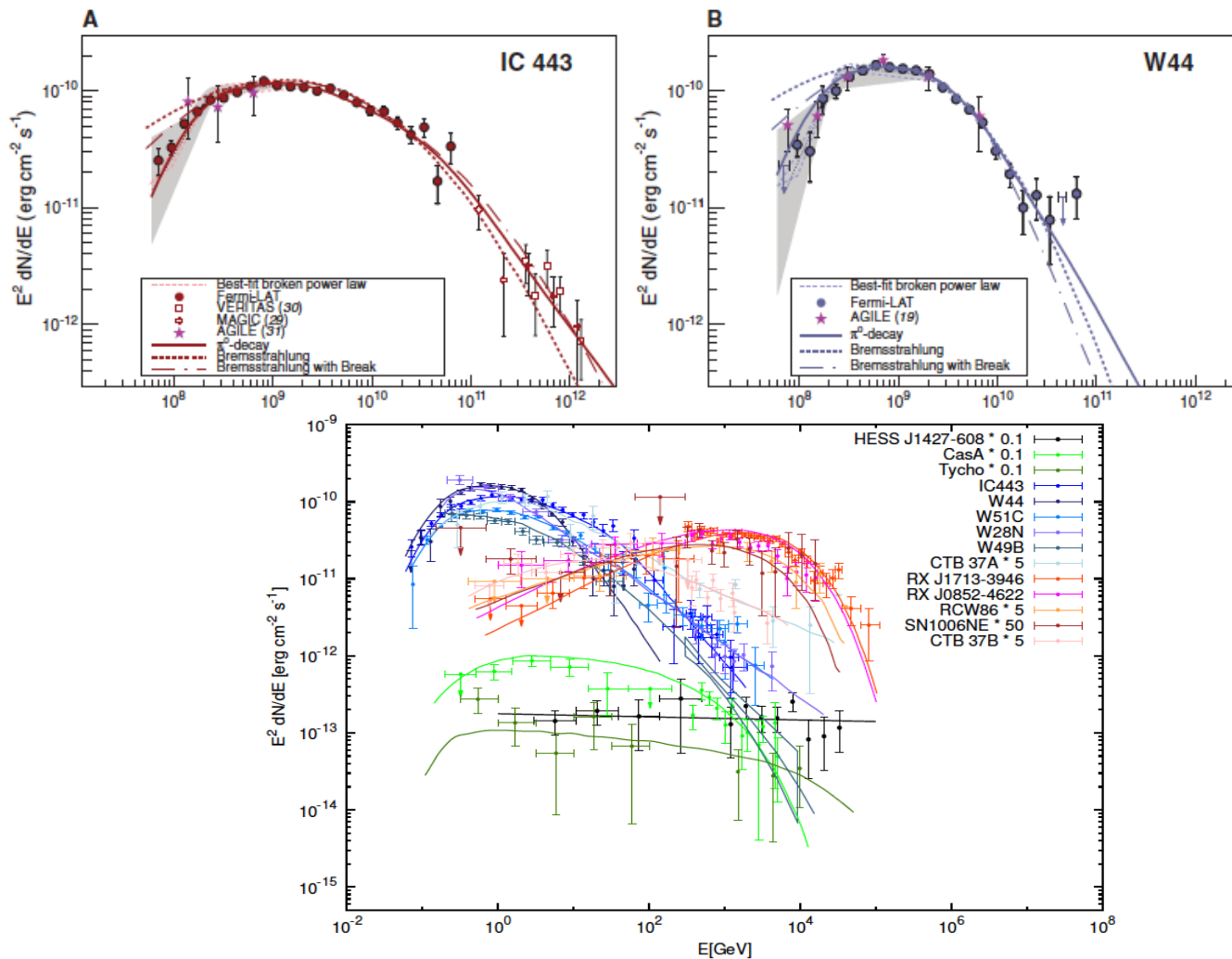
Fig. 2. Color composite *Chandra* X-ray image (in blue), infrared $2.12 \mu\text{m}$ molecular hydrogen (in red), and $1.64 \mu\text{m}$ [Fe II] (in green) images of W49B (from http://chandra.harvard.edu/press/04_releases/press_060204.html).



2: Hadronic Gamma-ray Emission



Detection of the Characteristic Pion-Decay Signature in Supernova Remnants
M. Ackermann *et al.*
Science 339, 807 (2013);
DOI: 10.1126/science.1231160





2: Observations of SNRs

Radio SNRs: 279 among them

Synchrotron X-Ray: >14

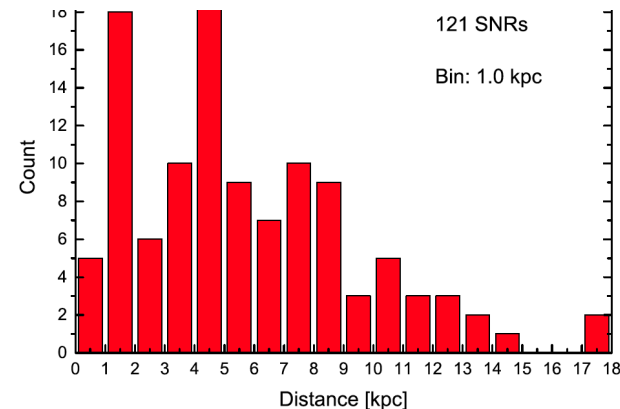
GeV SNRs: >30 among them

TeV SNRs: >10

$3/100 * 1e5 = 3000$

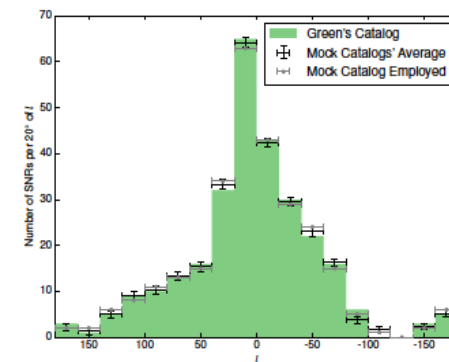
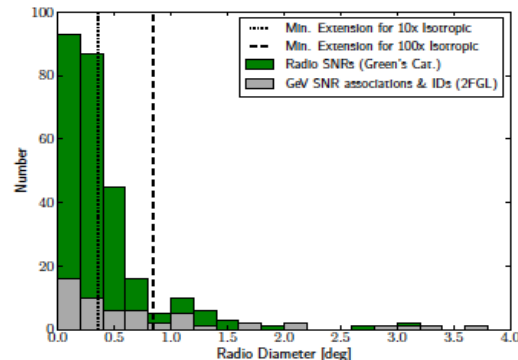
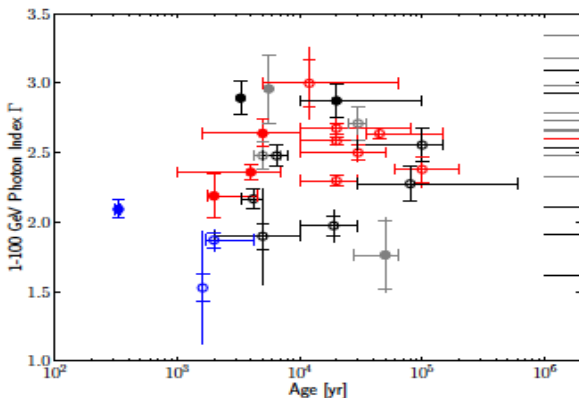
THE FIRST FERMI LAT SUPERNOVA REMNANT CATALOG

F. ACERO¹, M. ACKERMANN², M. AJELLO³, L. BALDINI^{4,5}, J. BALLETT¹, G. BARBIELLINI^{6,7}, D. BASTIERI^{8,9}, R. BELLAZZINI¹⁰,



Distribution of SNRs in Distance

Distribution of SNRs in Angular Diameter



Distribution of SNRs in Galactic Longitude

2: Observations of SNRs

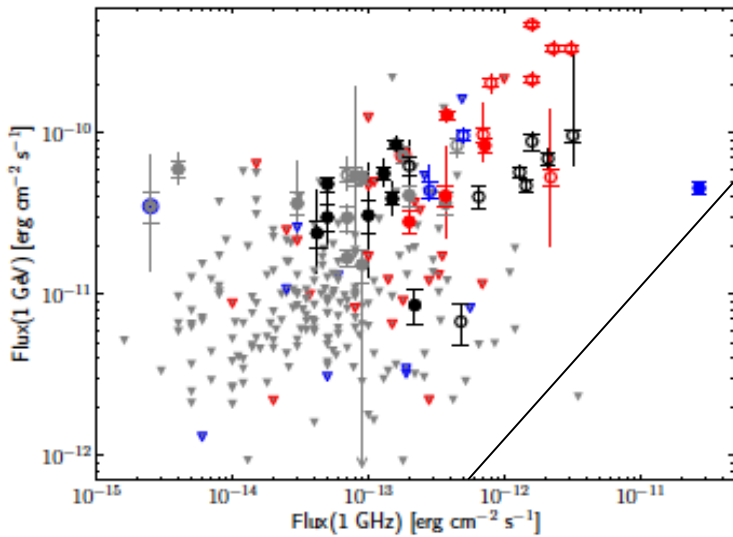
Radio vs GeV fluxes

Radio SNRs: 279 among them

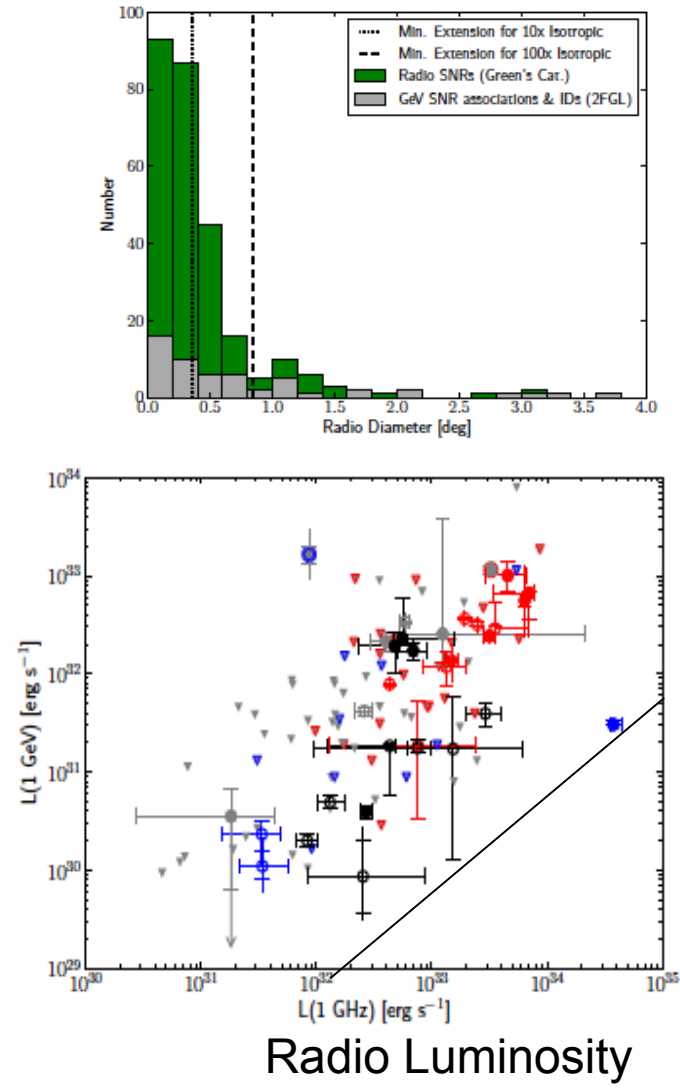
Synchrotron X-Ray: 14

GeV SNRs: 30 among them

TeV SNRs: >10



Radio Flux



Radio Luminosity

2: Observations of SNRs:

Spectral indexes

Radio SNRs: 279 among them

Synchrotron X-Ray: 14

GeV SNRs: 30 among them

TeV SNRs: >10

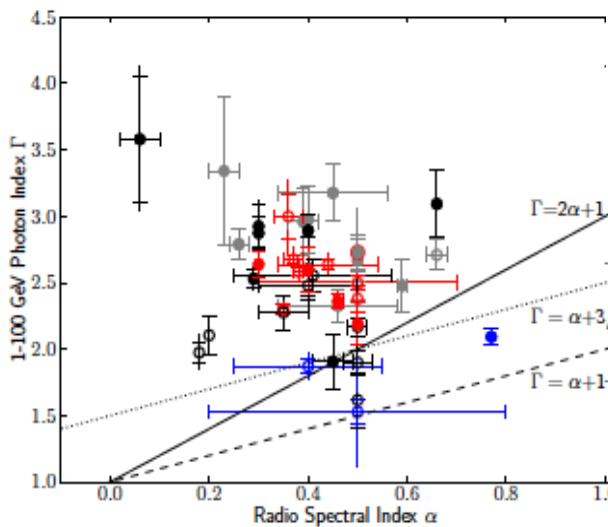
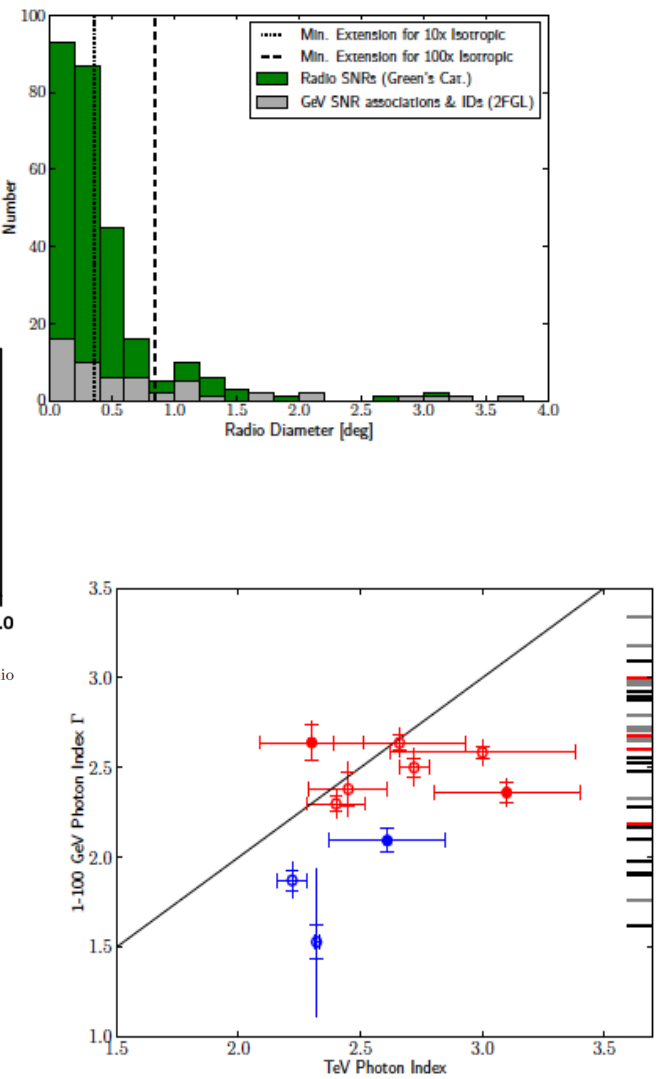
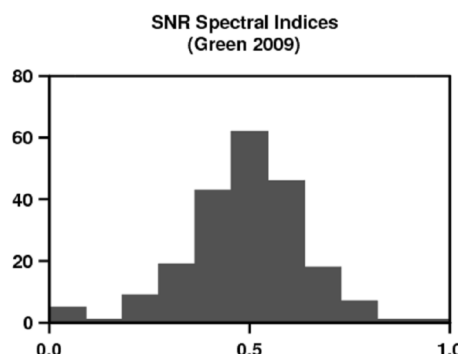


Fig. 1 Histogram of shell SNRs with fairly well-measured radio spectral indices, from Green 2009. PWNe are excluded.



2: Modeling of Cosmic Ray Spectra

$$q_f(R, z) \propto \left(\frac{R}{R_\odot}\right)^\alpha \exp\left[-\frac{\beta(R - R_\odot)}{R_\odot}\right] \exp\left(-\frac{|z|}{z_s}\right),$$

Injection Power :

Proton ~ 3e48 erg/year

Electron ~ 4e46 erg/year

3 SNRs/100 yrs with
1e50 erg protons and
1e48 erg electrons

For each SNR.

10% efficiency for type
Ia SNRs with a kinetic
energy of 1e51 ergs

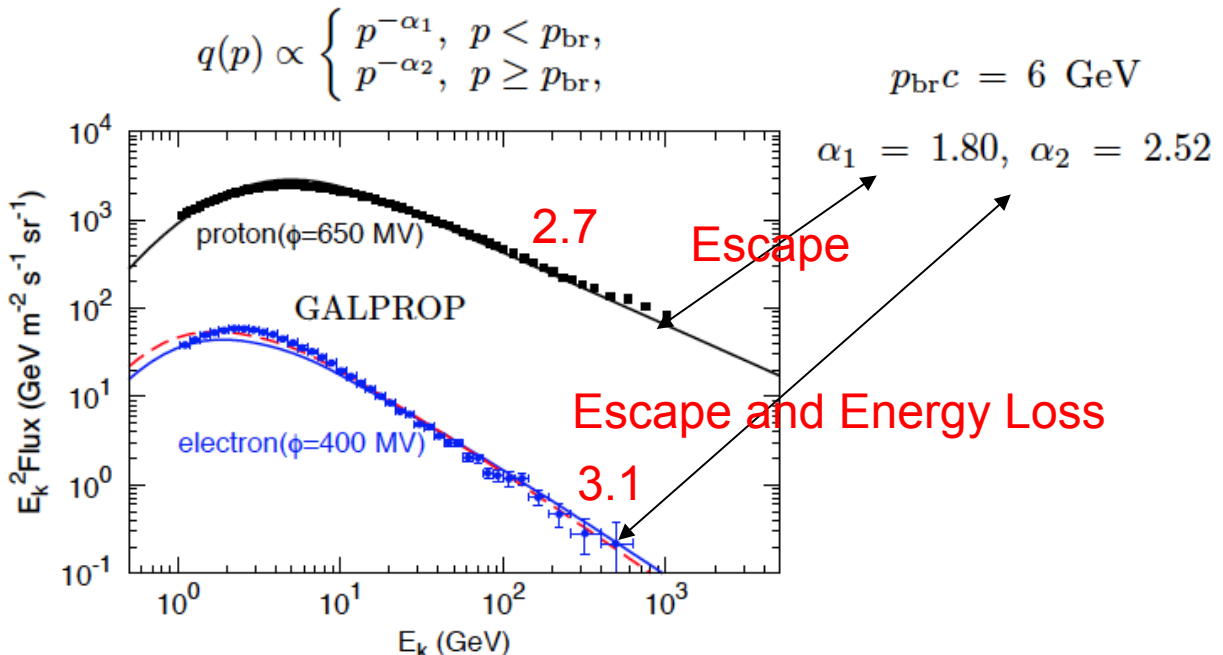
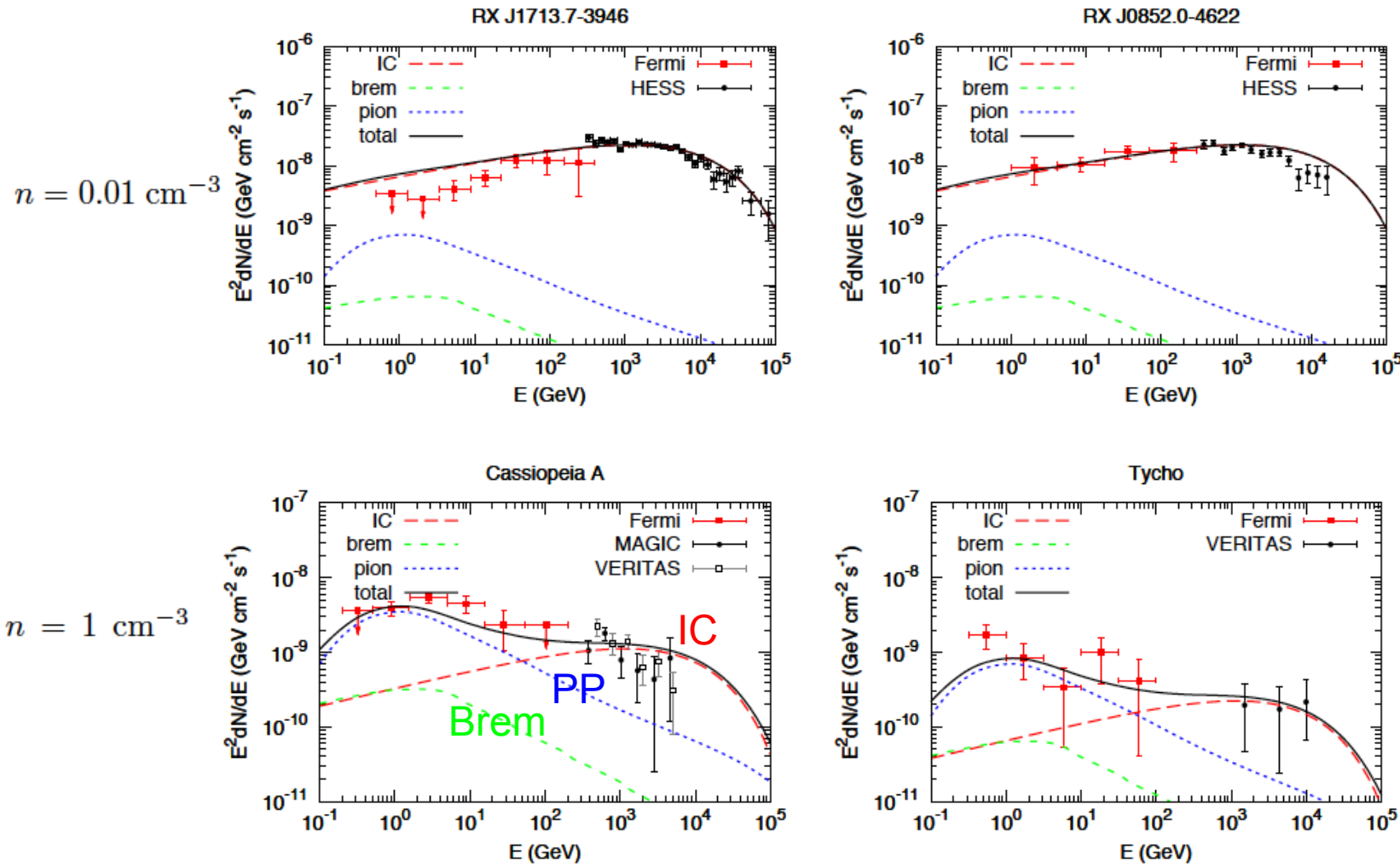


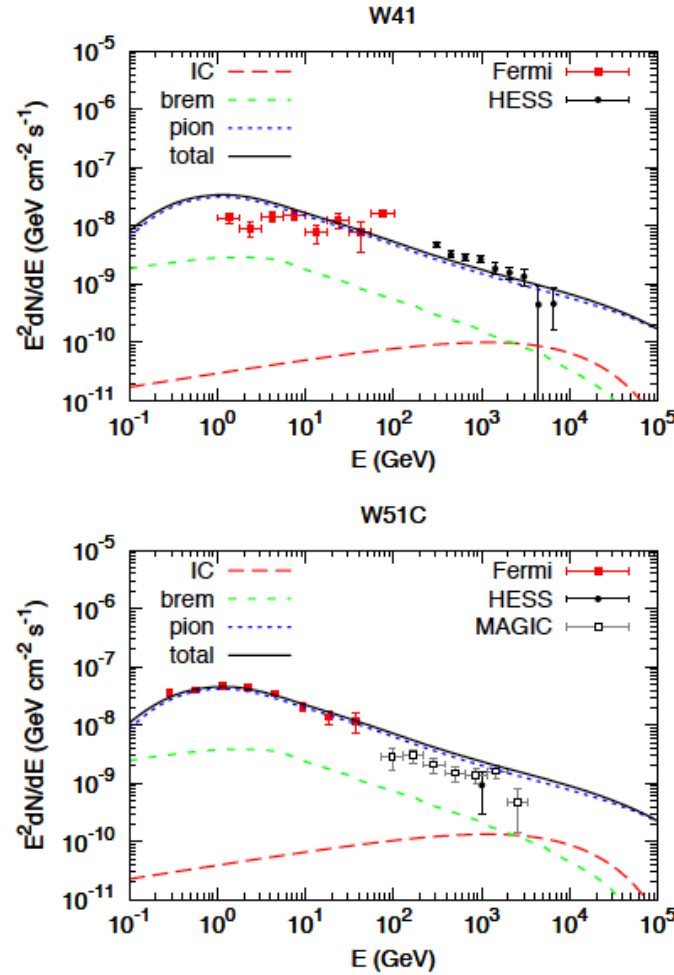
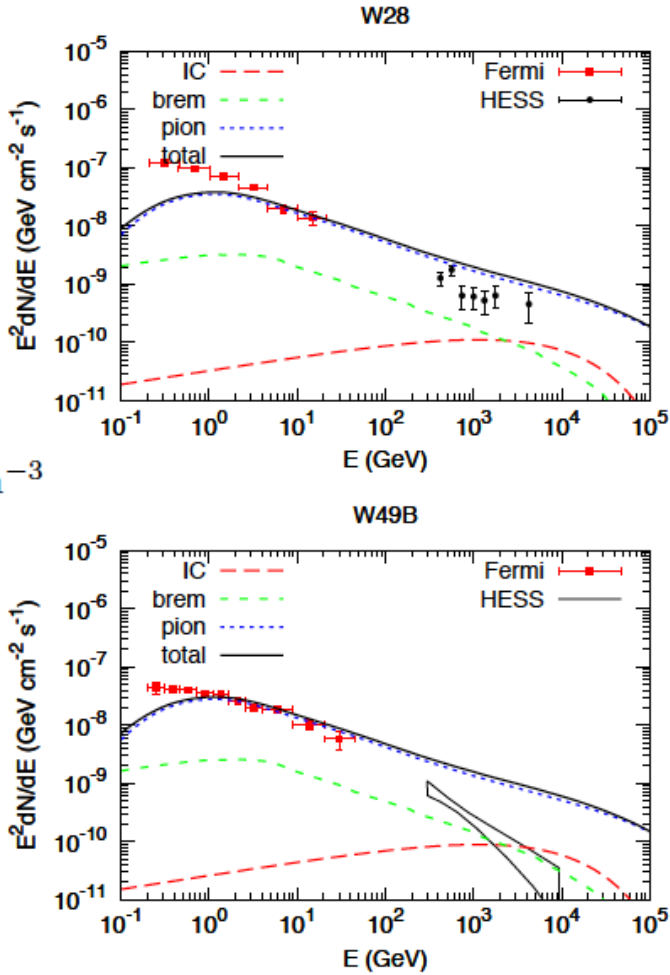
FIG. 1.— The expected fluxes of CR protons and electrons at the Earth, for the same spectral shape of the injected particles, compared with the PAMELA observational data (Adriani et al. 2011a,b). We adopt two parameter settings to calculate the electron spectrum: for solid line the magnetic field is the canonical one adopted in GALPROP and $K_{ep} \approx 1.3\%$; for dashed line the magnetic field is two times larger and $K_{ep} \approx 1.9\%$.

2: Emission Processes of Gamma-rays



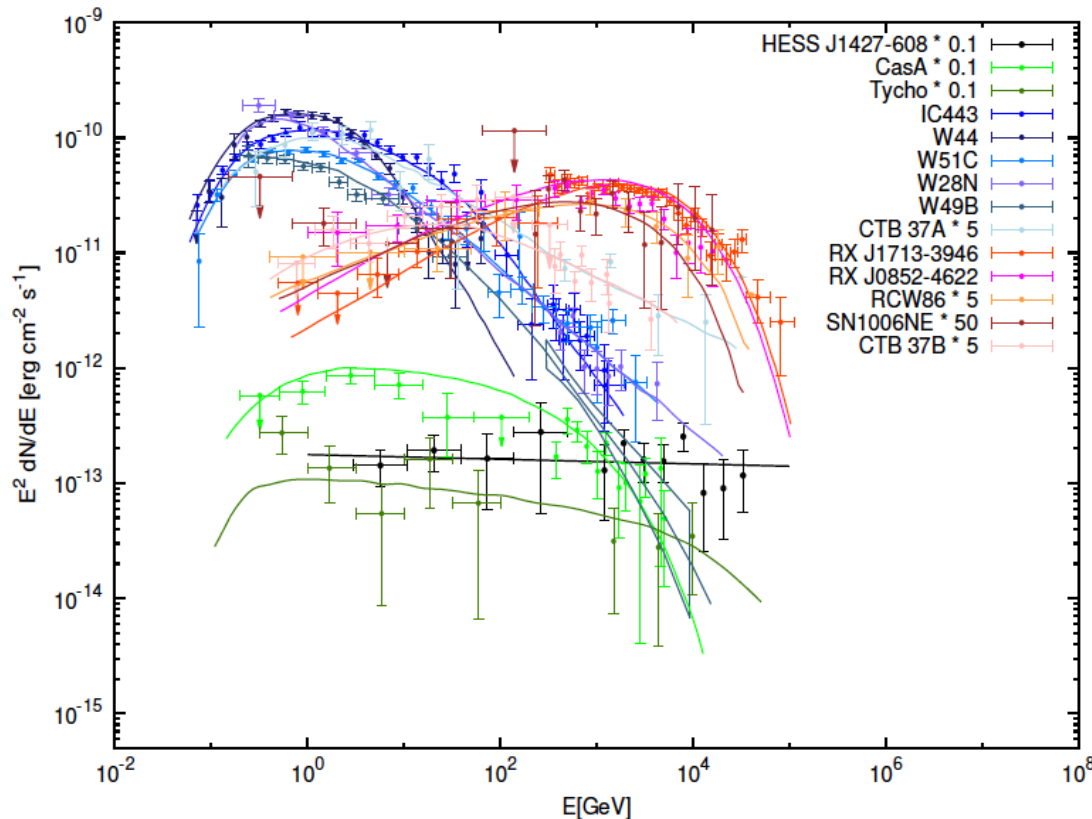
2: Modeling of Gamma-ray Spectra

$$n = 100 \text{ cm}^{-3}$$



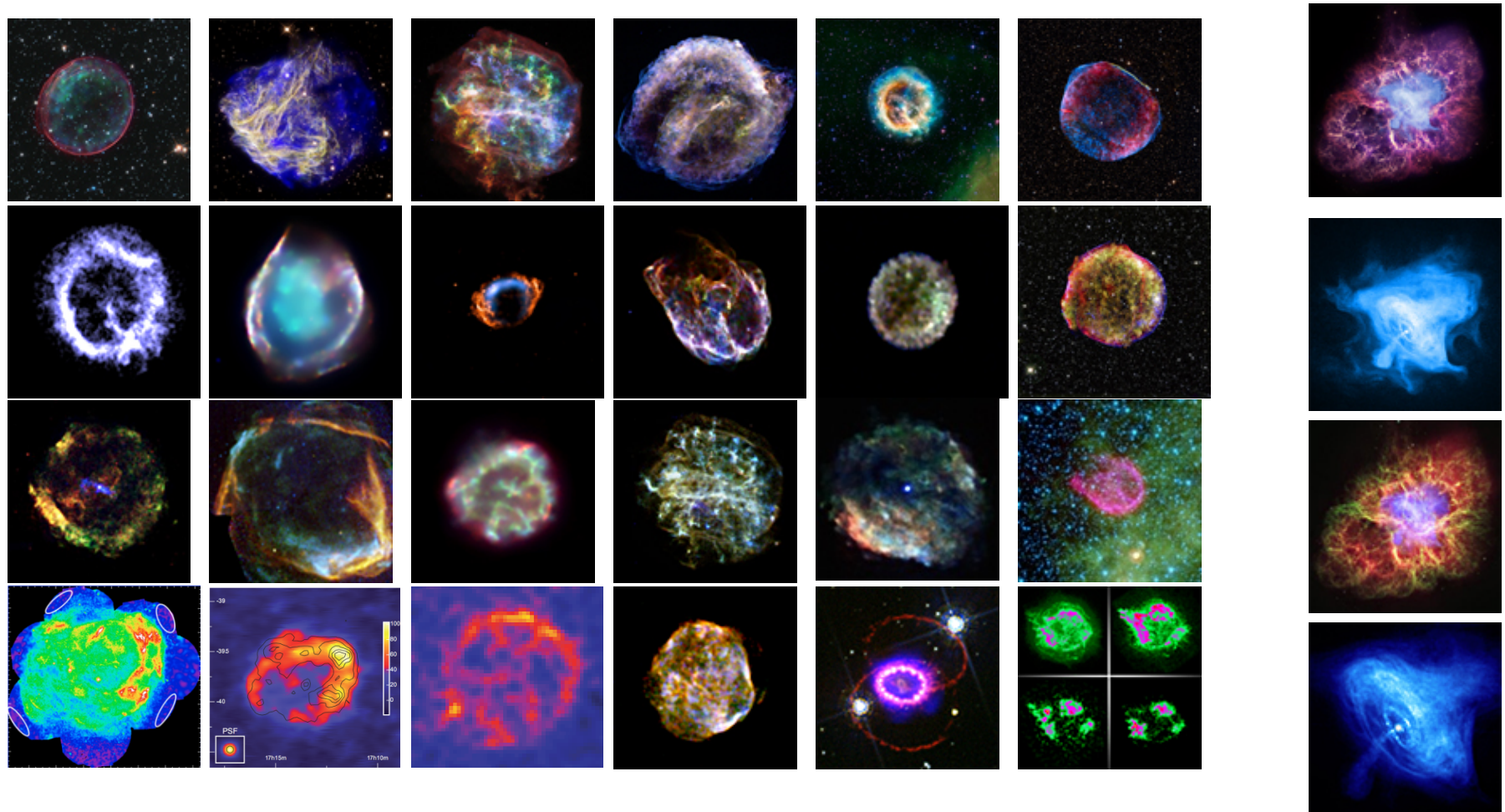
2: Summary

The spectra of SNRs show significant variations from source to source, which may be attributed to the evolution of shocks of SNRs and/or complexity of the environment.



3: Multi-wavelength Observations of Supernova Remnants

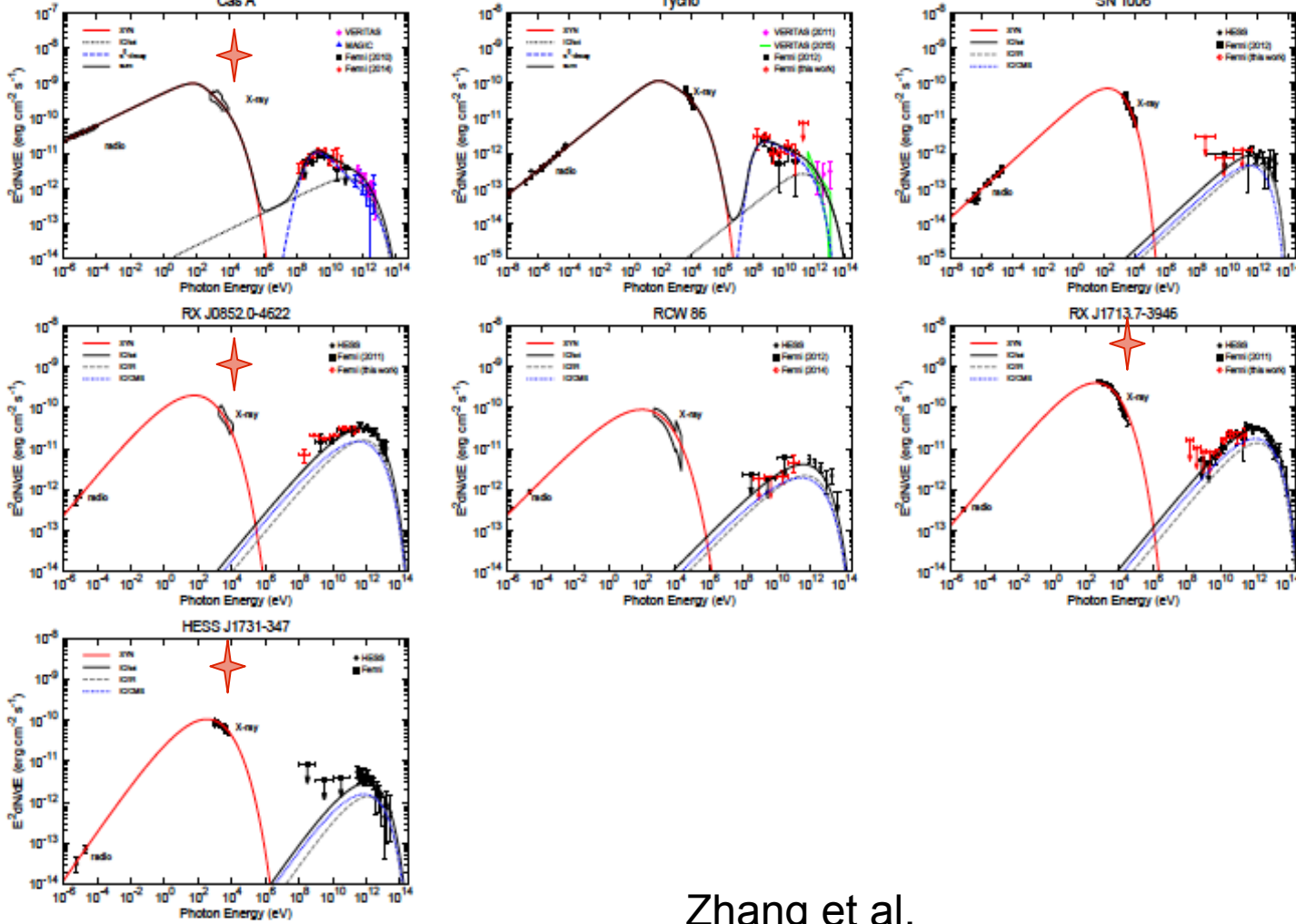
Pulsars are not energetically as important as shocks and may dominate the position excess at \sim 500GeV



3: Supernova Remnants with Synchrotron X-ray and TeV

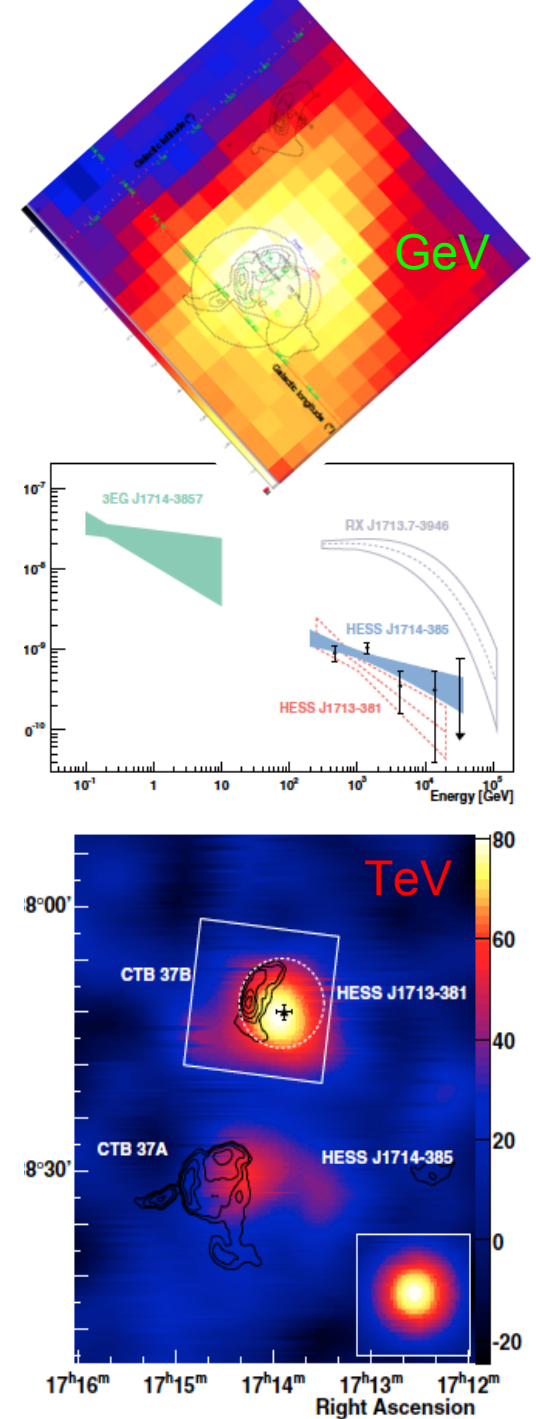
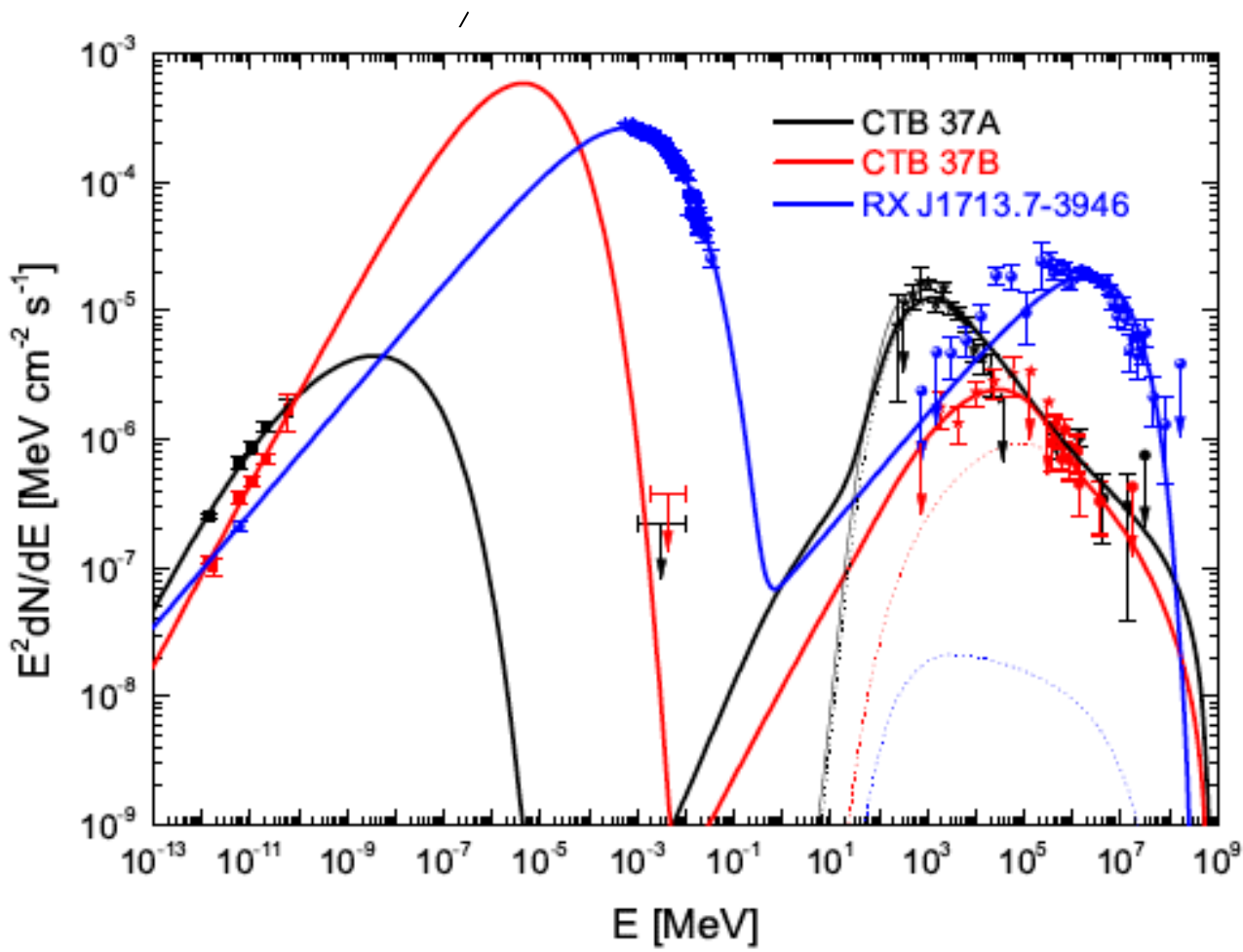


With a compact object at the center: Core Collapse SN

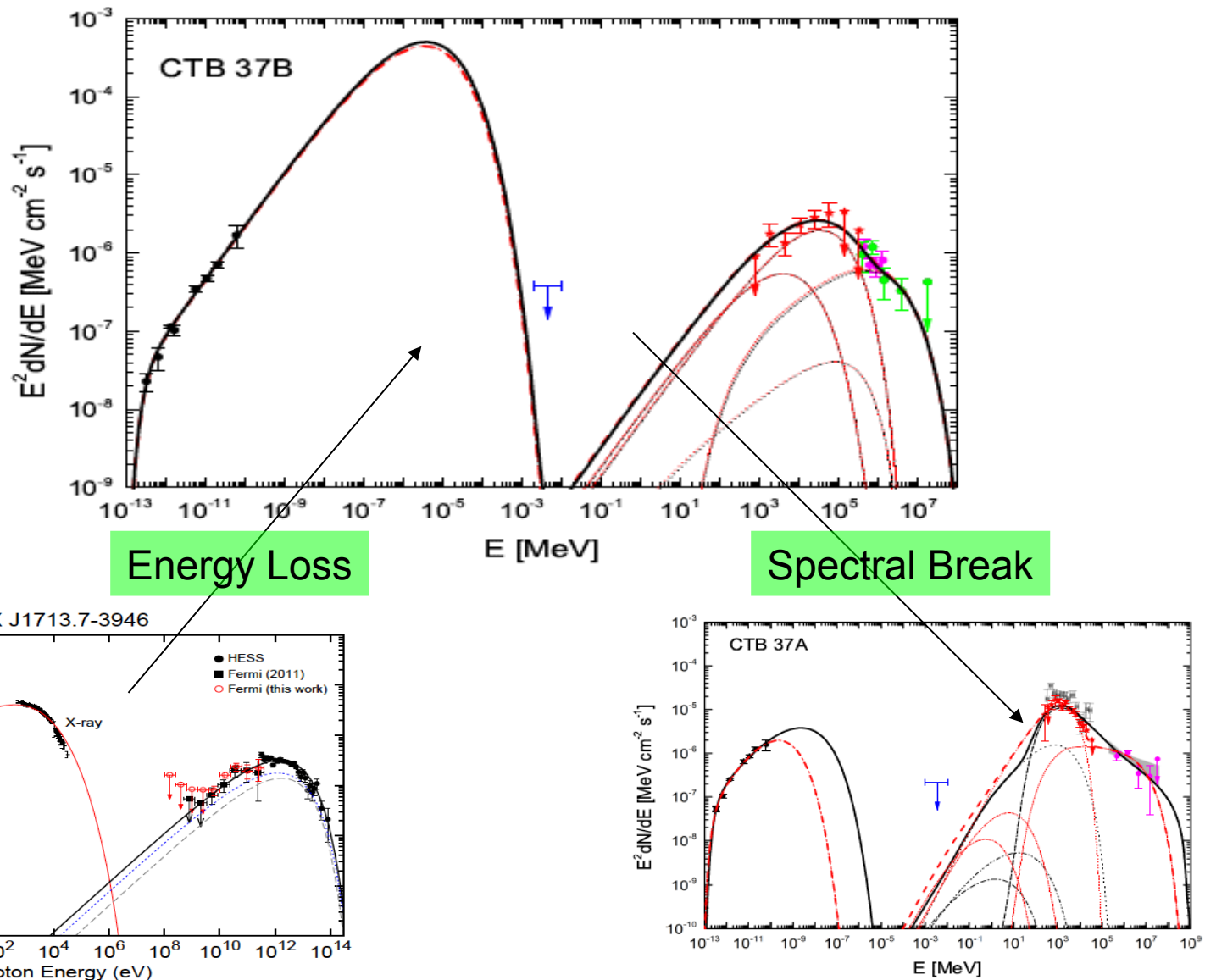


Zhang et al.

3: Three Supernova Remnants with compact central sources



3: Spectral Evolution



3: Model Parameters

| Source Name | α | $\log_{10} \frac{E_{br}}{\text{GeV}}$ | $\log_{10} \frac{E_{e,\text{cut}}}{\text{GeV}}$ | $\log_{10} \frac{E_{p,\text{cut}}}{\text{GeV}}$ | $\frac{B}{\mu\text{G}}$ | $\log_{10} \frac{W_p}{\text{erg}}$ | $\frac{W_B}{W_e}$ | Reduced χ^2 for the best-fit |
|-----------------|------------------------|---------------------------------------|-------------------------------------------------|-------------------------------------------------|--------------------------|-----------------------------------------------------------------------------------------------------------------------------------------------|---------------------------------------------------------------------------------------------------------------|-----------------------------------|
| RX J1713.7-3946 | $2.11^{+0.01}_{-0.01}$ | NA | $4.51^{+0.005}_{-0.006}$ | > 4.51 | $1.23^{+0.004}_{-0.004}$ | $49.41^{+0.04}_{-0.04} + \log_{10} \left[\left(\frac{n}{0.01\text{cm}^{-3}} \right)^{-1} \left(\frac{D}{1\text{kpc}} \right)^2 \right]$ | $5.46 \times \left(\frac{D}{1\text{kpc}} \right)^{-2} \left(\frac{R}{10\text{pc}} \right)^3$ | $\frac{509}{240-5} = 2.17$ |
| RX J1713.7-3946 | $2.11^{+0.01}_{-0.01}$ | NA | $4.51^{+0.005}_{-0.005}$ | $4.92^{+0.31}_{-0.31}$ | $1.24^{+0.005}_{-0.005}$ | $49.35^{+0.02}_{-0.02} + \log_{10} \left[\left(\frac{n}{1.0\text{cm}^{-3}} \right)^{-1} \left(\frac{D}{1\text{kpc}} \right)^2 \right]$ | $5.72 \times \left(\frac{D}{1\text{kpc}} \right)^{-2} \left(\frac{R}{10\text{pc}} \right)^3$ | $\frac{482}{240-5} = 2.05$ |
| CTB 37B | $1.59^{+0.07}_{-0.07}$ | $3.31^{+0.29}_{-0.31}$ | $2.70^{+0.18}_{-0.21}$ | > 4.57 | $2.00^{+0.13}_{-0.13}$ | $51.49^{+0.10}_{-0.09} + \log_{10} \left[\left(\frac{n}{0.5\text{cm}^{-3}} \right)^{-1} \left(\frac{D}{13.2\text{kpc}} \right)^2 \right]$ | $32.9 \times \left(\frac{D}{13.2\text{kpc}} \right)^{-2} \left(\frac{R}{20\text{pc}} \right)^3$ | $\frac{13.7}{19-6} = 1.05$ |
| CTB 37B | $1.51^{+0.11}_{-0.11}$ | $2.45^{+0.36}_{-0.34}$ | $1.57^{+0.79}_{-0.78}$ | > 4.60 | $2.71^{+0.14}_{-0.15}$ | $50.47^{+0.04}_{-0.04} + \log_{10} \left[\left(\frac{n}{10.0\text{cm}^{-3}} \right)^{-1} \left(\frac{D}{13.2\text{kpc}} \right)^2 \right]$ | $1.75 \times 10^4 \times \left(\frac{D}{13.2\text{kpc}} \right)^{-2} \left(\frac{R}{20\text{pc}} \right)^3$ | $\frac{14.3}{19-6} = 1.10$ |
| CTB 37A | $1.50^{+0.03}_{-0.03}$ | $0.25^{+0.16}_{-0.16}$ | $1.80^{+0.67}_{-0.61}$ | > 6.18 | $2.36^{+0.04}_{-0.04}$ | $49.77^{+0.02}_{-0.02} + \log_{10} \left[\left(\frac{n}{100\text{cm}^{-3}} \right)^{-1} \left(\frac{D}{7.9\text{kpc}} \right)^2 \right]$ | $575 \times \left(\frac{D}{7.9\text{kpc}} \right)^{-2} \left(\frac{R}{10\text{pc}} \right)^3$ | $\frac{33.8}{21-6} = 2.25$ |

EVOLUTION OF HIGH-ENERGY PARTICLE DISTRIBUTION IN MATURE SHELL-TYPE SUPERNOVA REMNANTS

HOUDUN ZENG^{1,3}, YULIANG XIN^{1,4}, SIMING LIU¹, J. R. JOKIPII⁵, LI ZHANG^{2,3}, AND SHUINAI ZHANG¹

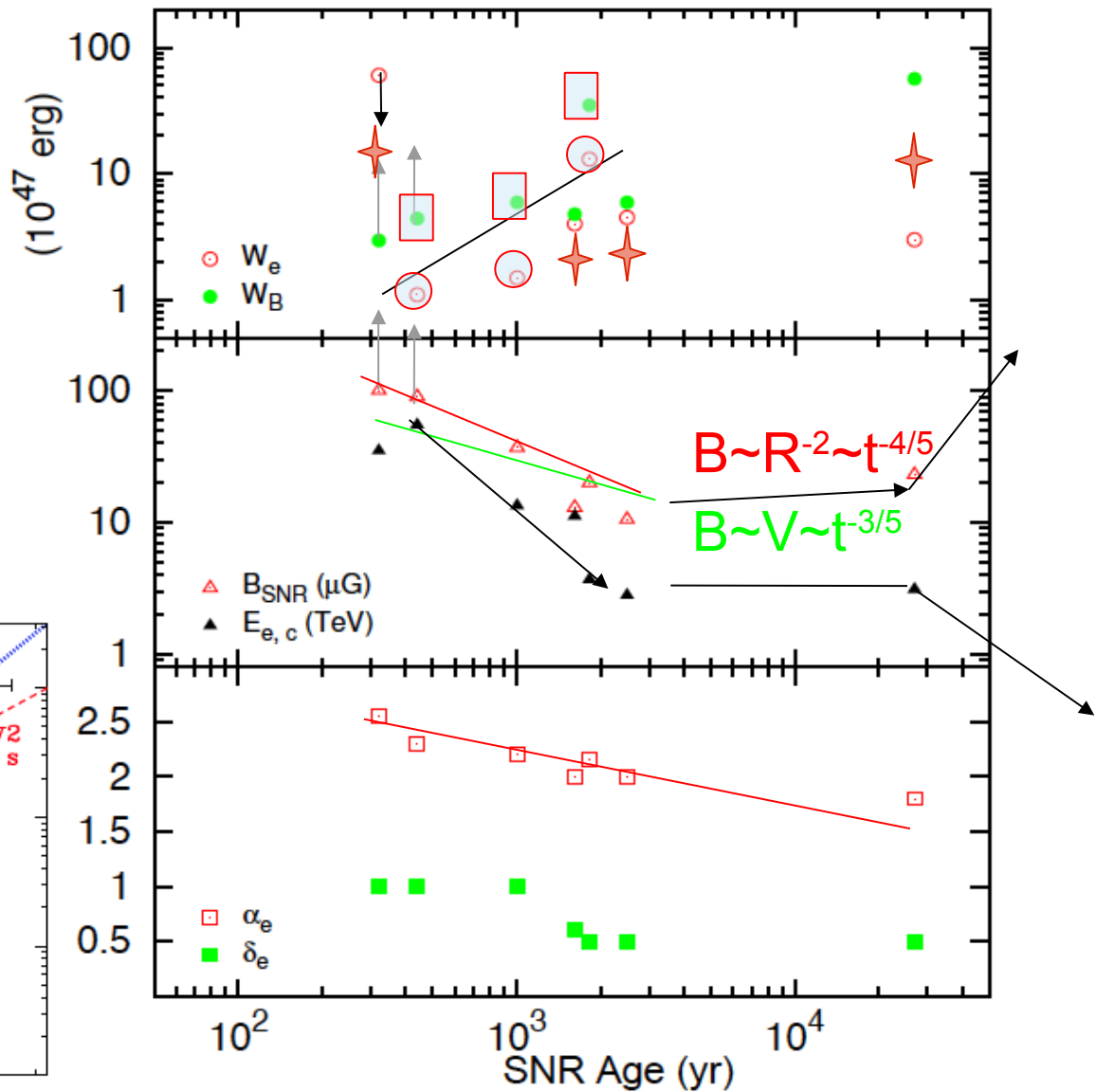
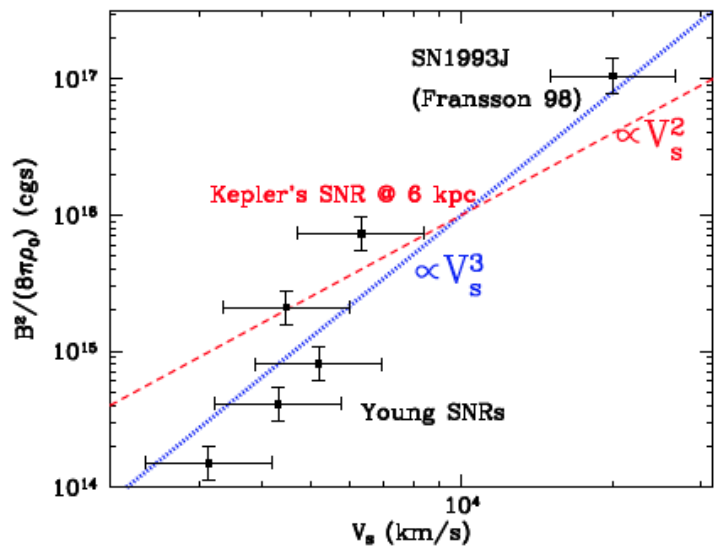
3: Evolution of Model Parameters

With a compact object at the center: Core Collapse SN

Astron Astrophys Rev (2012) 20:49
DOI 10.1007/s00159-011-0049-1

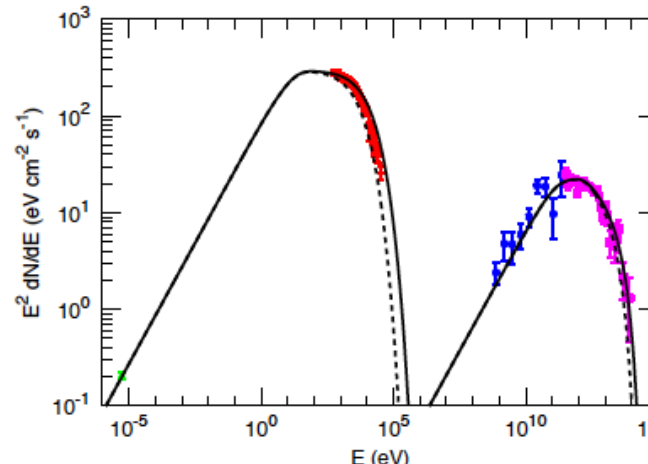
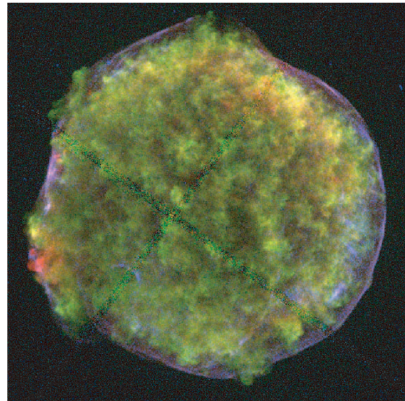
Supernova remnants: the X-ray perspective

Jacco Vink



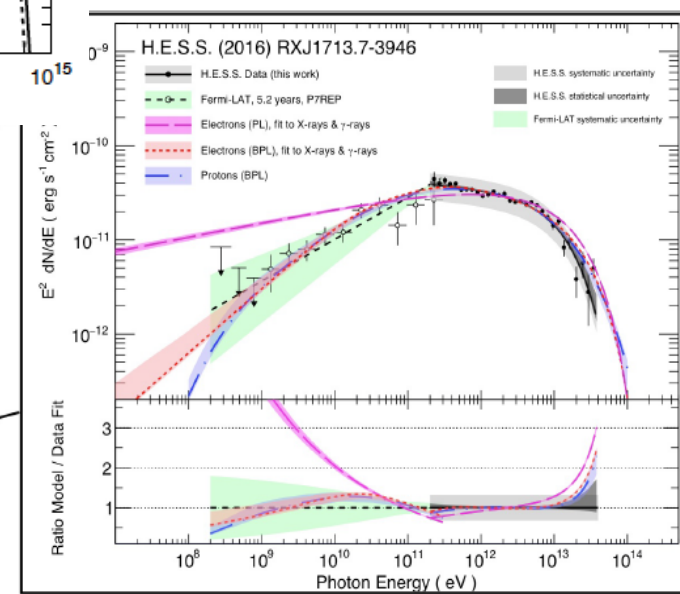
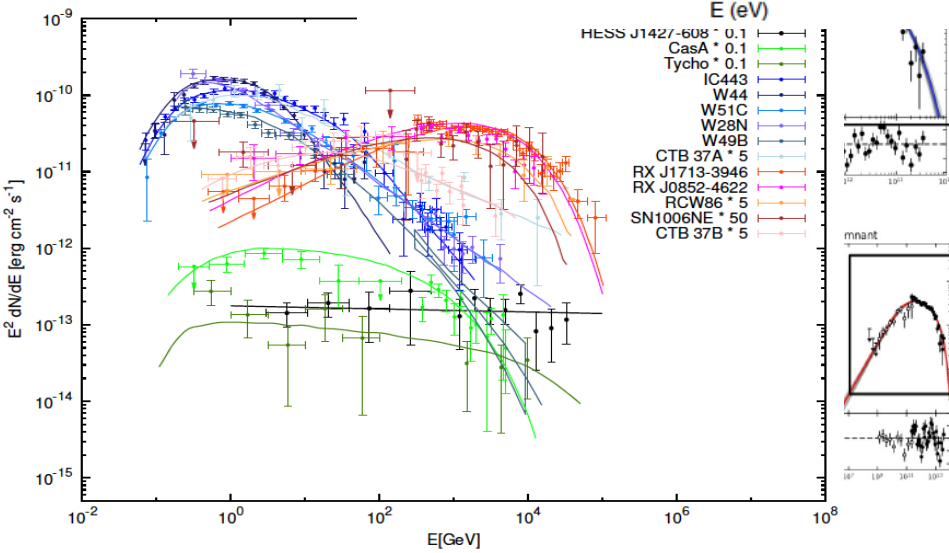
3: Future Studies

Expand the sample; Improve the spectral fit; Spatial structure of SNRs



INVERSE COMPTON EMISSION FROM A COSMIC-RAY PRECURSOR IN RX J1713.7-3946

YUTAKA OHIRA AND RYO YAMAZAKI



H.E.S.S. observations of RX J1713.7-3946 with improved angular and spectral resolution; evidence for gamma-ray emission extending beyond the X-ray emitting shell

4: Conclusions

A century after the discovery of cosmic rays (1912), recent achievements in Gamma-ray astronomy strengthen the scenario that

SNRs are important sources of Galactic cosmic rays and

The radio to gamma-ray spectra vary significantly from source to source

Environment plays an important role in determining the emission characteristics of SNRs.

4: Conclusions

By carrying out detailed modeling of multi-wavelength observations, we can study the details of the physics relevant to shocks of SNRs:

- 1) Radio spectrum hardens with time
- 2) B field decreases with time in the Sedov Phase(<2K year), *then starts to increase gradually*
- 3) When interacting with molecular clouds, B field increases dramatically and a spectral break appears.
- 4) Type Ia remnant shows continuous increase in the energy contents of electrons and magnetic field with time

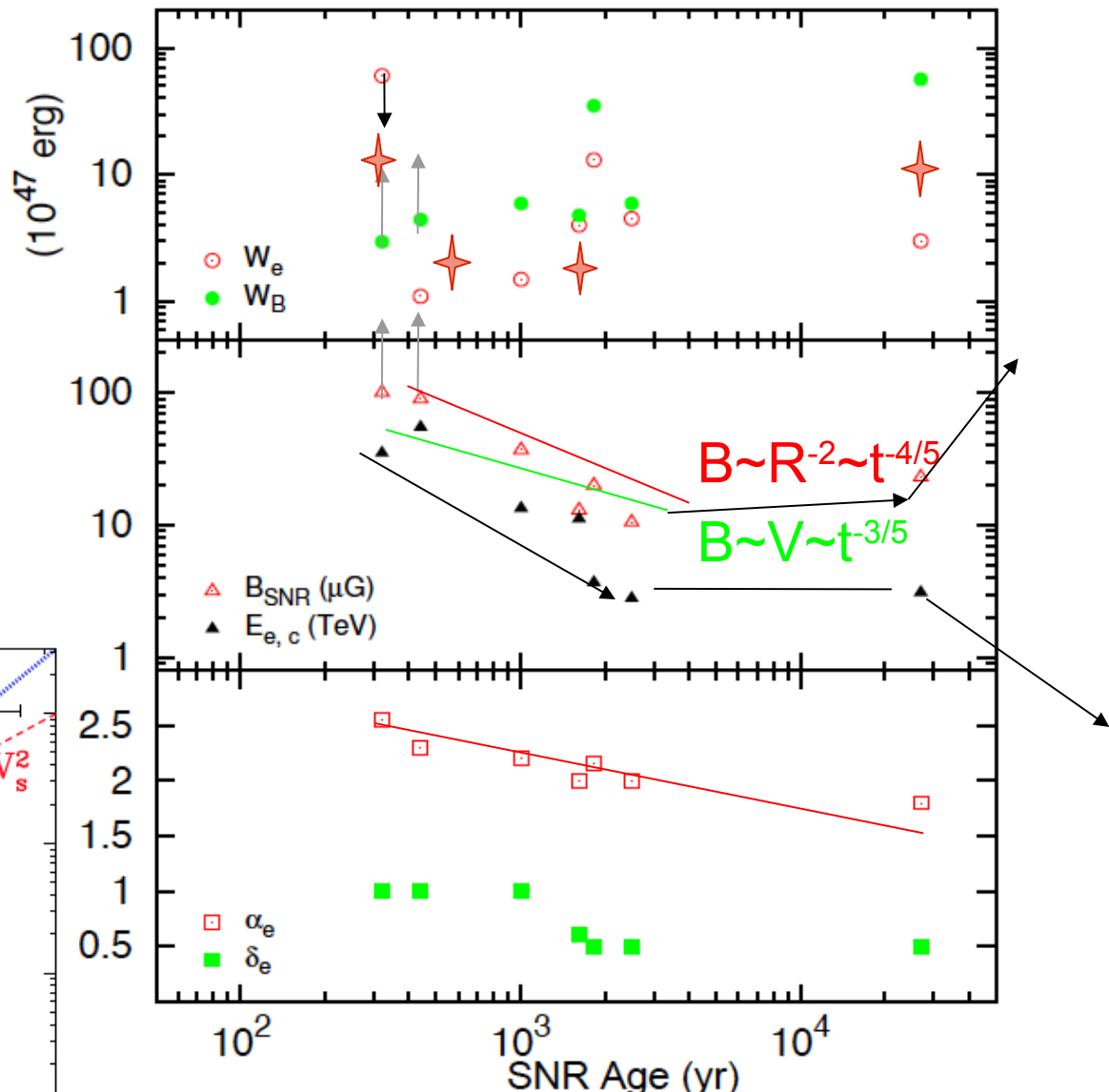
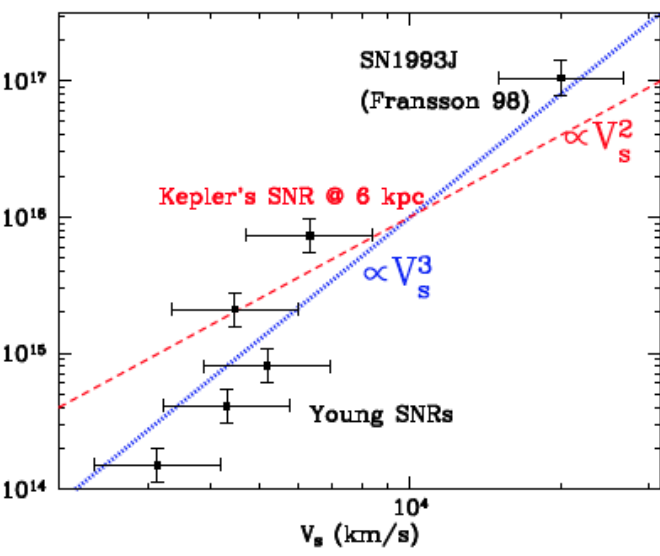
3: Evolution of Model Parameters

★ With a compact object at the center: Core Collapse SN

Astron Astrophys Rev (2012) 20:49
DOI 10.1007/s00159-011-0049-1

Supernova remnants: the X-ray perspective

Jacco Vink



2: Gamma-ray Observations of SNRs

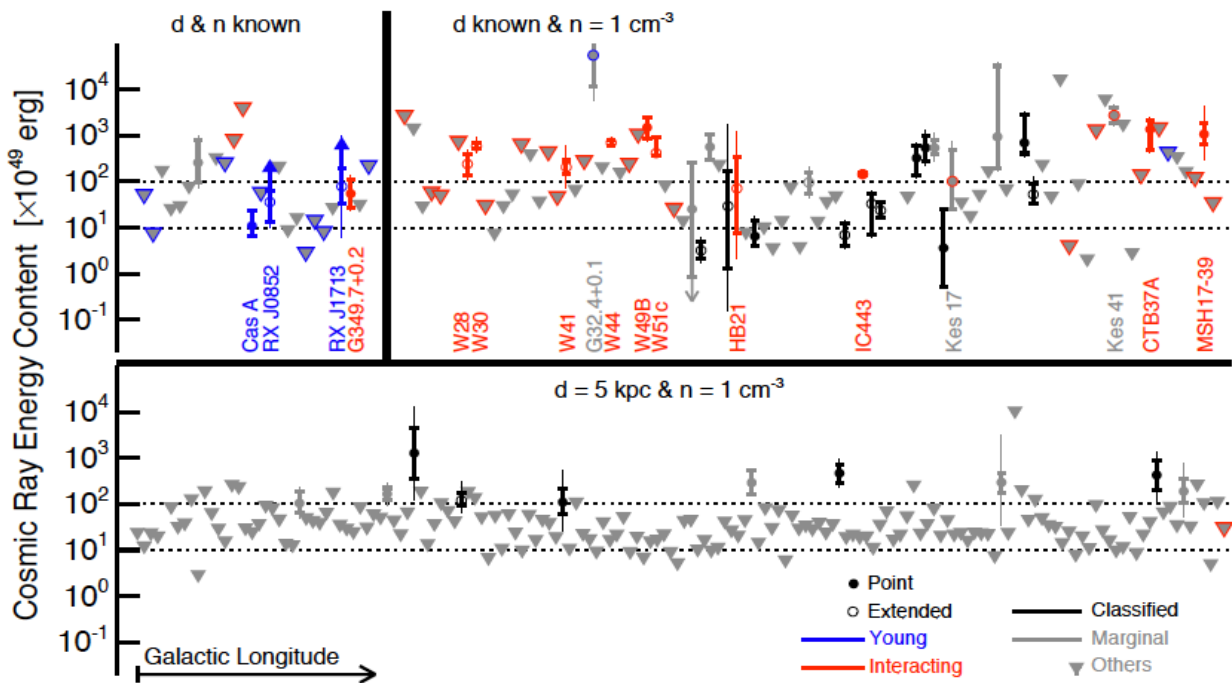
The 1st *Fermi* LAT Supernova Remnant Catalog

F. Acero², M. Ackermann³, M. Ajello⁴, L. Baldini^{5,6}, J. Ballet², G. Barbiellini^{7,8},
D. Bastieri^{9,10}, R. Bellazzini¹¹, E. Bissaldi¹², R. D. Blandford⁶, E. D. Bloom⁶,

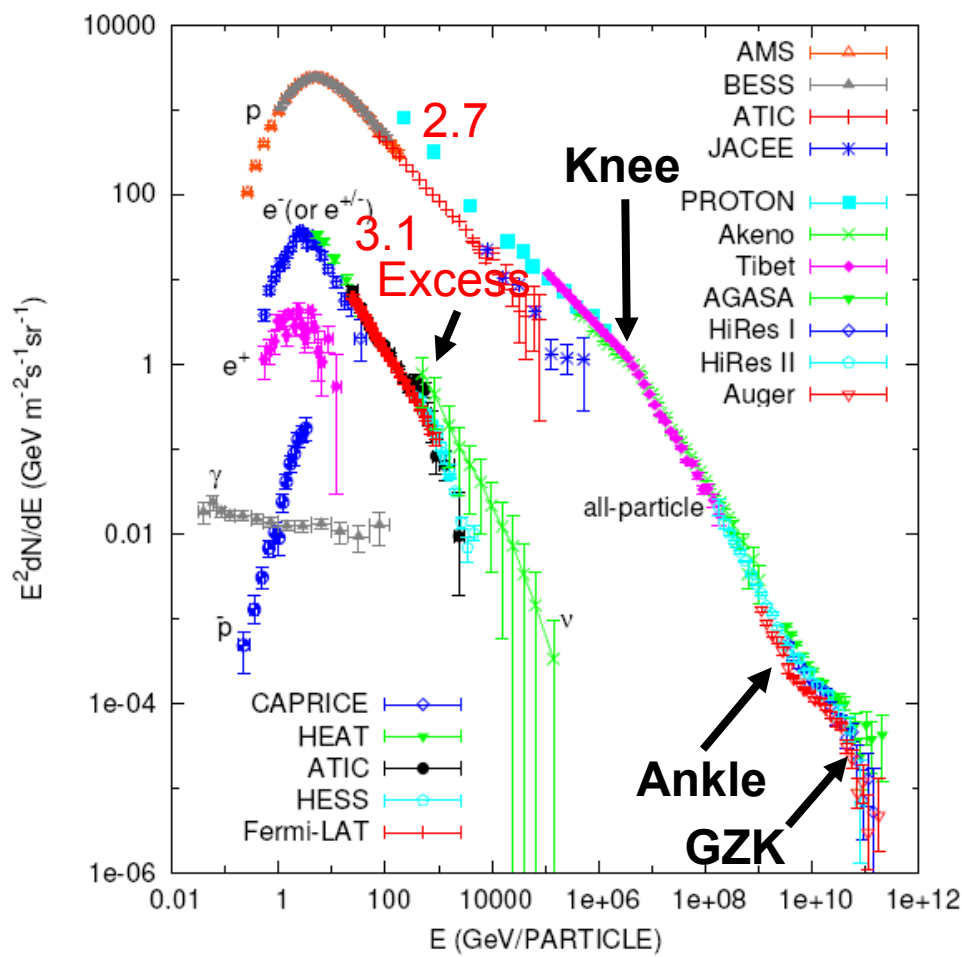
Radio SNRs: 279

Total Energy:
 $<300 \times 10^{51}$ ergs
 $=3 \times 10^{53}$ ergs
 $=1\%$ 3×10^{55} ergs

Age $<10^5$ years
 $=1\%$ 10^7 Years



2: Cosmic Rays



Dominated by Nuclei, there are also electrons, positrons and antiprotons

Age : $\sim 10^7$ Year

Energy density: $\sim 1\text{eV/cm}^3$

Power: $\sim 10^{41}\text{ erg/s}$
 $\sim 3e48\text{ erg/year}$

e/p $\sim 1\%$ at 1GeV

Leptonic Excess at $\sim 500\text{GeV}$

Spectral Knee at $\sim 1e15\text{eV}$

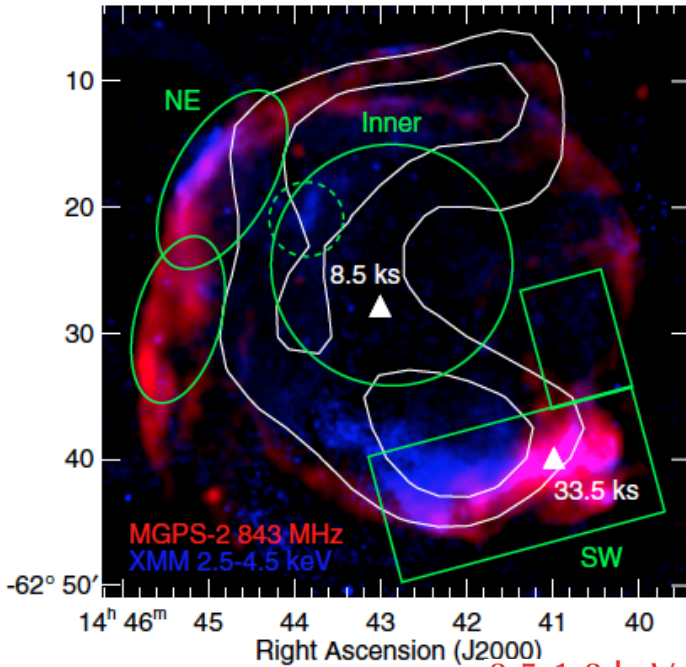
and Ankle at $\sim 1e18\text{eV}$

Maximum Energy: $3 \times 10^{20}\text{eV}$

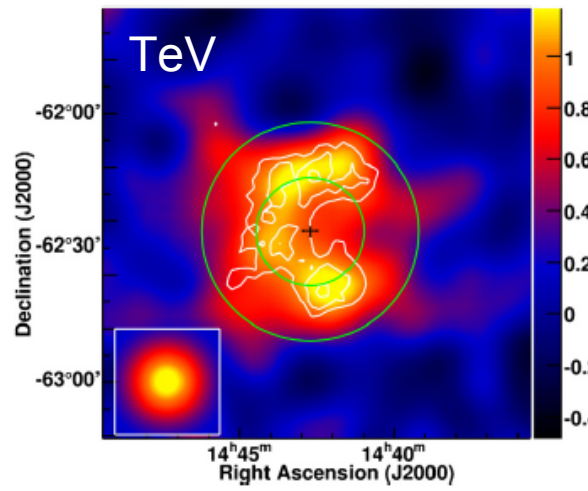
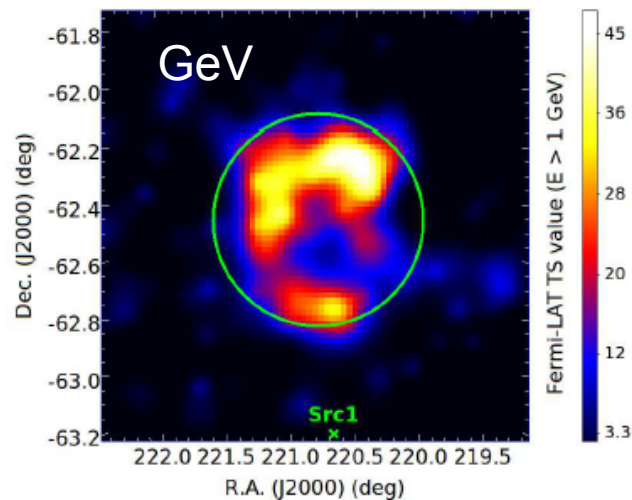
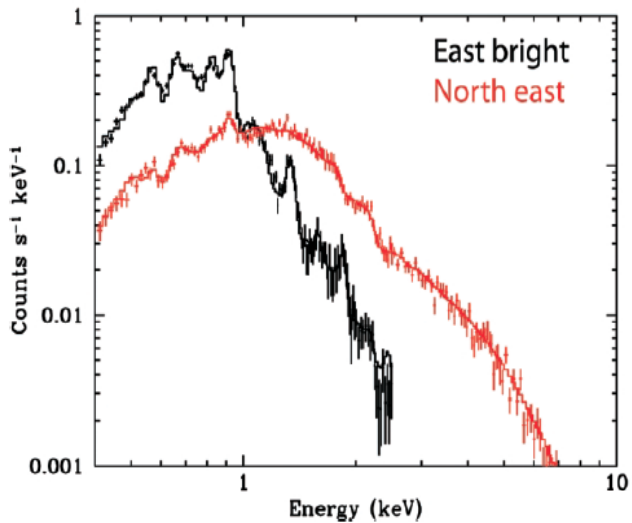
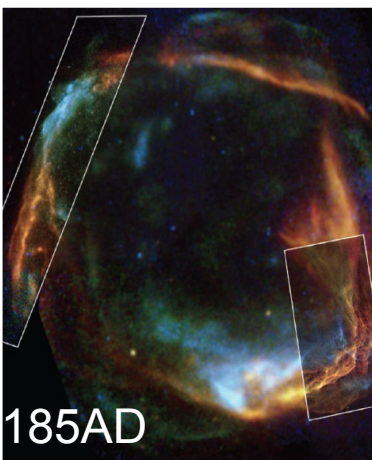
~ 50 Joule

GZK Cutoff at $\sim 1e20$ eV ²⁸

Declination (J2000)



3:RCW 86



DEEP MORPHOLOGICAL AND SPECTRAL STUDY OF THE SNR RCW 86 WITH *FERMI-LAT*

M. AJELLO², L. BALDINI^{3,4}, G. BARBIELLINI^{5,6}, D. BASTIERI^{7,8}, R. BELLAZZINI⁹, E. BISSALDI¹⁰, E. D. BLOOM⁴,

For region 1 (NW quadrant) $n_H \sim 1.5 \text{ cm}^{-3}$; for region 2 (NE quadrant) $n_H \sim 1 \text{ cm}^{-3}$; for region 3 (SE quadrant) $n_H \sim 1 \text{ cm}^{-3}$ and for region 4 (SW quadrant) $n_H \sim 1.2 \text{ cm}^{-3}$. In all cases the intrinsic error of the emitted numbers is of about 200% taking into account the

3:RCW 86

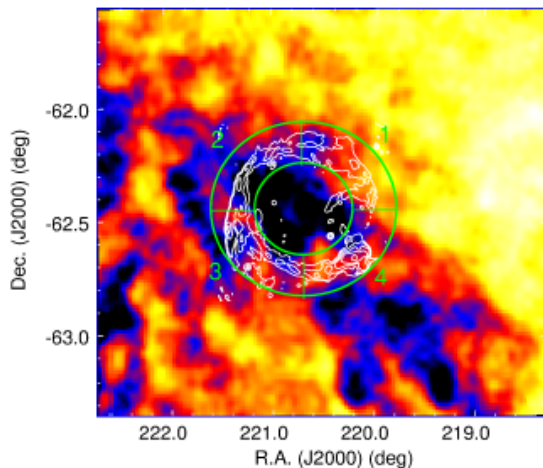
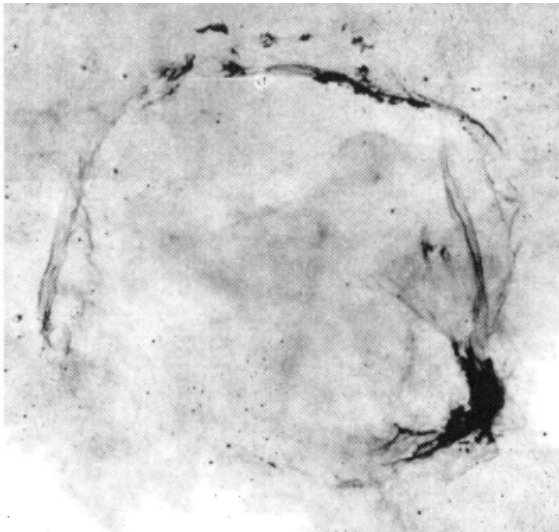
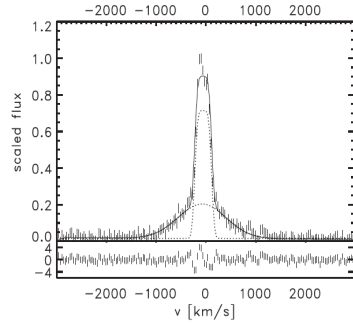
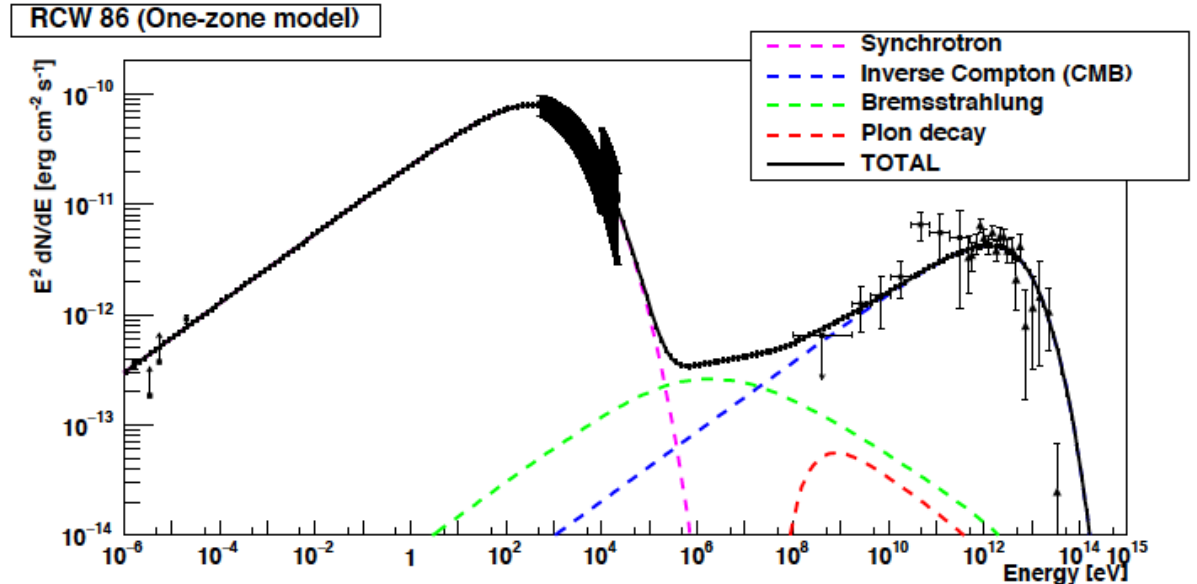


FIG. 8.— Neutral hydrogen distribution around RCW 86 at LSR radial velocity of -34 km s^{-1} . The green annulus delimits regions where the atomic density was estimated.



| Parameters | W ₁ One-zone |
|----------------------------------|----------------------------|
| Density (cm^{-3}) | 0.1 |
| B (μG) | 10.2 ± 0.5 |
| $\Gamma_{e,p}$ | 2.37 ± 0.03 |
| E_{max} (TeV) | 75 ± 5 |
| η_e (% of E_{SN}) | 3.84 ± 0.5 |
| η_p (% of E_{SN}) | 2 |
| $K_{ep} (\times 10^{-2})$ | 11.1 ± 1.5 |

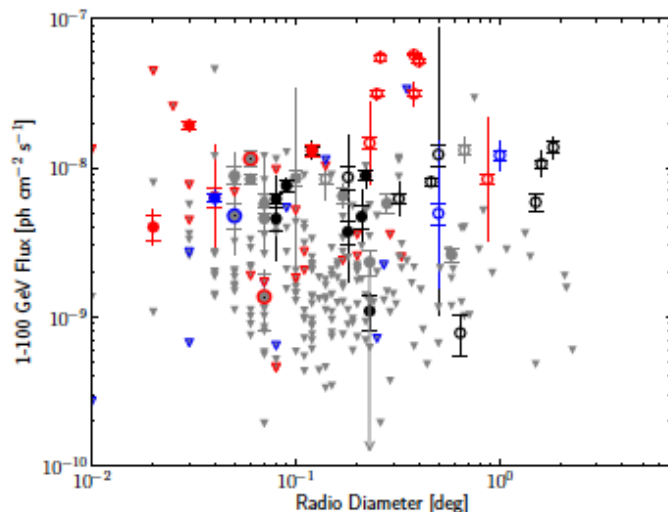
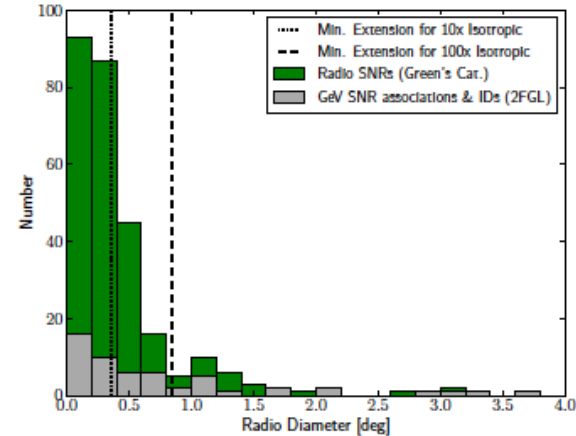
2: Observations of SNRs: Size vs Flux

Radio SNRs: 279 among them

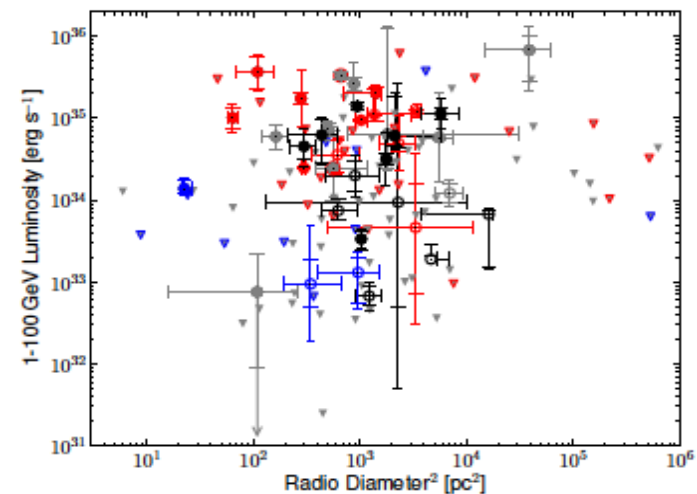
Synchrotron X-Ray: 14

GeV SNRs: 30 among them

TeV SNRs: 10



Radio Angular Diameter



Radio Area

2: Observations of SNRs:

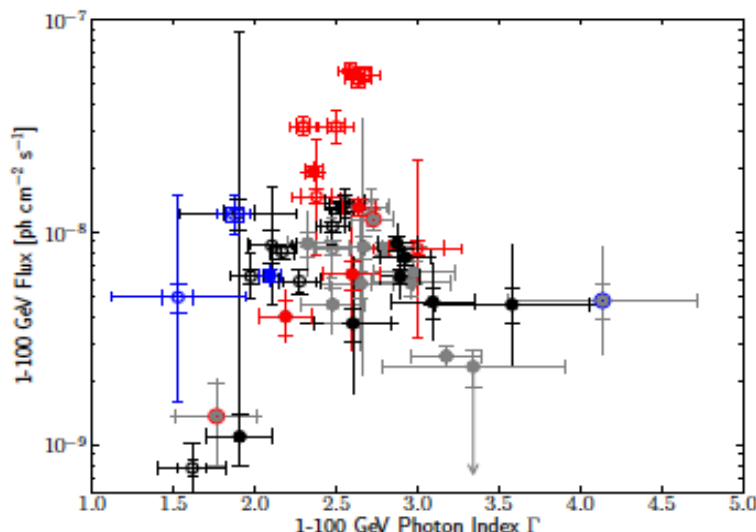
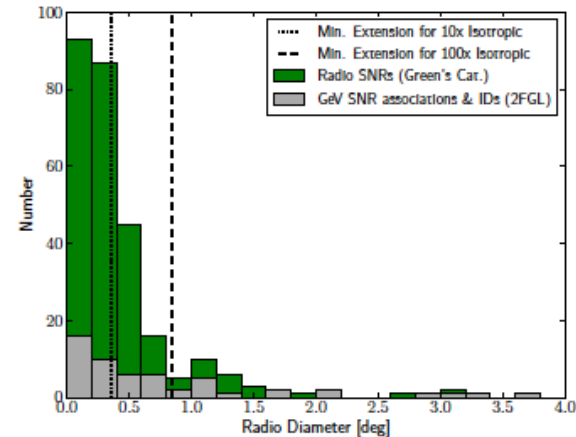
Spectral Index vs Flux

Radio SNRs: 279 among them

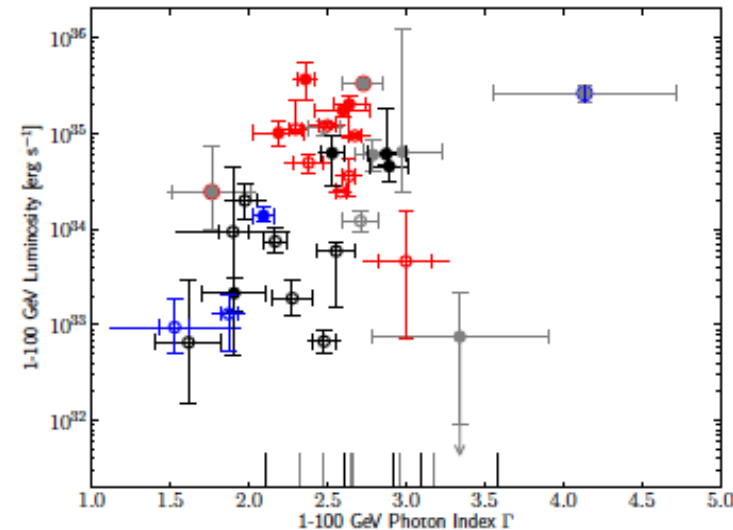
Synchrotron X-Ray: 14

GeV SNRs: 30 among them

TeV SNRs: 10



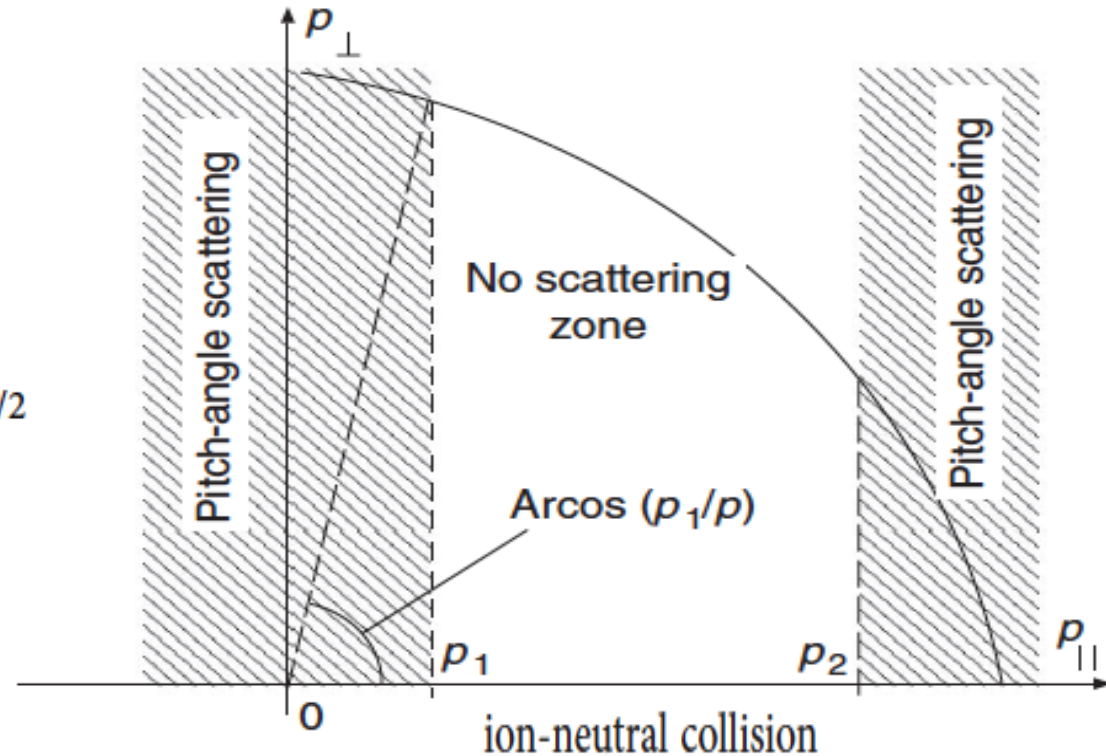
GeV Spectral Index



3: Shock interaction with partially ionised gas: the origin of broken power-laws

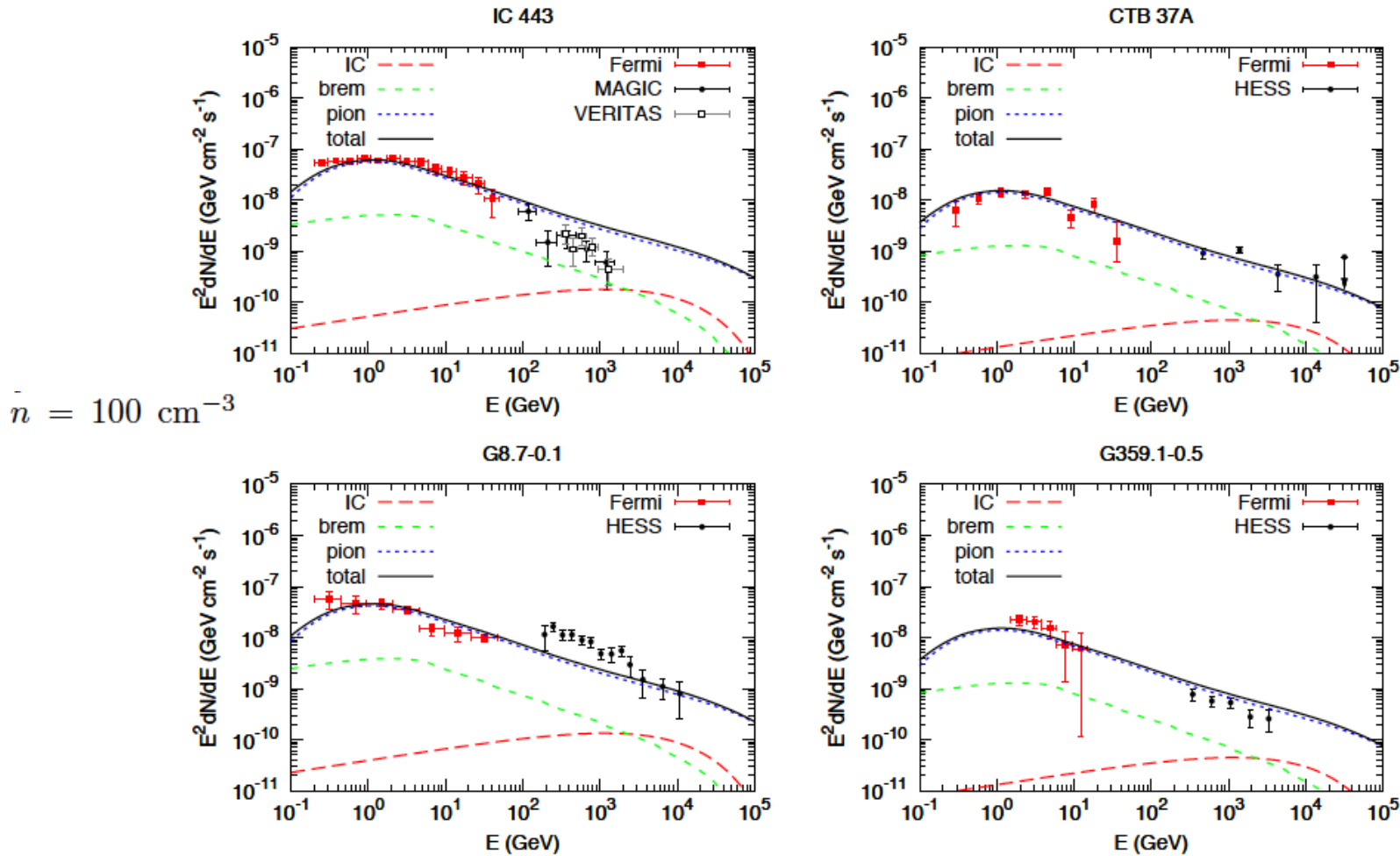
$$kp_{\parallel}/m = \pm \omega_c$$

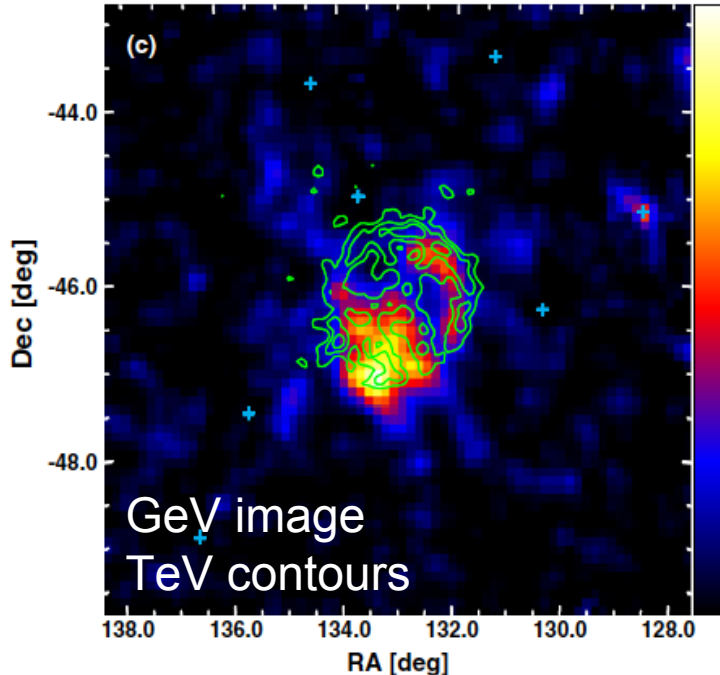
$$p_{\text{br}}/mc \simeq 10B_{\mu}^2 T_4^{-0.4} n_0^{-1} n_i^{-1/2}$$



Mechanism for spectral break in cosmic ray proton spectrum of supernova remnant W44

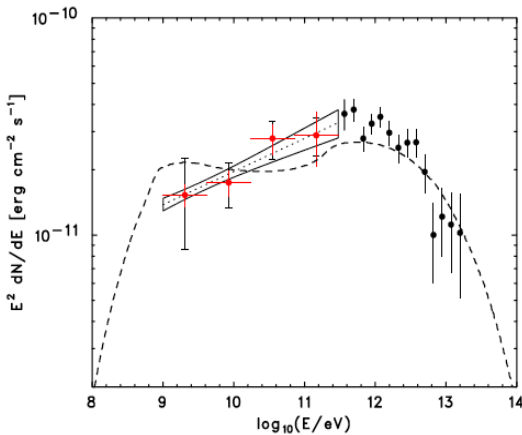
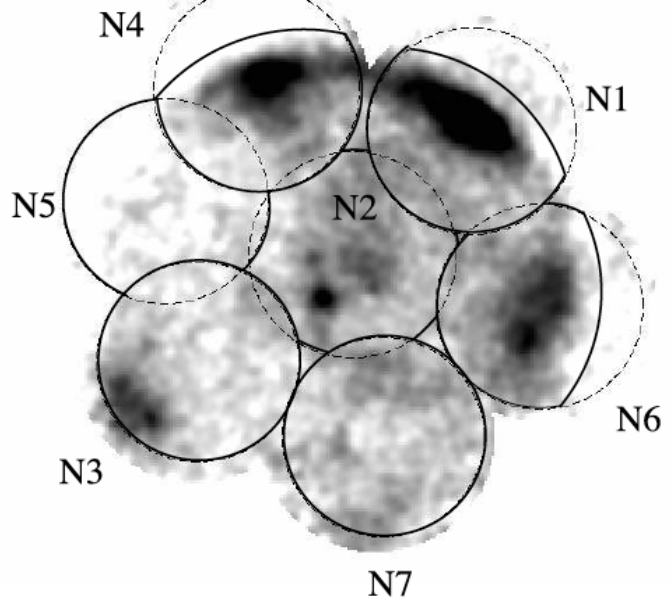
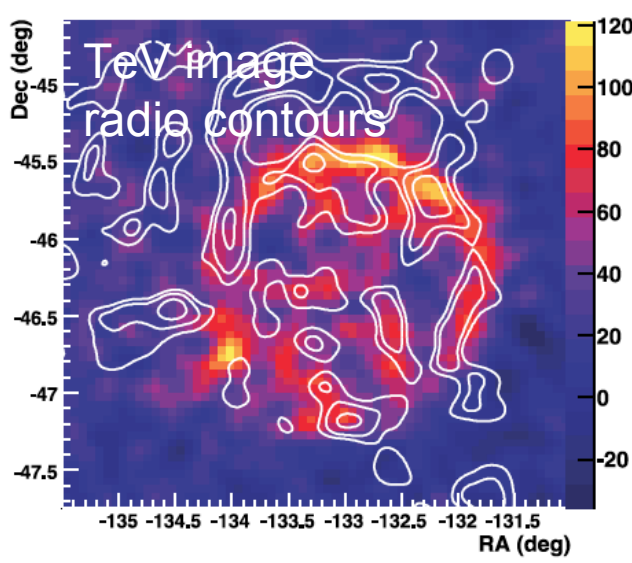
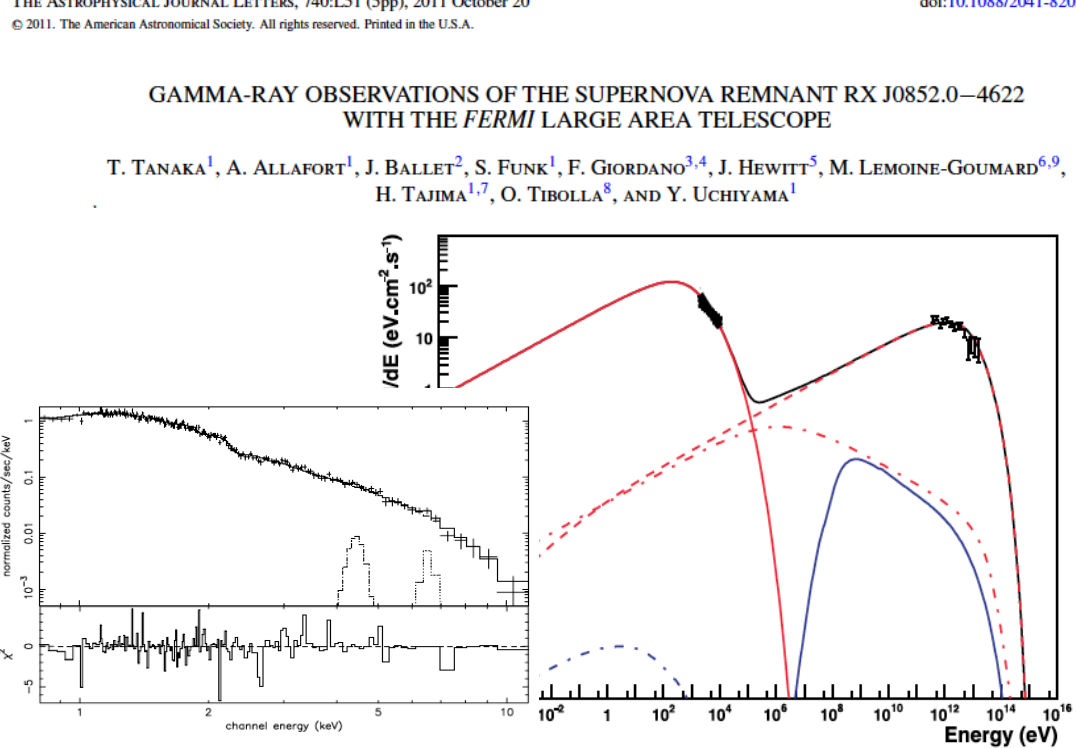
2: Modeling of Gamma-ray Spectra





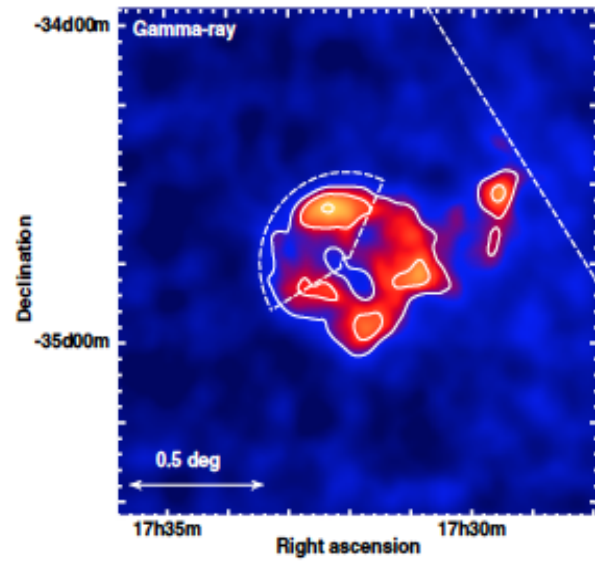
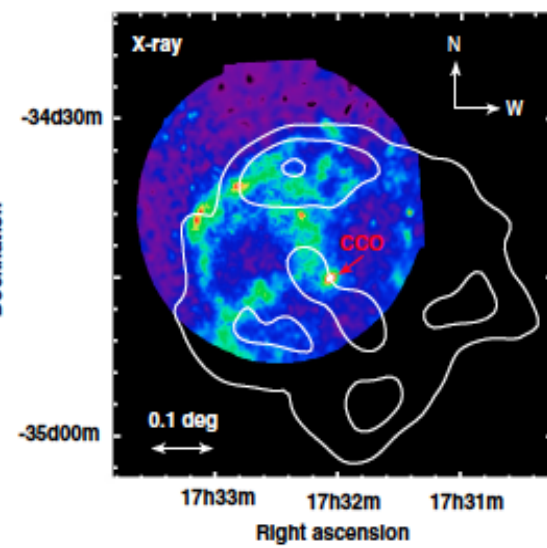
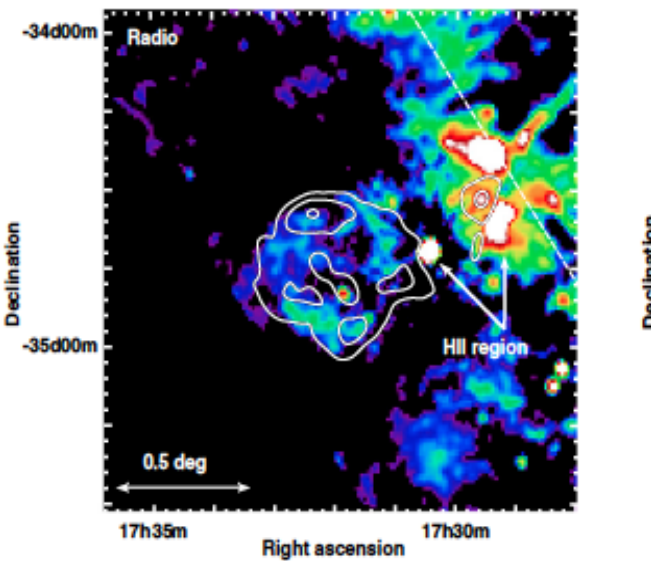
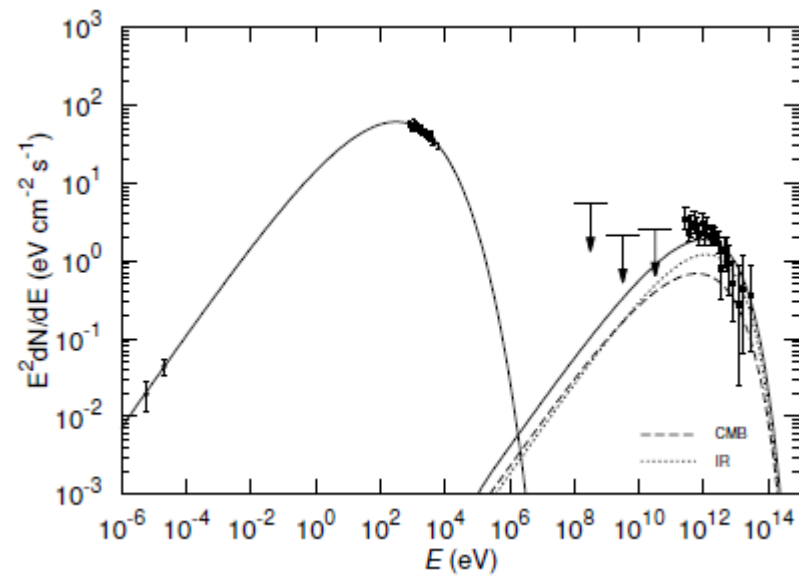
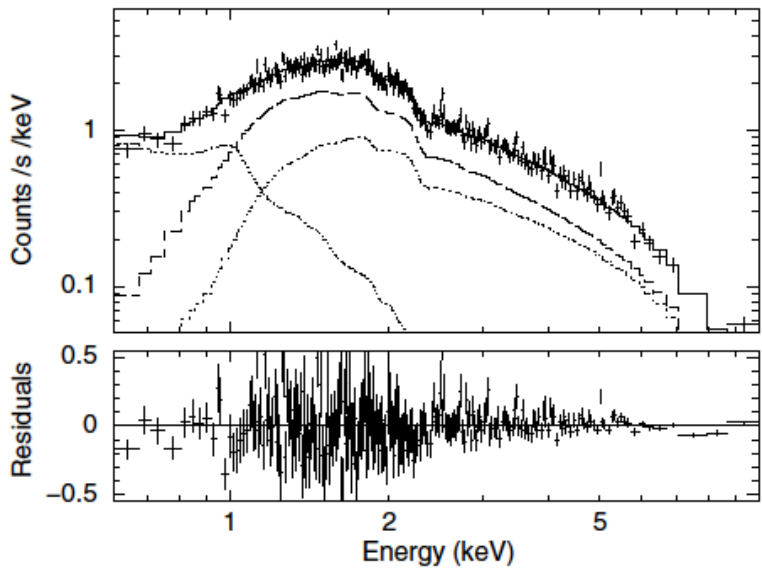
H.E.S.S. OBSERVATIONS OF THE SUPERNOVA REMNANT RX J0852.0-4622 AND SPECTRUM OF A WIDELY EXTENDED VERY HIGH ENERGY ELECTRON SOURCE

F. AHARONIAN,¹ A. G. AKHPERJANIAN,² A. R. BAZER-BACHI,³ M. BEILICKE,⁴ W. BENBOW,¹ D. BERGE,^{1,5}



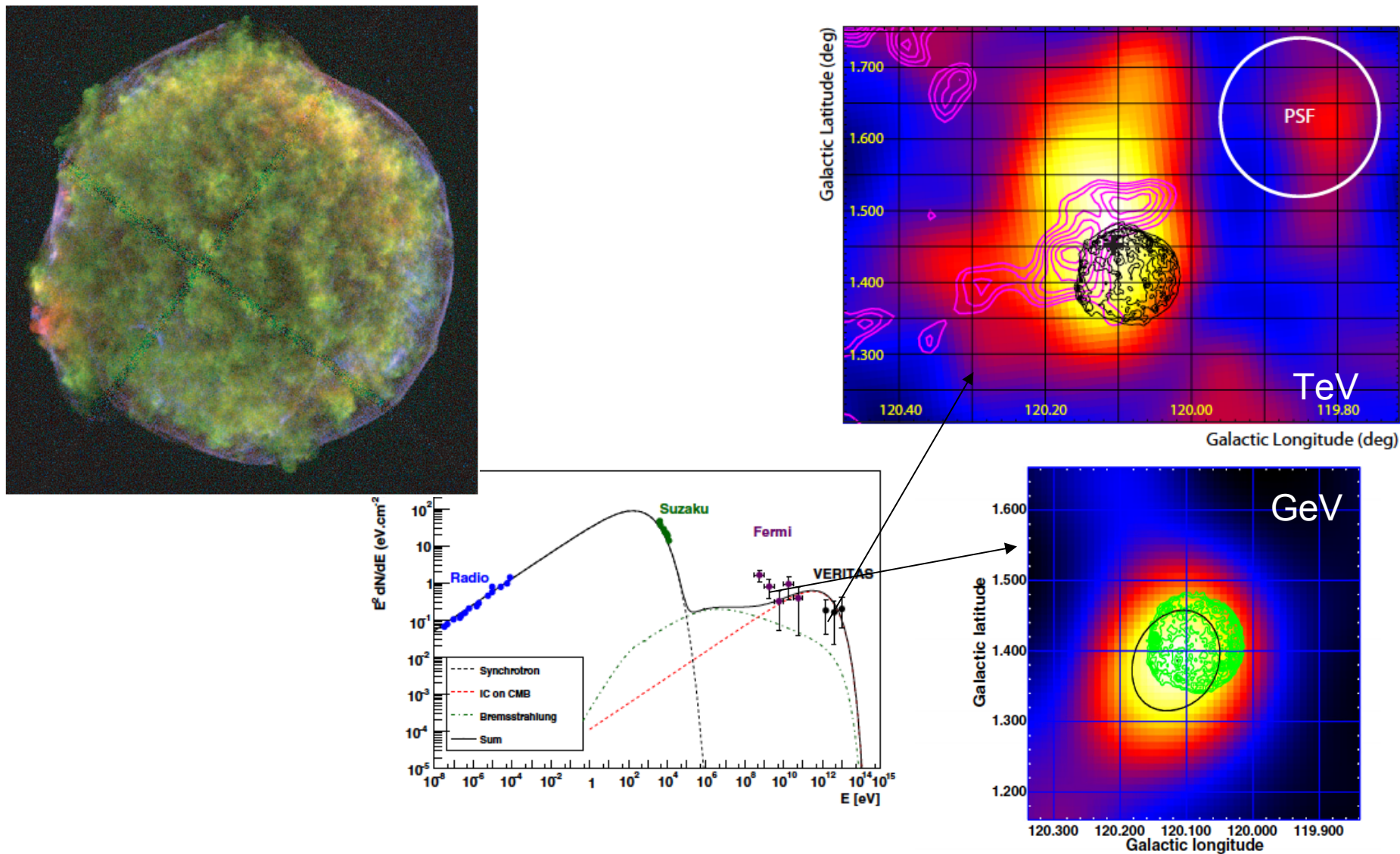
A new SNR with TeV shell-type morphology: HESS J1731-347

HESS Collaboration, A. Abramowski¹, F. Acero², F. Aharonian^{3,4,5}, A. G. Akhperjanian^{6,5}, G. Anton⁷, A. Balzer⁷,



DISCOVERY OF TEV GAMMA RAY EMISSION FROM TYCHO'S SUPERNOVA REMNANT

V. A. ACCIARI¹, E. ALIU², T. ARLEN³, T. AUNE⁴, M. BEILICKE⁵, W. BENBOW¹, S. M. BRADBURY⁶, J. H. BUCKLEY⁵,

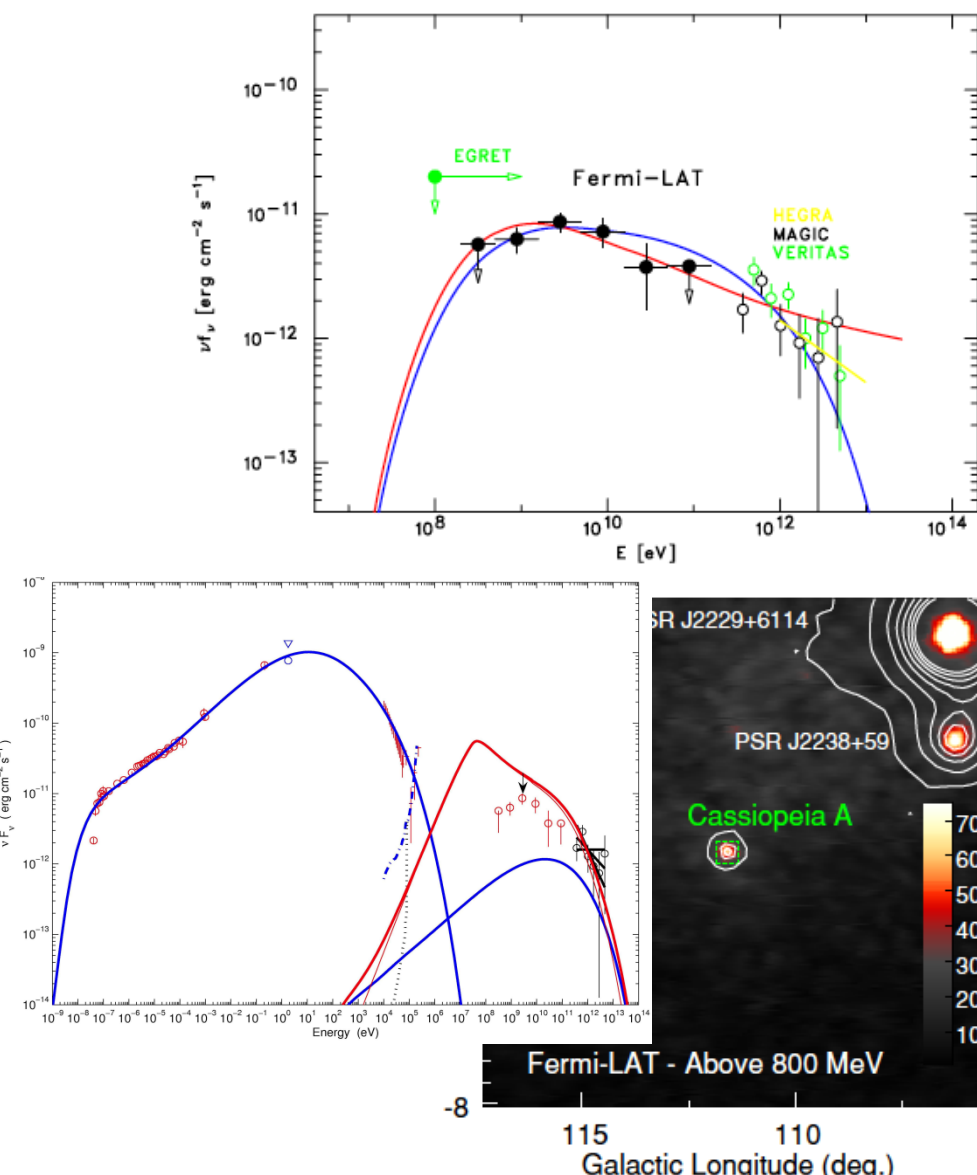
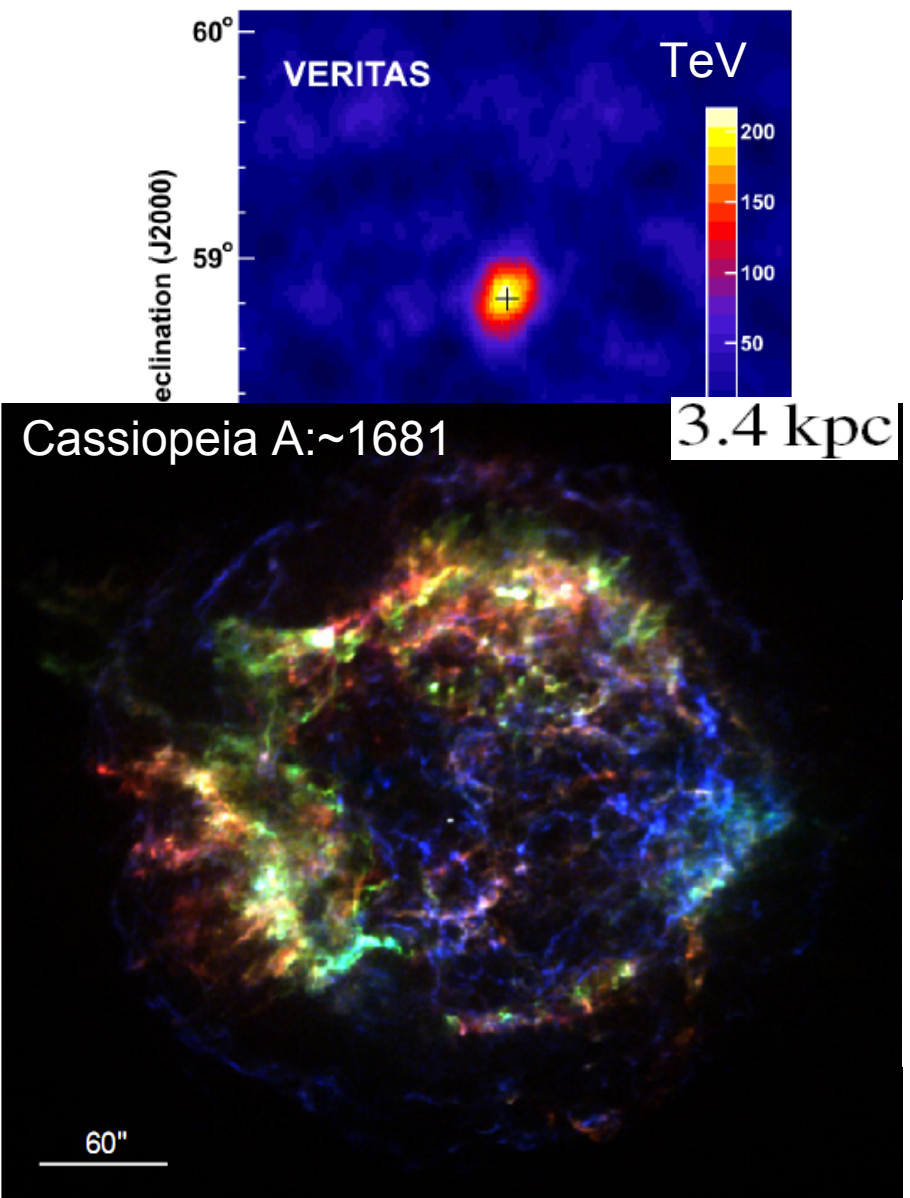


FERMI LARGE AREA TELESCOPE DETECTION OF THE YOUNG SUPERNOVA REMNANT TYCHO

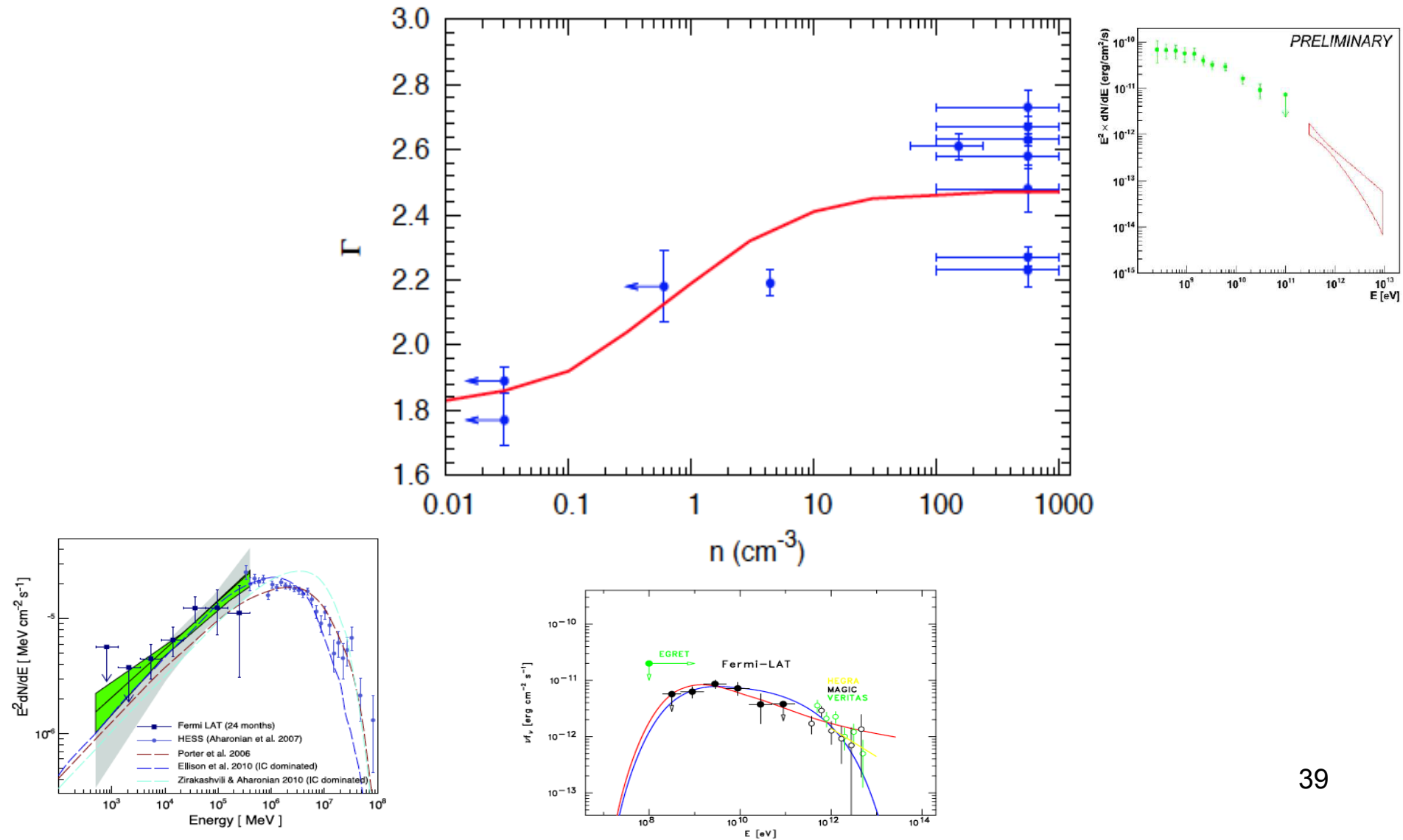
F. GIORDANO^{1,2}, M. NAUMANN-GODO³, J. BALLET³, K. BECHTOL⁴, S. FUNK⁴, J. LANDE⁴, M. N. MAZZIOTTA², S. RAINÒ²,

FERMI-LAT DISCOVERY OF GeV GAMMA-RAY EMISSION FROM THE YOUNG SUPERNOVA REMNANT CASSIOPEIA A

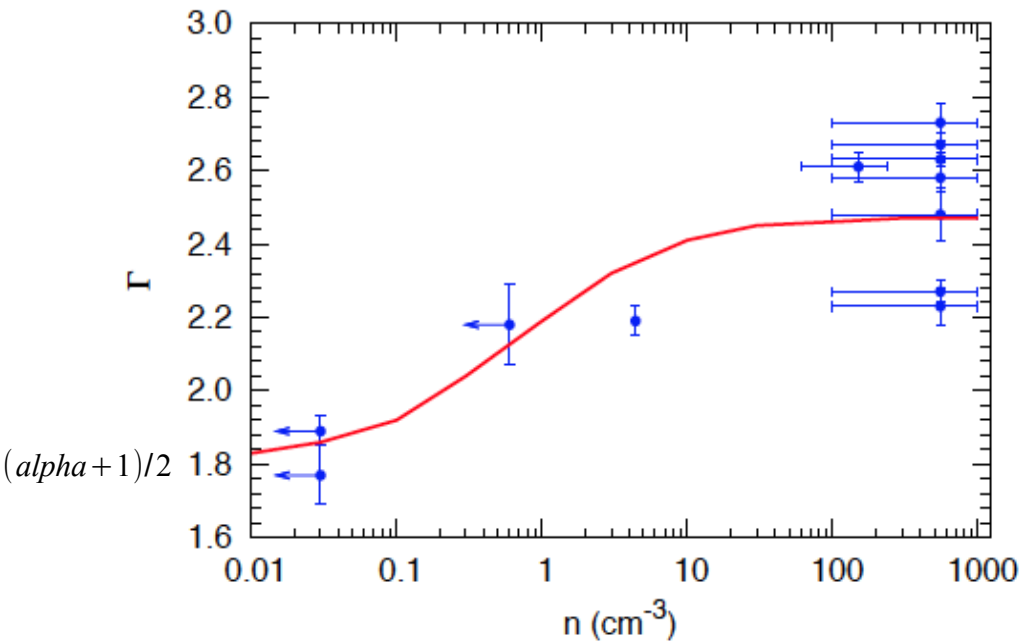
A. A. ABDO^{1,2}, M. ACKERMANN³, M. AJELLO³, A. ALLAFORT³, L. BALDINI⁴, J. BALLET⁵, G. BARBIELLINI^{6,7}, M. G. BARING⁸,



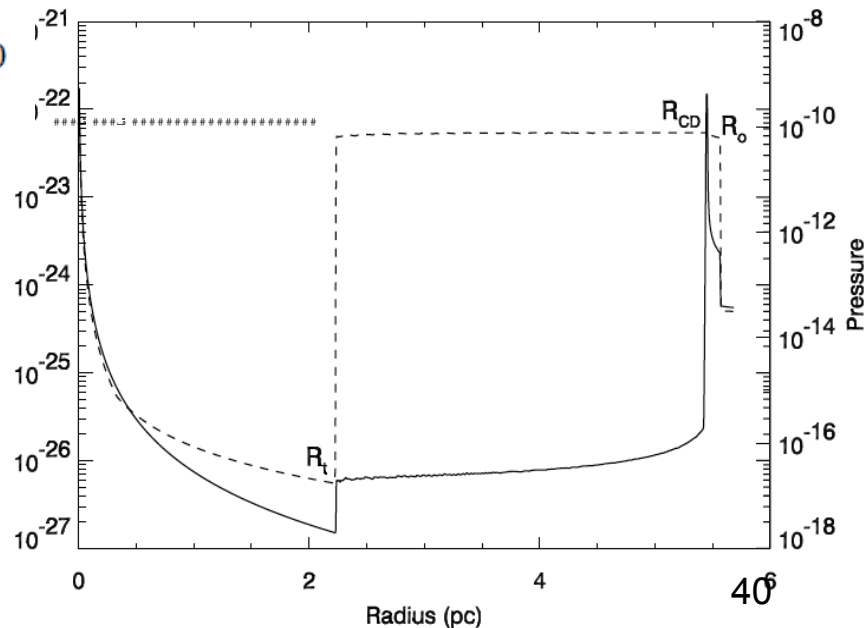
1: Summary



1: Modeling of Gamma-ray Spectra



$$\alpha = 2.52$$



THE EVOLUTION OF SUPERNOVAE IN CIRCUMSTELLAR WIND-BLOWN BUBBLES. I.
INTRODUCTION AND ONE-DIMENSIONAL CALCULATIONS

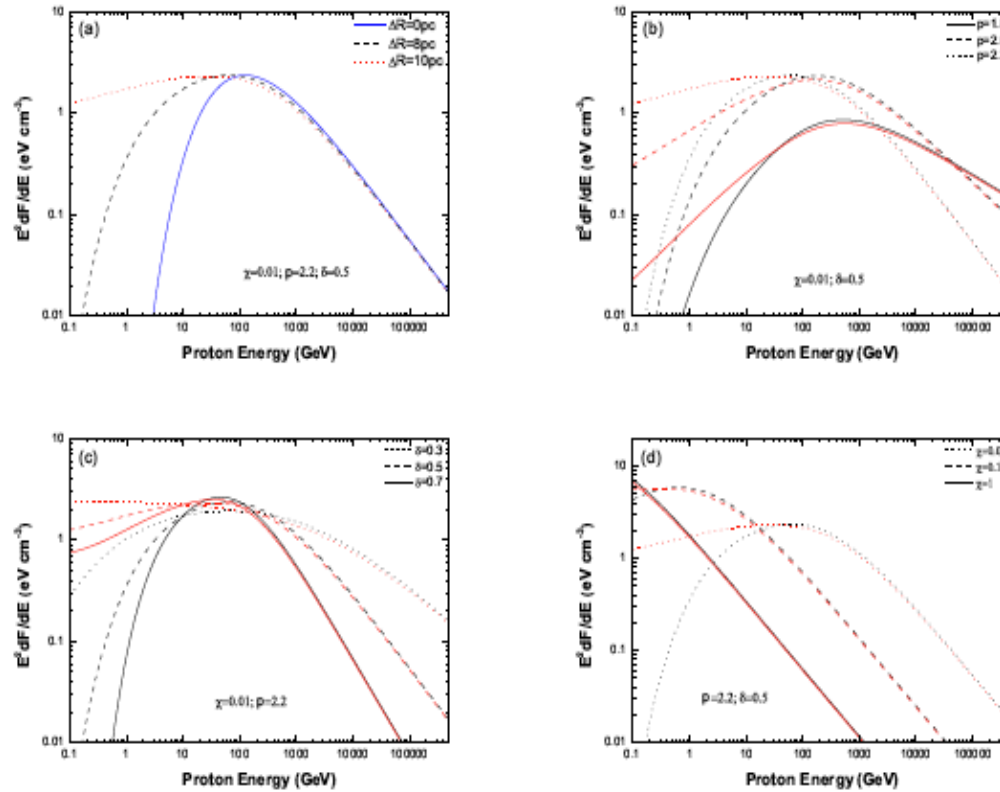
VIKRAM V. DWARKADAS

γ -rays from molecular clouds illuminated by accumulated diffusive protons. II: interacting supernova remnants

Hui Li¹ and Yang Chen^{1,2*}

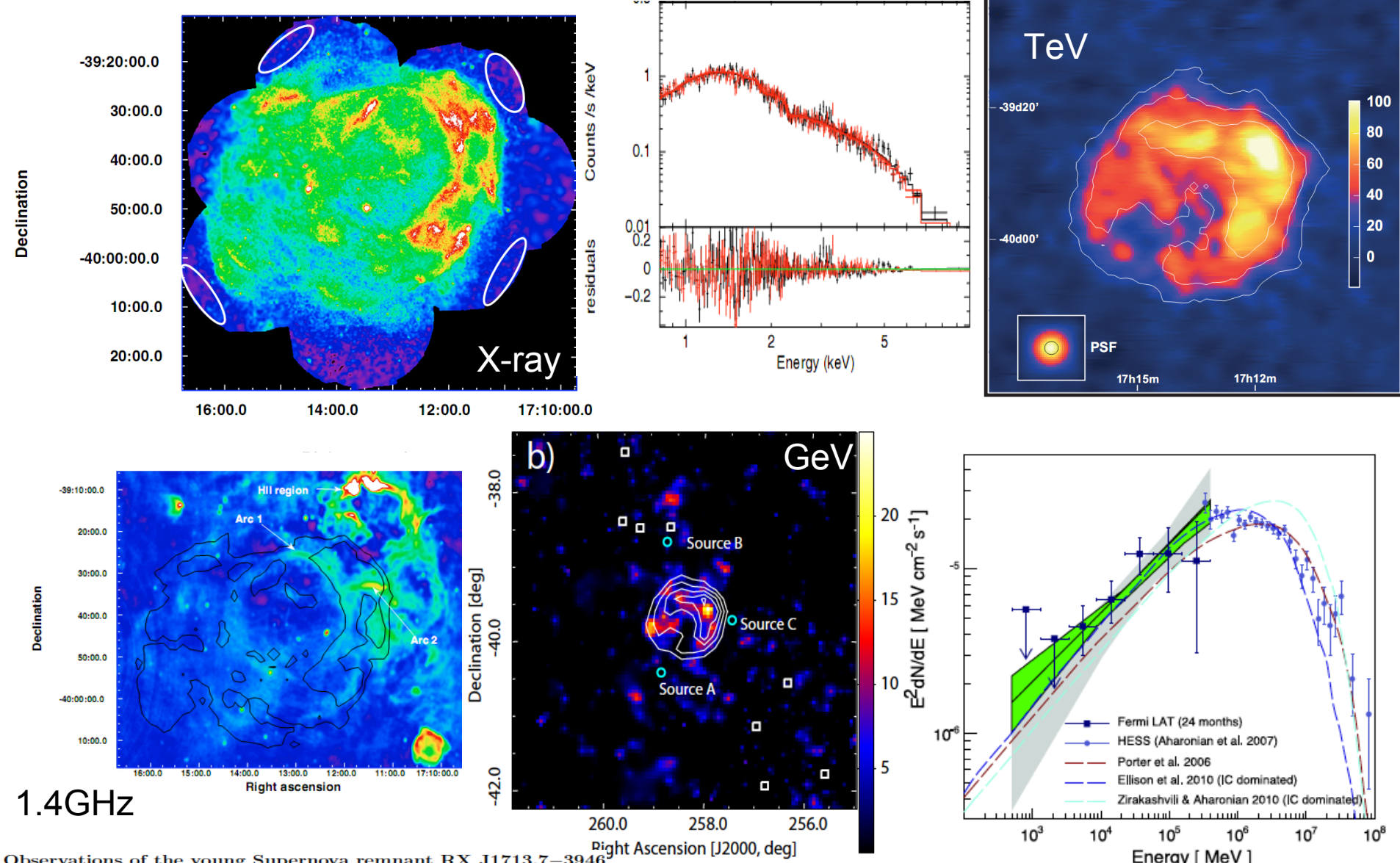
¹Department of Astronomy, Nanjing University, Nanjing 210093, P. R. China

²Key Laboratory of Modern Astronomy and Astrophysics, Nanjing University, Ministry of Education, Nanjing 210093, China



2: Shell Type TeV SNRs

F. Acero¹, J. Ballet¹, A. Decourchelle¹, M. Lemoine-Goumard^{2,3}, M. Ortega⁴, E. Giacani⁴, G. Dubner⁴, and G. Cassam-Chenaï⁵

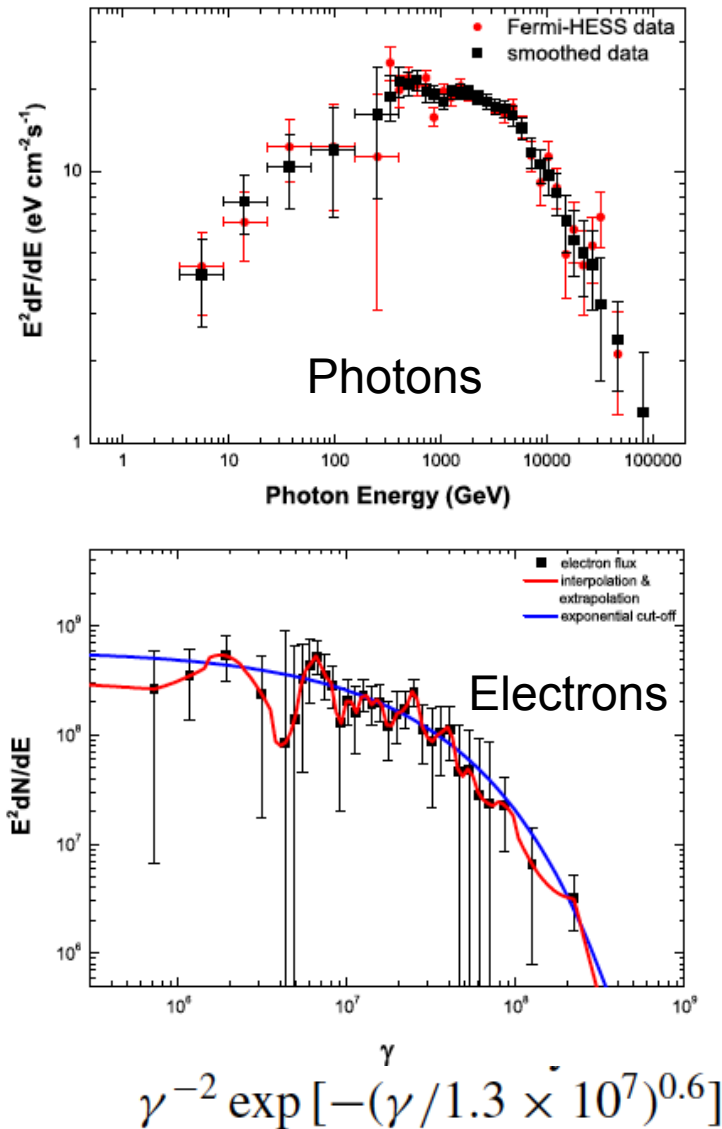


DERIVATION OF THE ELECTRON DISTRIBUTION IN SUPERNOVA REMNANT RX J1713.7–3946 VIA A SPECTRAL INVERSION METHOD

HUI LI¹, SIMING LIU², AND YANG CHEN^{1,3}

¹ Department of Astronomy, Nanjing University, Nanjing 210093, China

² Key Laboratory of Dark Matter and Space Astronomy, Purple Mountain Observatory, Chinese Academy of Sciences, Nanjing 210008, China



$$P(k) = ck \int d\gamma N(\gamma) \int d\epsilon n_{\text{ph}}(\epsilon) \sigma_{\text{IC}}(k, \epsilon; \gamma),$$

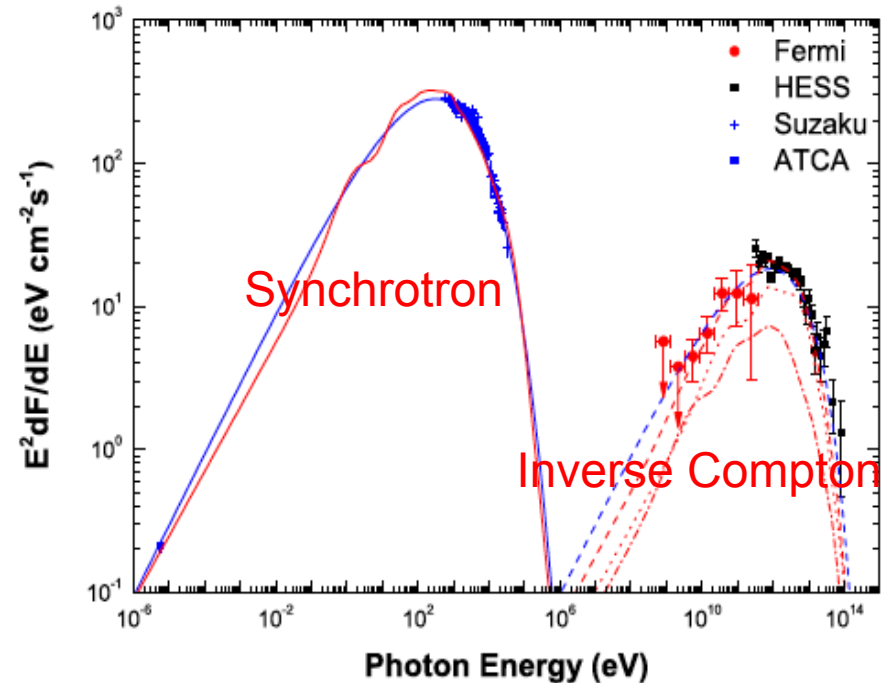
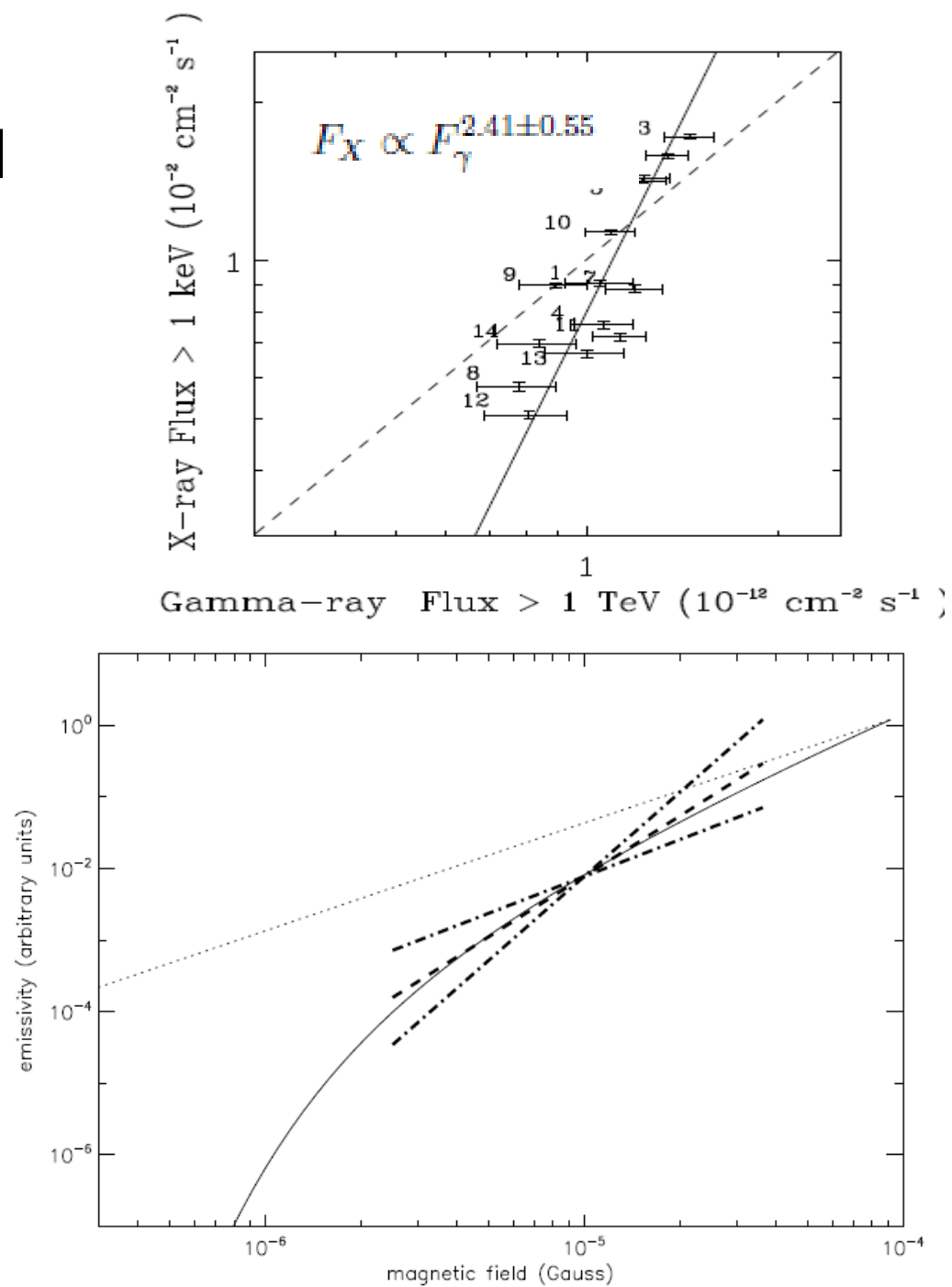
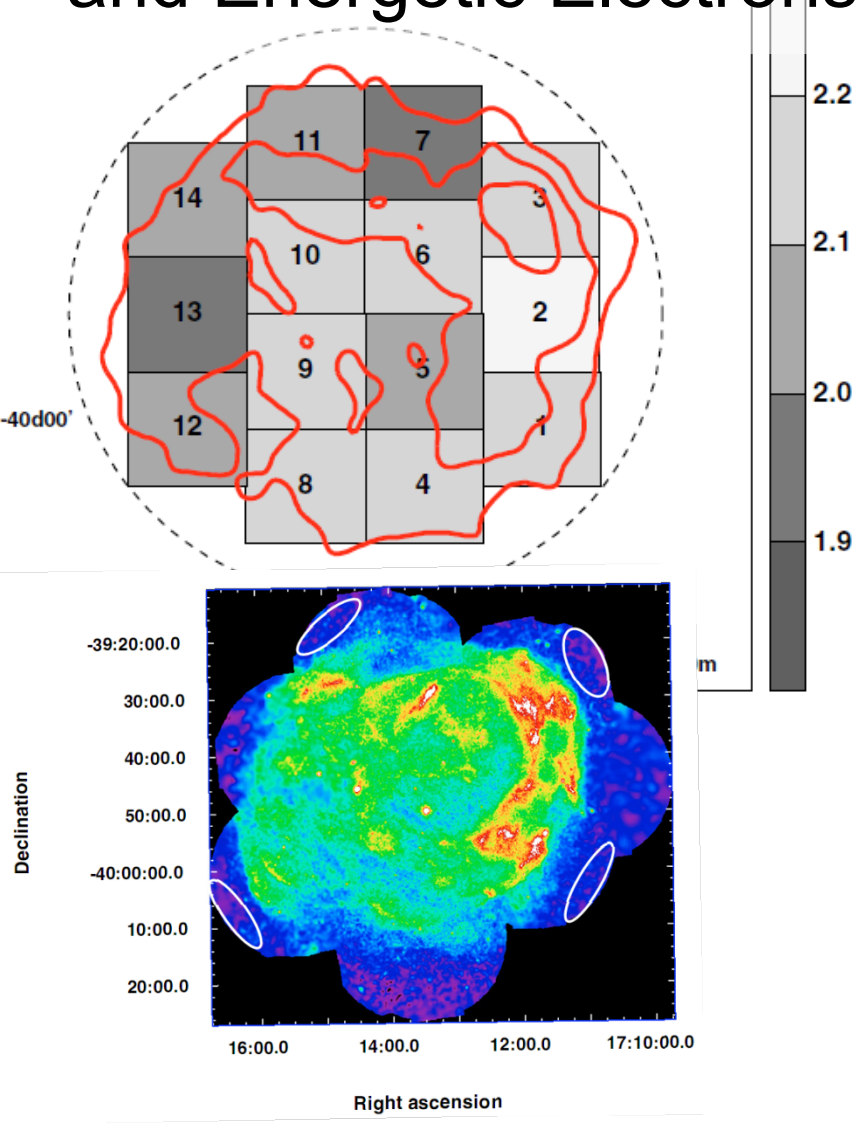
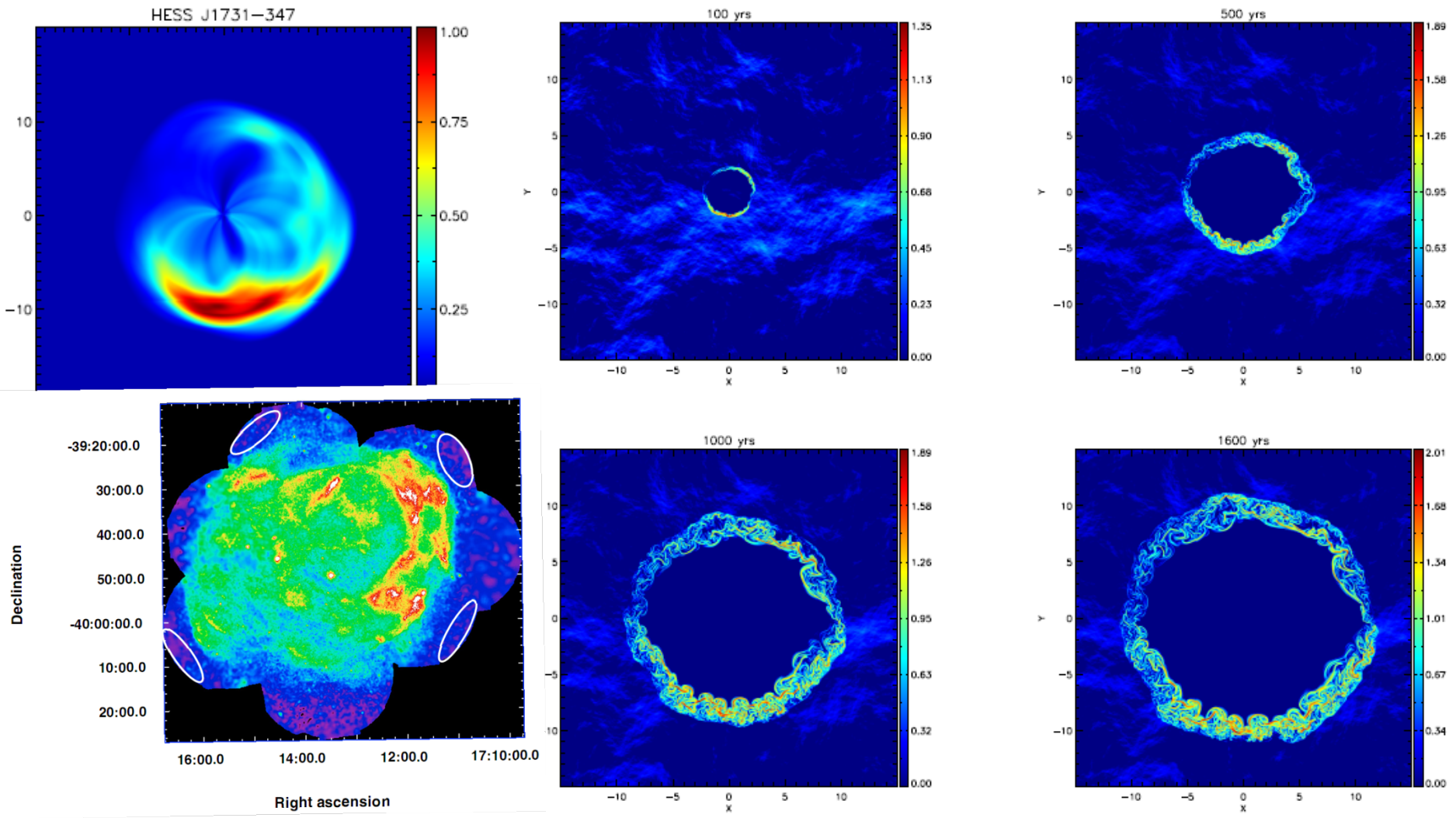


Figure 2. Comparison of the observed radio (Acero et al. 2009), X-ray (Tanaka et al. 2008), and γ -ray fluxes with the synchrotron (solid) and IC (dashed) spectra of the derived electron distributions using our inversion method. The blue lines are for the analytical distribution, whose parameters are described in Section 3. The red lines are the inter- and extrapolated electron distribution, where the dotted and dot-dashed lines are for the IC of IR and CMB photons, respectively.

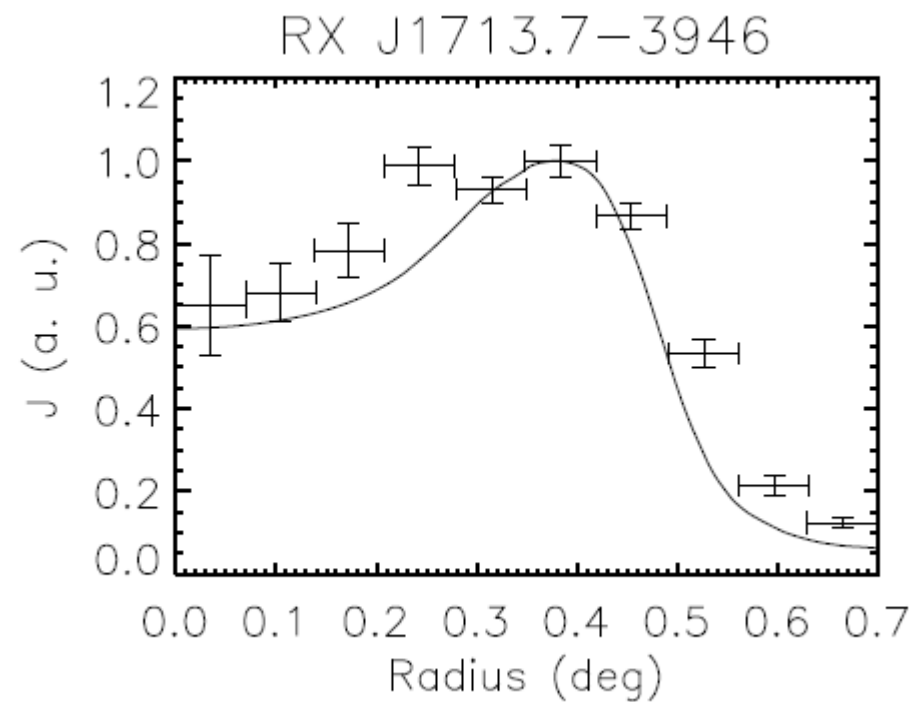
2: Energy Partition between Magnetic Field and Energetic Electrons



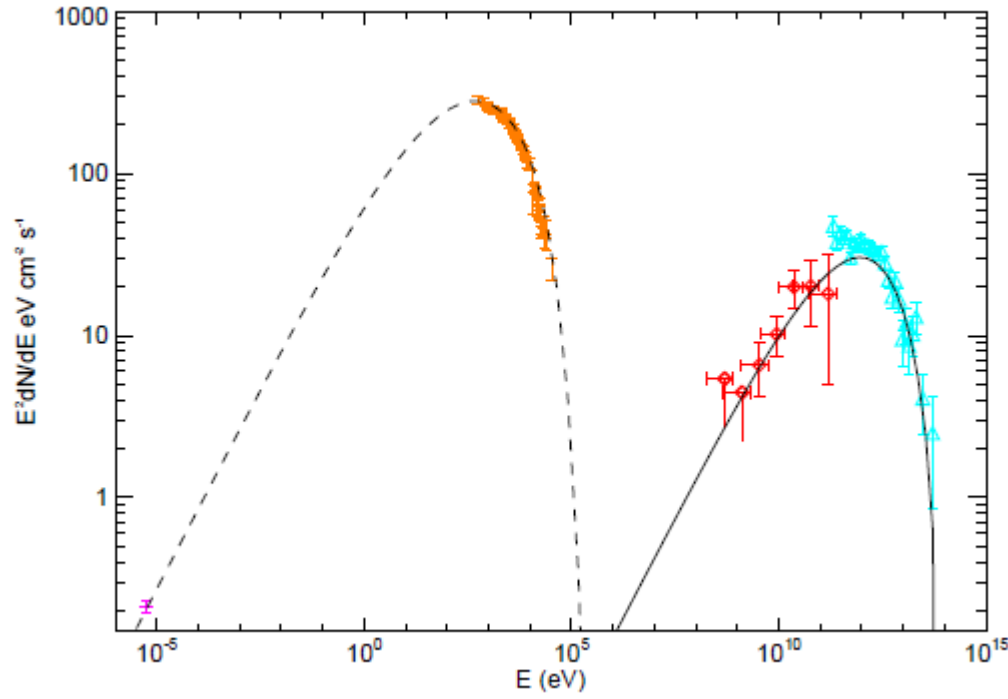
1: Energy Partition between Magnetic Field and Energetic Electrons



1 Radial Brightness Profiles

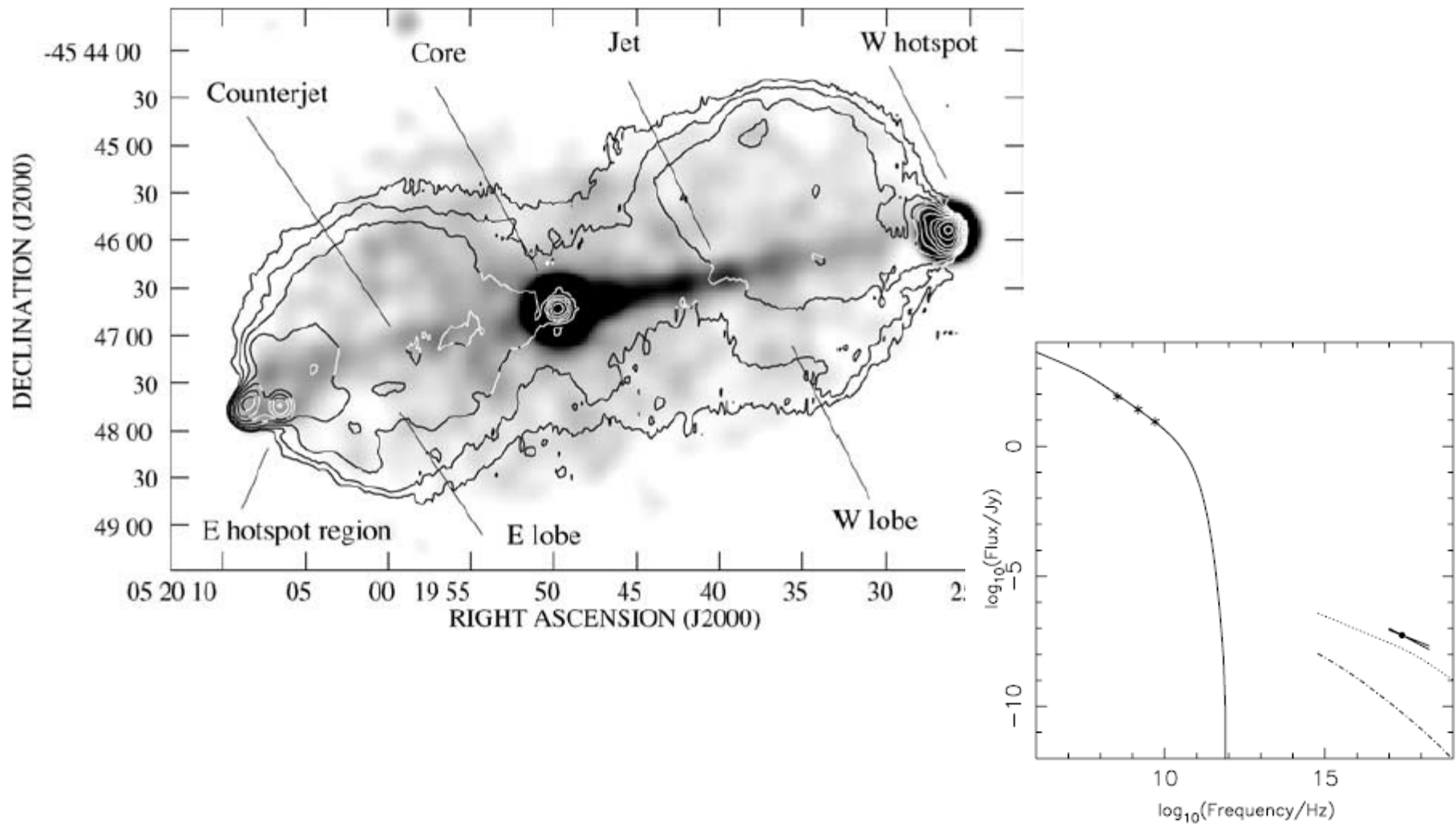


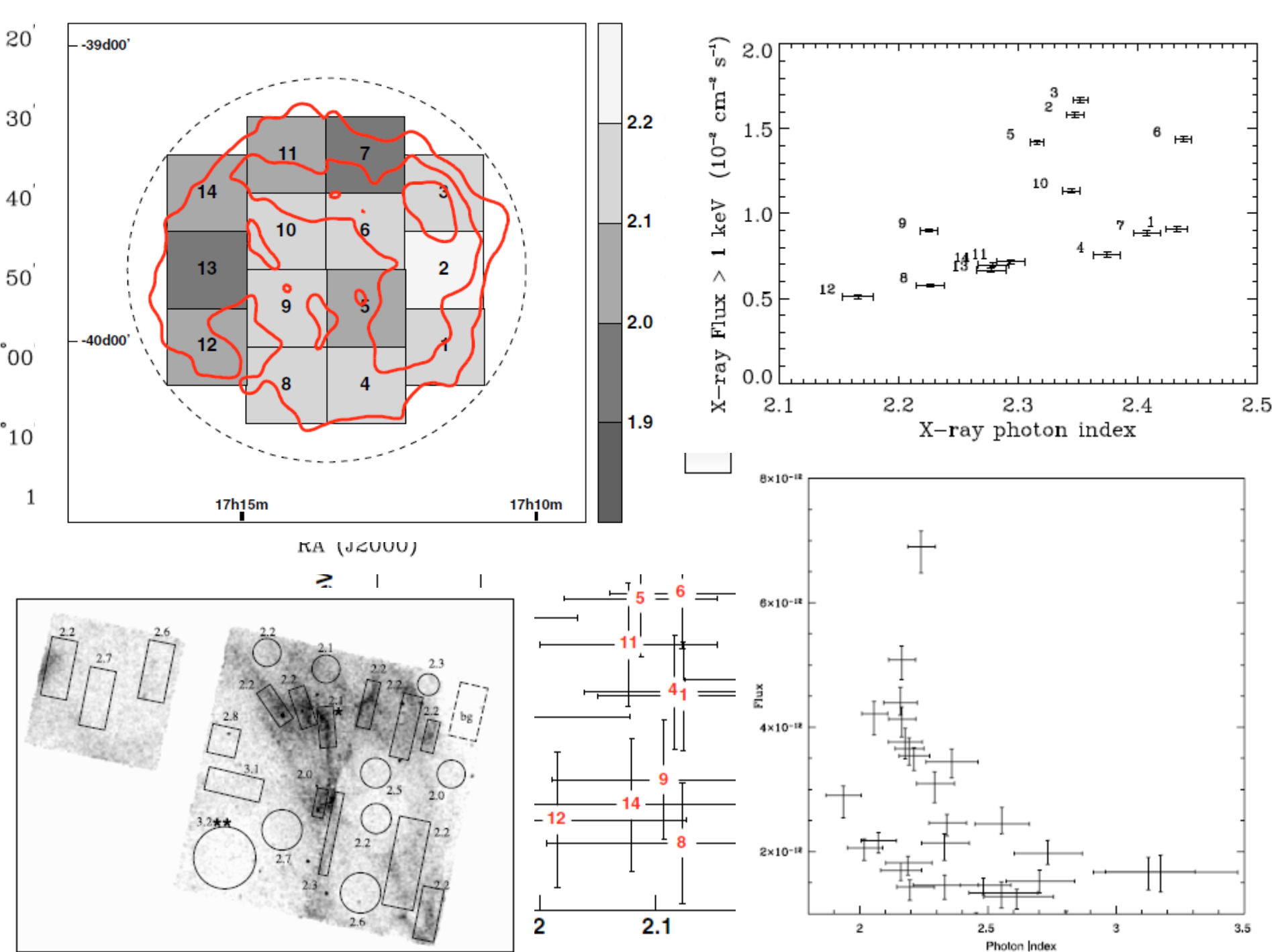
1 Multi-wavelength overall spectral fit



| Name | $F_\gamma^{\text{a}}/F_X^{\text{b}}$ $10^{-10} \text{ erg s}^{-1} \text{ cm}^{-2}$ | Diameter ^c pc | B^{d} μG | W_e^{d} 10^{47} erg | W_B 10^{47} erg |
|-----------------|---------------------------------------------------------------------------------------|-----------------------------|---------------------------------|-------------------------------------------|--------------------------------|
| RX J1713.7-3946 | 0.68/5.4 | $17.4(D/1)$ | 12 | $3.9(D/1)^2$ | $4.0(D/1)^3(f/0.87)^e$ |
| RX J0852-4622 | $0.66^{\text{e,f}}/0.83$ | $34(D/1)$ | 9.4 | $10(D/1)^2$ | $10(D/1)^3(f/0.49)^f$ |
| J1731-347 | 0.09/1.0 ^a | $27(D/3.2)$ | 28 | $2.3(D/3.2)^2$ | $85(D/3.2)^3(f/0.9)^a$ |

1 Energy Partition between Magnetic Field and Energetic Electrons

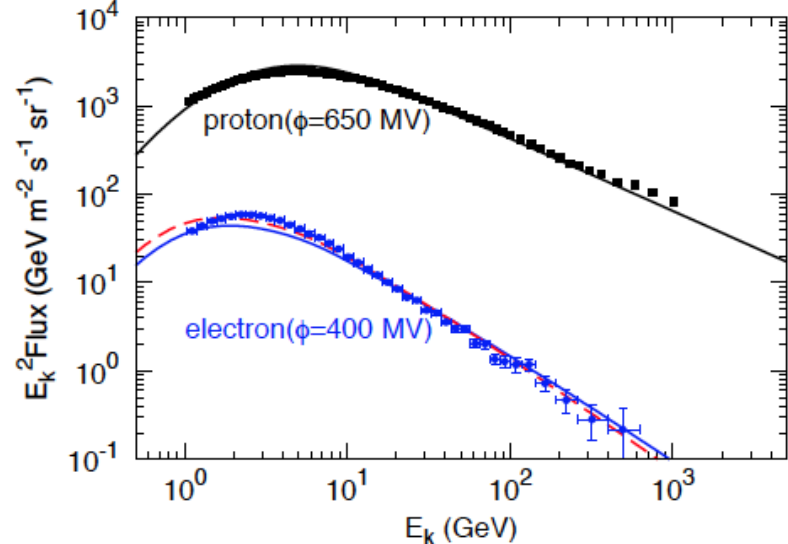
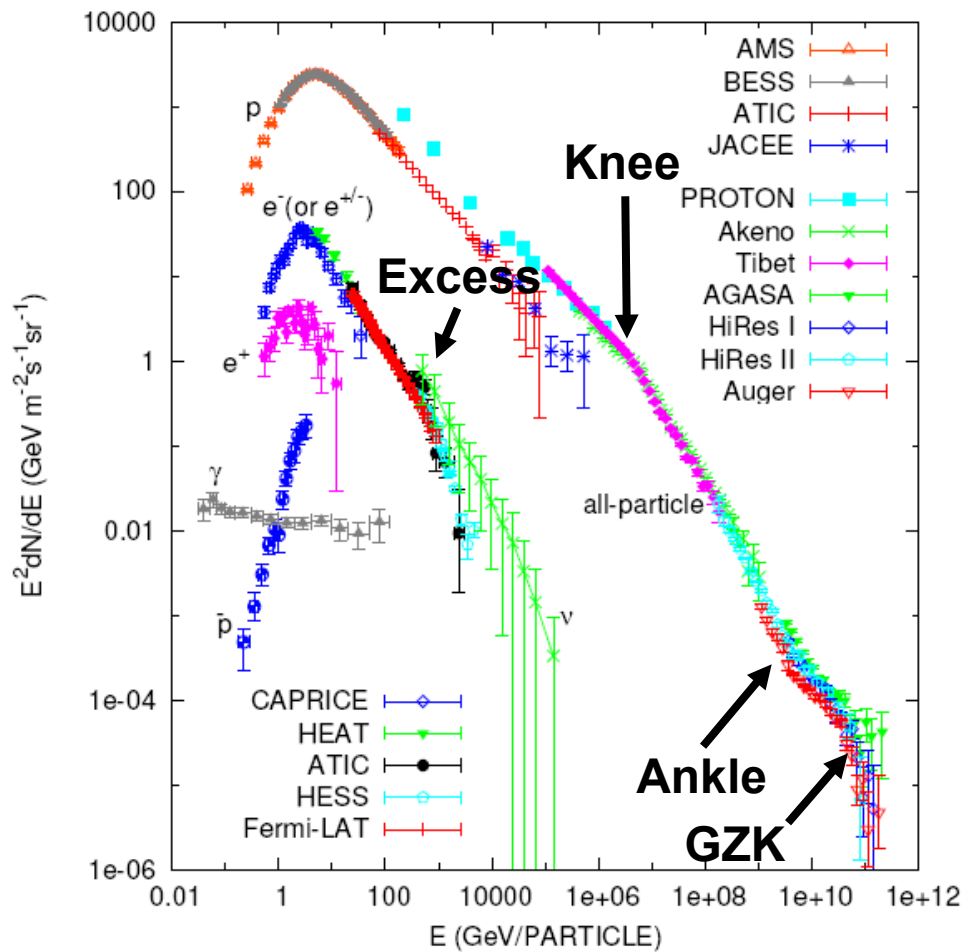




3: Future Studies

- 1: 3D MHD Simulations to Study Source structure
- 2: Multi-wavelength spectral fit
- 3: Evolution of SNRs
- 4: Incorporating the thermal component

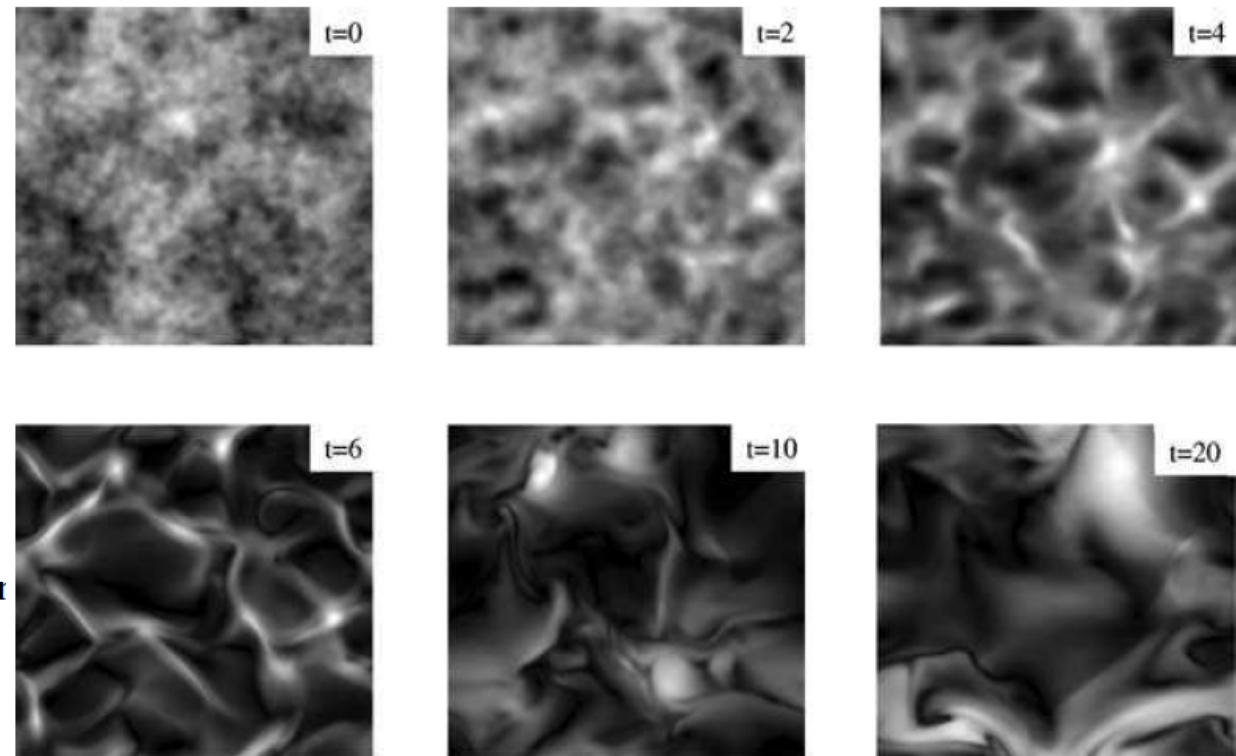
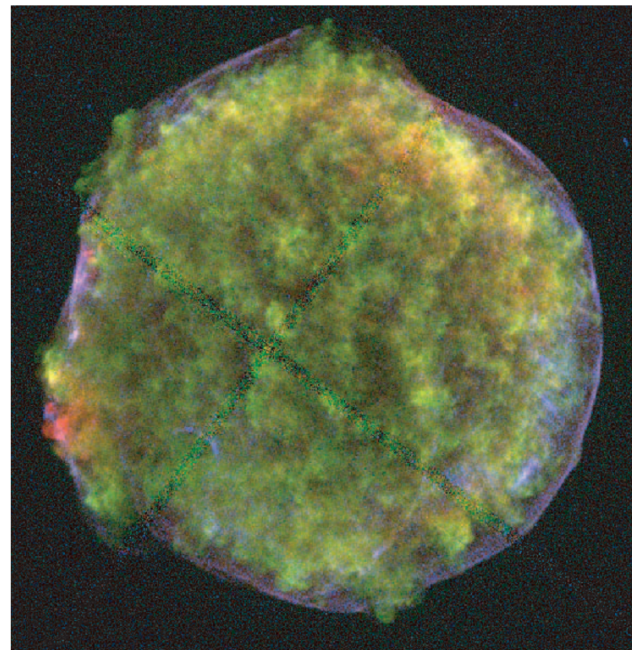
2: Cosmic Rays



G. 1.— The expected fluxes of CR protons and electrons at Earth, for the same spectral shape of the injected particles, pared with the PAMELA observational data (Adriani et al. a,b). We adopt two parameter settings to calculate the elec-spectrum: for solid line the magnetic field is the canonical adopted in GALPROP and $K_{ep} \approx 1.3\%$; for dashed line the netic field is two times larger and $K_{ep} \approx 1.9\%$.

J. GIACALONE AND J. R. JOKIPII
Magnetic Field Strength

4.1 Source Structure: Magnetic Field Amplification



Turbulent amplification of mag
acceleration of cosmic rays

A. R. Bell[★]

4.2 Multi-wavelength spectral fit

GAMMA RAYS FROM THE TYCHO SUPERNOVA REMNANT: MULTI-ZONE VERSUS SINGLE-ZONE MODELING

ARMEN ATOYAN¹ AND CHARLES D. DERMER²

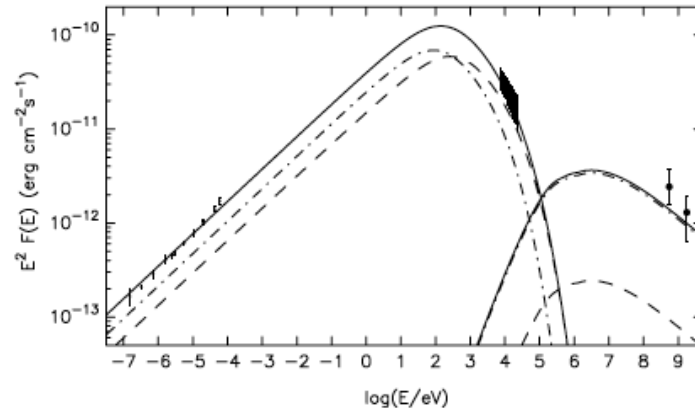
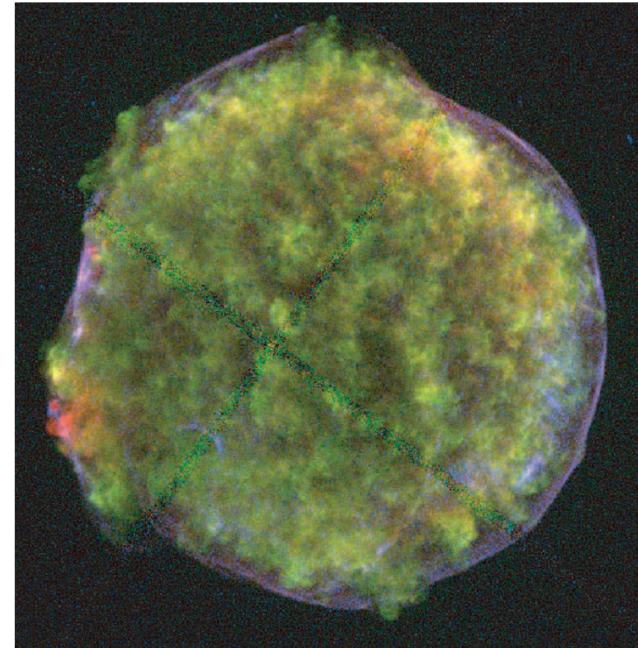


Figure 1. Synchrotron fluxes from radio through X-rays in the two-zone model. Dashed and dot-dashed lines show the fluxes from zone 1 and zone 2, respectively, and the total flux is shown by the solid line. Calculations assume density $n_2 \approx 3 \text{ cm}^{-3}$ at $d_{\text{kpc}} = 2.8$, $n_1 \approx n_2$, $B_1 = 100 \mu\text{G}$ and $B_2 = 34 \mu\text{G}$, $\eta = 0.2$, $\alpha = 2.31$, and $E_{\text{cut}} = 40 \text{ TeV}$. Also shown are the lower-energy ($\lesssim \text{GeV}$) bremsstrahlung fluxes produced by relativistic electrons in zones 1 and 2.

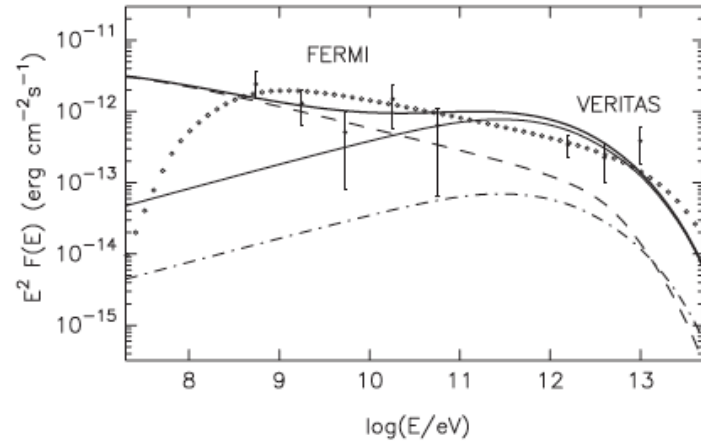


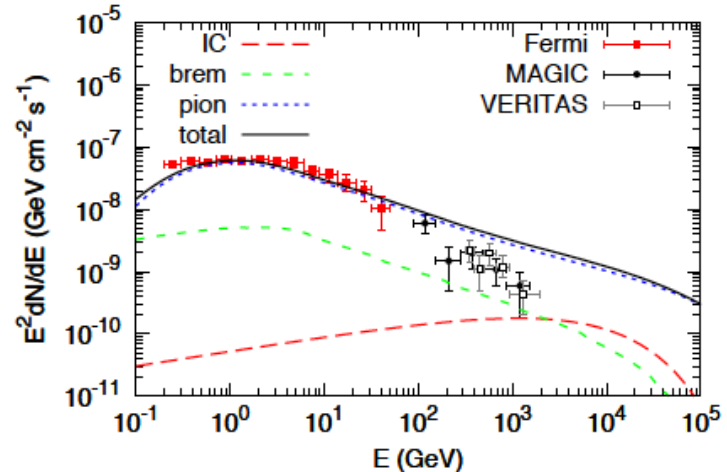
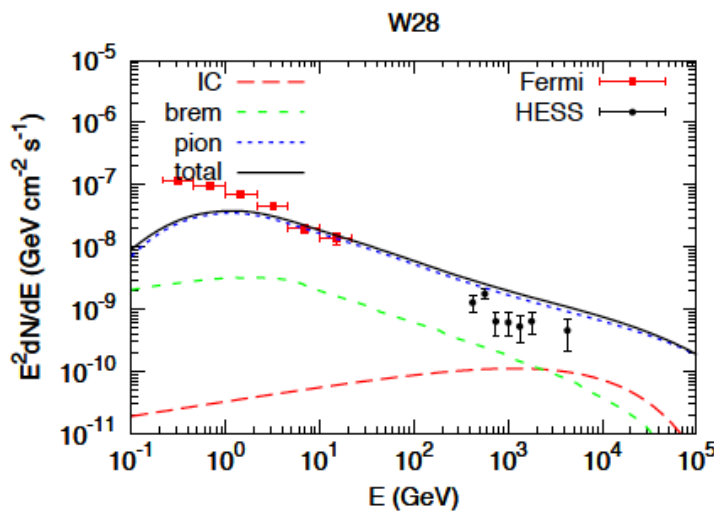
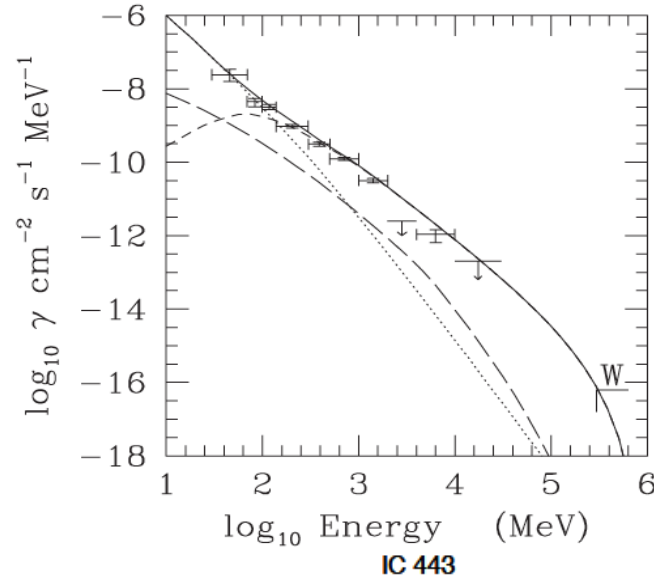
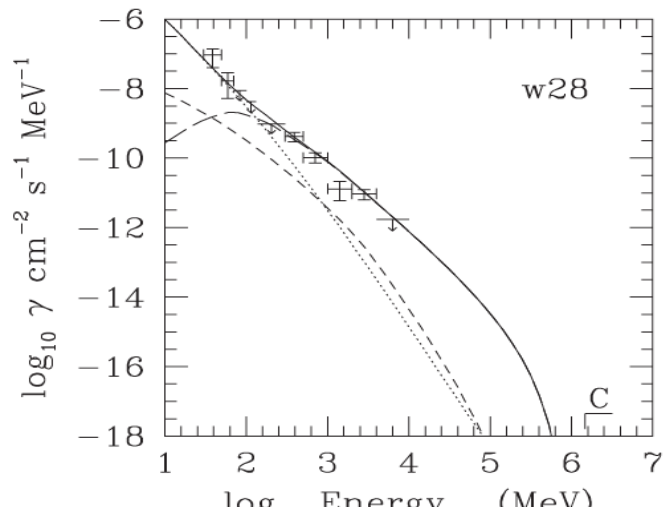
Figure 2. γ -ray fluxes in the two-zone model with parameters described in Figure 1. The heavy solid line shows the total flux of leptonic origin. The total bremsstrahlung and Compton radiation fluxes are shown by dashed and solid (thin) lines, respectively. For comparison, the Compton flux contribution from zone 1 is also shown (dot-dashed line). The open dotted curve shows the flux of hadronic origin calculated for protons with total energy $E_p = 3 \times 10^{49} \text{ erg}$.

4.2 Multi-wavelength spectral fit

PRIMARY VERSUS SECONDARY LEPTONS IN THE EGRET SUPERNOVA REMNANTS

MARCO FATUZZO¹ AND FULVIO MELIA²

Received 2004 December 17; accepted 2005 May 6



RADIO TO GAMMA-RAY EMISSION FROM SHELL-TYPE SUPERNOVA REMNANTS: PREDICTIONS FROM NONLINEAR SHOCK ACCELERATION MODELS

MATTHEW G. BARING¹

Laboratory for High-Energy Astrophysics, Code 661, NASA Goddard Space Flight Center, Greenbelt, MD 20771; baring@lheavx.gsfc.nasa.gov

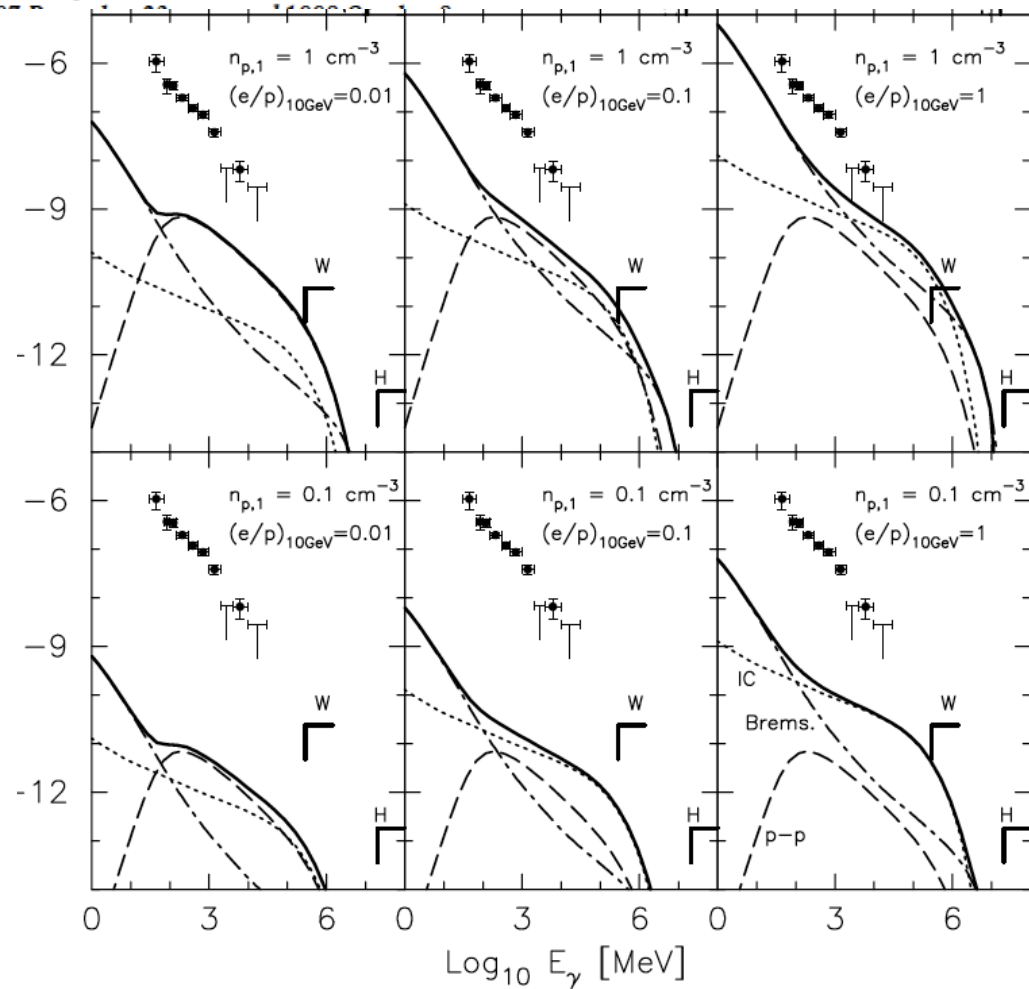
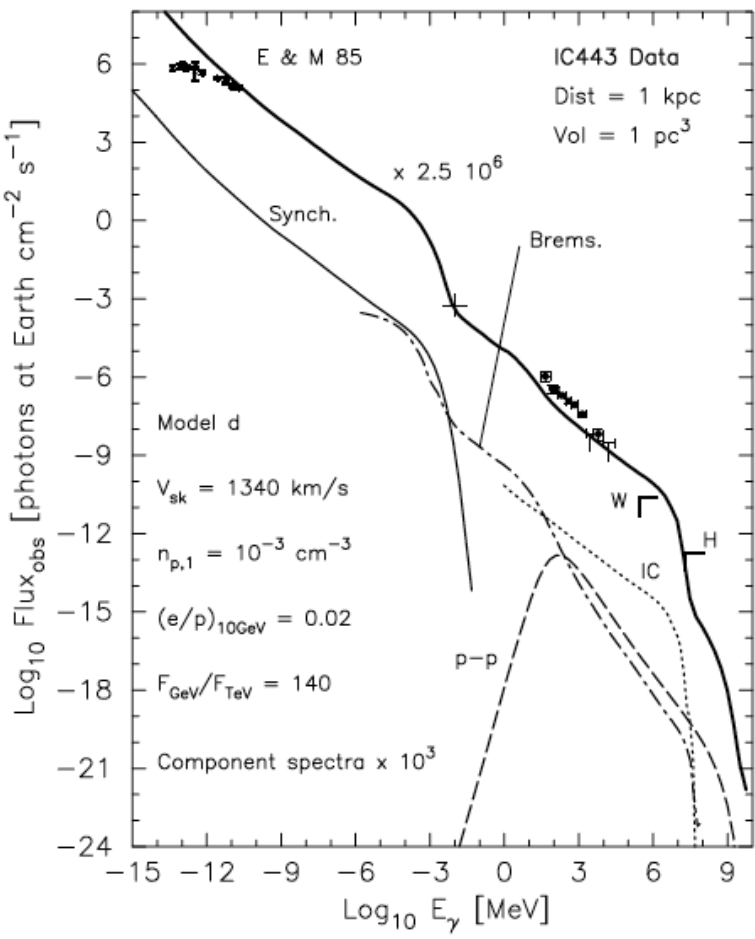
DONALD C. ELLISON AND STEPHEN P. REYNOLDS

Department of Physics, North Carolina State University, Box 8202, Raleigh NC 27695; don_ellison@ncsu.edu, steve_reynolds@ncsu.edu

AND

ISABELLE A. GRENIER AND PHILIPPE GORET

Service d'Astrophysique, CEA, DSM, DAPNIA, Centre d'Etudes de Saclay, 91191 Gif-sur-Yvette, France; isabelle.grenier@cea.fr,
goret@sapvsg.saclay.cea.fr



4.4 Thermal Emission

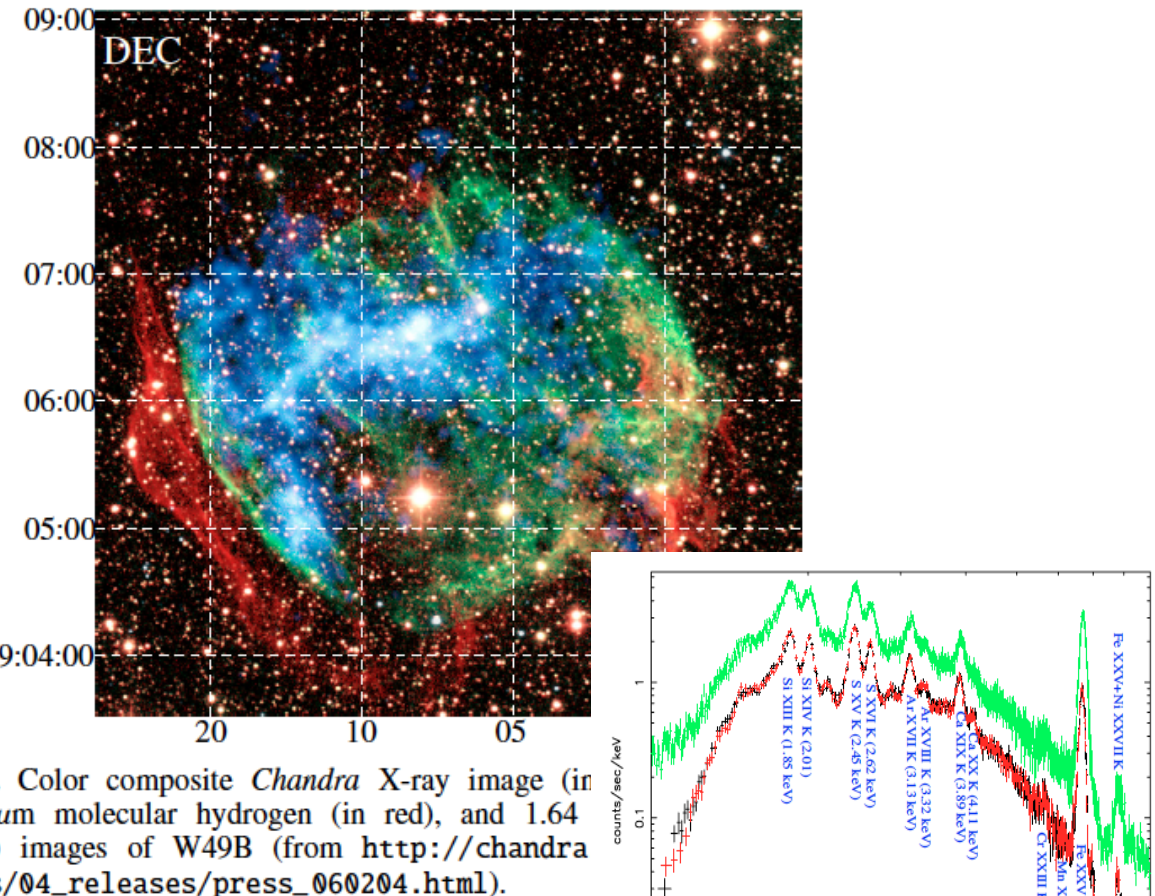
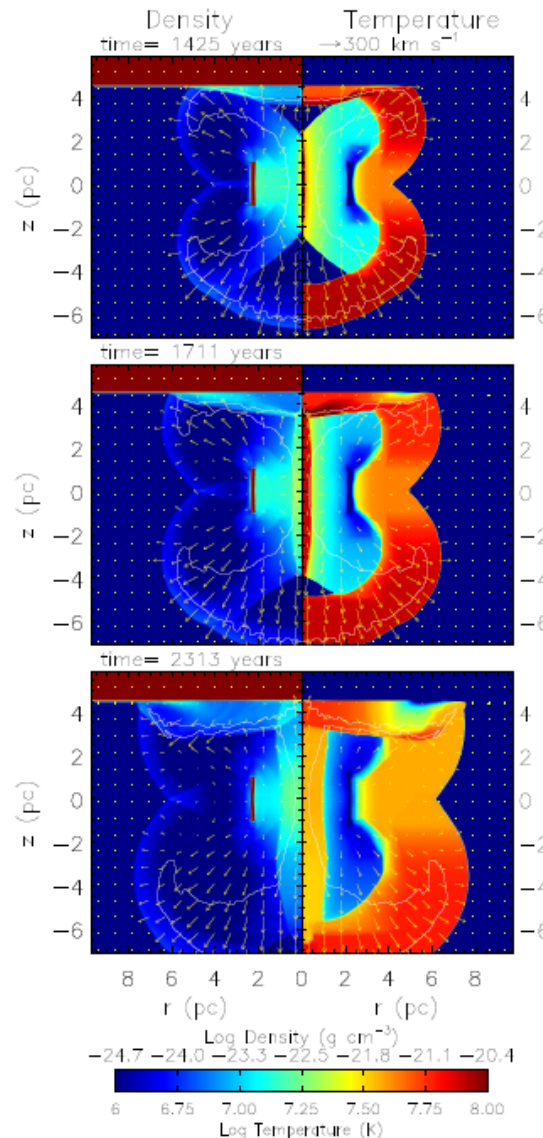


Fig. 2. Color composite *Chandra* X-ray image (in $2.12 \mu\text{m}$ molecular hydrogen (in red), and $1.64 \mu\text{m}$ green) images of W49B (from http://chandra.press/04_releases/press_060204.html).



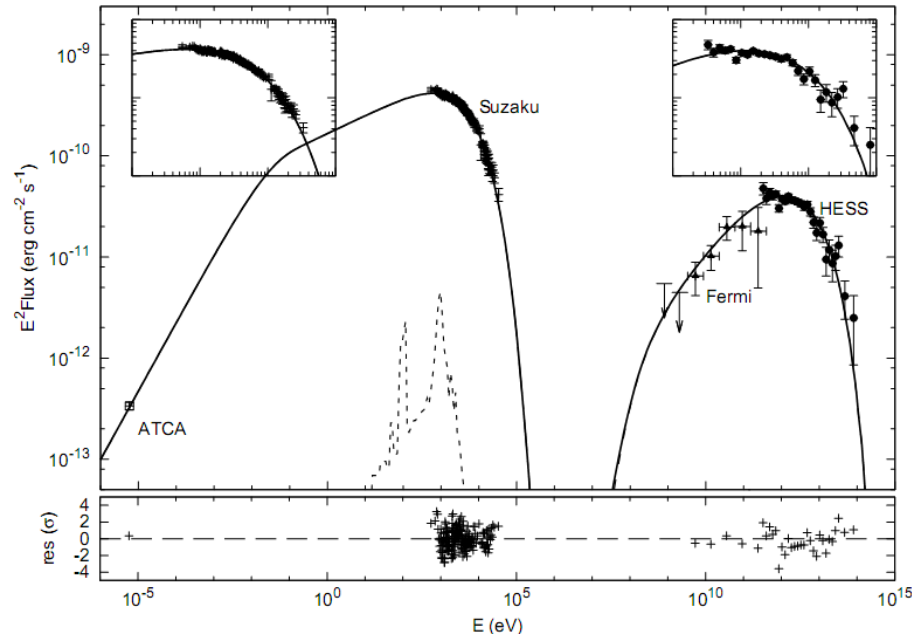
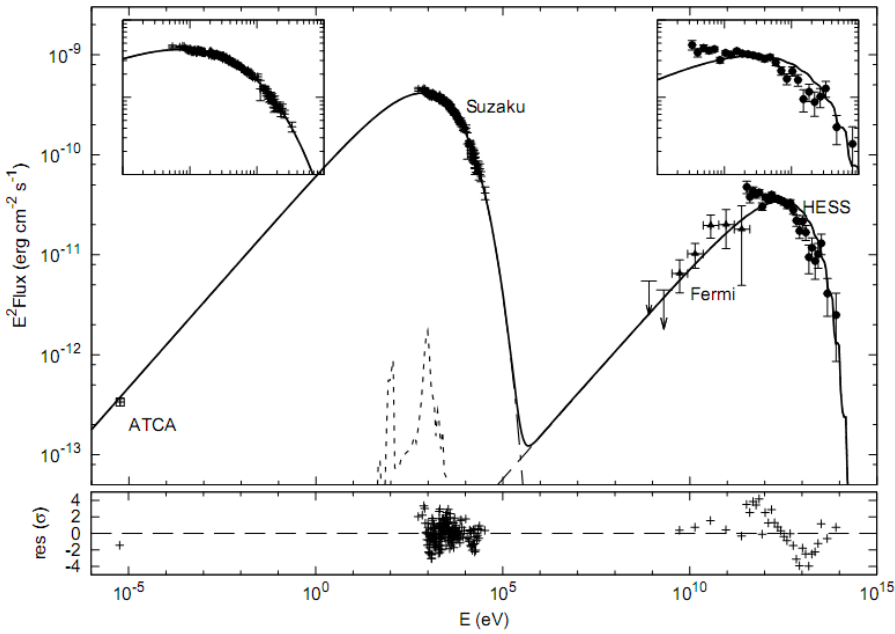
Unveiling the spatial structure of the overionized plasma in the supernova remnant W49B

1: Two emission models for SNR RX J1713.7-3946

Leptonic

$$F_e(E) \propto E^{-\alpha_e} \exp [-(E/E_c^e)^{\delta_e}]$$

Hadronic



| | α_e | E_c^e (TeV) | W_e (10^{47} erg) | δ_e | B (μ G) | n_{ISM} (10^{-2} cm $^{-3}$) | α_p | E_c^p (TeV) | W_p (10^{52} erg) |
|-----------|------------------------|----------------------|---------------------------|------------------------|---------------------------|---------------------------------------|------------------------|----------------------|---------------------------|
| leptonic | $2.15^{+0.01}_{-0.01}$ | $51.3^{+2.3}_{-2.2}$ | $5.5^{+0.3}_{-0.3}$ | $1.21^{+0.04}_{-0.04}$ | $11.6^{+0.1}_{-0.1}$ | < 0.7 | — | — | — |
| hadronic | $1.64^{+0.09}_{-0.08}$ | $14.5^{+4.8}_{-3.9}$ | $0.05^{+0.05}_{-0.02}$ | $2.1^{+0.2}_{-0.2}$ | $428.2^{+233.9}_{-159.6}$ | < 1.1 | $1.58^{+0.06}_{-0.06}$ | $53.7^{+7.1}_{-6.2}$ | > 1.6 |
| hadronic* | $1.58^{+0.05}_{-0.05}$ | $12.3^{+2.1}_{-1.8}$ | $0.03^{+0.01}_{-0.01}$ | $1.9^{+0.1}_{-0.1}$ | $596.8^{+173.0}_{-129.0}$ | < 1.2 | — | $54.7^{+6.0}_{-5.7}$ | > 1.4 |

THE ASTROPHYSICAL JOURNAL, 735:120 (9pp), 2011 July 10
 © 2011. The American Astronomical Society. All rights reserved. Printed in the U.S.A.

doi:10.1088/0004-637X/

3: Future Studies

- 1: 3D MHD Simulations to Study Source structure
- 2: Multi-wavelength spectral fit
- 3: Evolution of SNRs
- 4: Incorporating the thermal component

4.3 Time Evolution

Declination

